UNIVERSITAT POLITÈCNICA DE CATALUNYA

DOCTORAL THESIS

Relaxation dynamics and crystallization kinetics of glass-forming drugs

---

Author:
Guadalupe Natalia RUIZ

Supervisor:
Dr. Luis Carlos PARDO and
Dr. Roberto MACOVEZ
Tutor:
Josep LLuis TAMARIT

A thesis submitted in fulfillment of the requirements
for the degree of Doctor of Philosophy

in the

Group of Characterization of Materials (GCM), PhD programme in
Computational and Applied Physics
Department of Physics

July 3, 2018

Declaration of Authorship

I, Guadalupe Natalia RUIZ, declare that this thesis titled, "Relaxation dynamics and crystallization kinetics of glass-forming drugs" and the work presented in it are my own. I confirm that:

- This work was done wholly or mainly while in candidature for a research degree at this University.
- Where any part of this thesis has previously been submitted for a degree or any other qualification at this University or any other institution, this has been clearly stated.
- Where I have consulted the published work of others, this is always clearly attributed.
- Where I have quoted from the work of others, the source is always given. With the exception of such quotations, this thesis is entirely my own work.
- I have acknowledged all main sources of help.
- Where the thesis is based on work done by myself jointly with others, I have made clear exactly what was done by others and what I have contributed myself.

Signed:

_____

Date:

_____

"I tore myself away from the safe comfort of certainties through my love for truth - and truth rewarded me."

Simone de Beauvoir

UNIVERSITAT POLITÈCNICA DE CATALUNYA

Abstract

Group of Characterization of Materials

Department of Physics

Doctor of Philosophy

Relaxation dynamics and crystallization kinetics of glass-forming drugs

by Guadalupe Natalia RUIZ

Glassy phases play an important role in our daily life and in many industries such as the food, pharmaceutical, and construction industries, and are critical in applications such as organic (opto) electronics and fiber optics. They are responsible for certain vital mechanisms in living species: some animals and plants, for instance, have the ability of achieving cryopreservation by vitrifying liquid substances within them (Fahy et al., 1984). Whereas crystals are solid phases that show periodicity of the constituent atoms or molecules, glasses are disordered solids that lack long-range positional order but behave mechanically like solids. Chapter 1 of the current thesis presents an introduction to the characteristics and dynamics of glassy phases. How they are derived from the liquid phase, and how they transform into the crystalline solid phase, thermodynamically more stable. The temperature at which a liquid transforms to the amorphous (glassy) phase is called the glass transition temperature, T_g.

Along this thesis the relaxation dynamics of prilocaine and stiripentol, and the isothermal crystallization process of the latter have been studied with experimental techniques. Both prilocaine and stiripentol are drugs used in medical applications mainly as anesthesia and for the treatment of epilepsy, respectively. The studied materials have been analyzed by the concurrent use of Broadband Dielectric Spectroscopy, Differential Scanning Calorimetry, X-Ray diffraction, Raman spectroscopy, I.R spectroscopy and confocal microscopy. The physical principles governing the dielectric technique (which is the main experimental tool employed for the present work) are presented in Chapter 2. The details of the experimental set-ups are stated in Chapter 3.

In the case of a pharmaceutical product, being able to control and foresee the aggregation phase and dissolution rate of the substance is of the uttermost relevance. Many drugs are poorly soluble in water and thus, in biological media. The glass state of a drug is a non-equilibrium state that presents higher free energy than the crystal state. This implies, that a drug in the glassy phase dissolves more rapidly and can be absorbed in larger amounts in the intestine. Nevertheless, the higher free energy of glassy phases represents at the same time a major problem for shelf-life, since metastable phases are prone to spontaneously transforming into the stable crystalline state. This is of course a potentially major problem, since wrong dosage or agglomeration of a drug could render it useless or even worse, toxic for the human body. Being able to understand the glass and crystallization dynamics of drugs,

and their interaction with water, is a very powerful tool in order to develop more efficient products.

Water is the universal biological solvent, key to the formation of biological structures as well as many other biological processes (Mallamace et al., 2016; Ball, 2008). For most materials the addition of water leads to a decrease in viscosity, or equivalently, an increase of molecular mobility, which results in a lower glass transition temperature T_g (the higher the water content the lower the T_g). This is referred to as the plasticizing effect of water. Chapter 4 presents a detailed analysis of both pure and hydrated prilocaine. Results show that the addition of water to the prilocaine drug leads to the formation of prilocaine-water complexes, possibly water-bridged monomers or dimers that increase the glass transition temperature. This antiplasticizing effect of water on the molecular mobility of a simple glass former represents a significant exception to the alleged universality of water as drug plasticizer. The physico-chemical origins of this behavior have been confirmed by studying the effect of confinement of the pure and hydrated drug in the pores of a nonporous structure (Chapter 5).

In the case of stiripentol, not only the glassy dynamics were studied, but also the crystallization process (Chapter 6). A sublinear correlation between the characteristic crystal-growth time and the relaxation time of the cooperative relaxation dynamics of stiripentol was found. This correlation was observed also in other substances, which suggests that it is a general correlation at temperatures above T_g. This may allow predicting a substance's crystallization time as a function of temperature.

The results of this thesis provide valuable insight into the kinetics and relaxation dynamics, as well as the phase stability, of both studied drugs that could be general to other amorphous drugs. Global conclusions are outlined in Chapter 7.

Contents

List of Abbreviations

BDS	**B**roadband **D**ielectric **S**pectroscopy
BNN	**B**arton **N**akajama **N**amikawa
CC	**C**ole **C**ole
CM	**C**oupling **M**odel
DSC	**D**ifferential **S**canning **C**alorimetry
HN	**H**avriliak **N**egami
IR	**I**nfra **R**ed
JG	**J**ohari **G**oldstein
KWW	**K**ohlrausch **W**illiams **W**atts
ODIC	**O**rientationally **D**isordered **C**rystals
PLC	**P**rilocaine
SG	**S**tructural **G**lasses
STP	**S**tiripentol
UDR	**U**niversal **D**ielectric **R**esponse
VFT	**V**ogel-**T**ammann-**F**ulcher
XRD	**X**-**R**ay **D**iffraction

Physical Constants

Permittivity of vacuum	$\epsilon_0 = 8.854\,187\,817 \times 10^{-12}\,\mathrm{F/m}$
Boltzmann constant	$k_b = 1.380\,648\,52 \times 10^{-23}\,\mathrm{J\,K^{-1}}$

List of Symbols

C_p	heat capacity at constant pressure	$\mathrm{J\,K^{-1}}$
E	electric field	$\mathrm{V\,m^{-1}}$
E	activation energy	$\mathrm{kJ\,mol^{-1}}$
E_{Loc}	local electric field	$\mathrm{V\,m^{-1}}$
g	gravity	$\mathrm{m\,s^{-2}}$
G	shear modulus	Pa
j	current density	$\mathrm{A\,m^{-2}}$
h	enthalpy	J
m	fragility index	
M^*	complex electric modulus	$\mathrm{m\,F^{-1}}$
$M^{'}$	real part of electric modulus	$\mathrm{m\,F^{-1}}$
$M^{''}$	imaginary part of electric modulus	$\mathrm{m\,F^{-1}}$
P	macroscopic polarization	$\mathrm{A\,s\,m^{-2}}$
P	pressure	bar
P_g	glass transition pressure	bar
p_i	microscopic polarization	$\mathrm{A\,s\,m^{-2}}$
t	time	s
t_c	crystallization time	s
T	temperature	K
T_c	crystallization temperature	K
T_g	glass transition temperature	K
T_m	melting temperature	K
T_{VF}	Volgel-Fulcher temperature	K
V	volume	$\mathrm{m^3}$
α_p	thermal expansion coefficient at constant pressure	$\mathrm{m^3\,K^{-1}}$
η	viscosity	$\mathrm{N\,s\,m^{-2}}$
ϵ^*	complex dielectric permittivity	$\mathrm{F\,m^{-1}}$

ϵ'	real part of dielectric permittivity	$\mathrm{F\,m^{-1}}$
ϵ''	imaginary part of dielectric permittivity	$\mathrm{F\,m^{-1}}$
ϵ_r	relative dielectric permittivity	scalar
ν	technical frequency	Hz
σ^*	complex electric conductivity	$\mathrm{S\,m^{-1}}$
σ'	real part of electric conductivity	$\mathrm{S\,m^{-1}}$
σ''	imaginary part of electric conductivity	$\mathrm{S\,m^{-1}}$
σ_{DC}	DC conductivity	$\mathrm{S\,m^{-1}}$
σ_{AC}	AC conductivity	$\mathrm{S\,m^{-1}}$
τ	relaxation time	s
ω	angular frequency	$\mathrm{rad\,s^{-1}}$
χ	dielectric susceptibility	scalar

A Lucho, a mis hermanxs y a mis amigxs del alma.

Chapter 1

Introduction to solid state

Common matter is composed by molecules held together by forces, and the relative strength of these intermolecular interactions determine in which phase it is. A gas is a phase in which molecules are separated from one another, constantly move about and tend to occupy the maximum space available. In liquids, molecules are more closely packed together, they collectively have a definite volume, but undergo diffusional motions leading to fluid properties. Solids, on the other hand, represent an aggregation phase where diffusional and molecular motions are generally hindered. The balance between the average kinetic energy and the attractive intermolecular forces between the particles determine whether a substance is a solid, a liquid or a gas. If the attractive potential energy between the particles is smaller than the average kinetic energy, then the substance will be in the glass phase and will not be able to condense to form a liquid or a solid. Inversely, if the attractive potential is larger than the kinetic energy, a more compact, denser structure either in the form of a liquid with a higher level of order will form, in the phase of liquid below the critical point, or a solid phase.

Different types of solid phases can be formed. Crystals are solid phases with high level of order, in the sense that a certain pattern of atoms, molecules or ions is repeated along a periodic lattice. Glasses, on the contrary, are disordered solids. This means they do not display long-range positional periodicity but have mechanical properties similar to those of crystals.

When it comes to formulation and storing of drugs, whether the solid phase is ordered (crystalline) or disordered (glass) is a key point that needs to be considered. Whereas the glass state presents a higher free energy and hence dissolves more rapidly inside the human body, the same property is a problem for shelf life, since it makes it less resistant to transforming into the stable crystalline state (Yoshioka and

V.J.Stella, 2002).

Avoiding phase transformation or change in physico-chemical properties in pharmaceutical products is of course of paramount importance, as well as providing a drug formulated in a phase that can be easily absorbed and metabolized by the human body and is highly compatible with water. Along this thesis I have studied the glassy state and crystallization of Prilocaine and Stiripentol. Both of these substances are drugs used in medical applications mainly as anesthesia and for the treatment of epilepsy, respectively.

1.1 Ordered and disordered solid phases

1.1.1 Solid Ordered Phases: The crystal

Crystals (crystalline solids) are materials whose components are arranged in a highly ordered microscopic structure. These periodic arrangements may have atoms, molecules or ions as its constituents and are repeated in a pattern in all directions, conforming a crystal lattice (Lower, 2016). The pattern that is periodically repeated is called a unit cell.

Figure 1.1 shows, as an example, the crystalline arrangement of silicon dioxide (SiO_2). This compound occurs naturally as quartz sand in its crystalline phase. The crystal lattice represents a state of minimal entropy and high order.

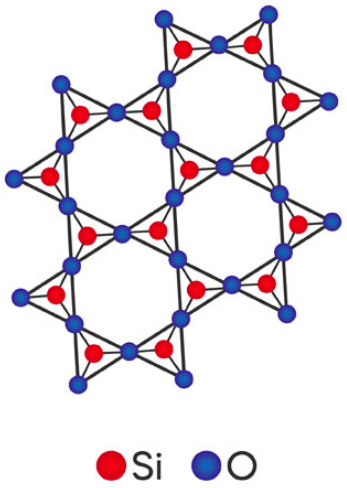

FIGURE 1.1: Schematic representation of the periodic arrangement observed in a SiO_2 crystal lattice. Red dots represent Si atoms whereas blue ones stand for O.

Most inorganic solids are not single crystals, but polycrystals, which means many crystalline sections are held together into a single solid. Many ceramics, metals, rocks and ice show this kind of arrangement (Lower, 2016; Ashcroft and Mermin, 1976).

1.1.2 Solid Disordered Phases: The glass

Whereas crystalline materials show a periodic structure where a positional arrangement or unit cell of atoms is reproduced along a periodical matrix, glasses are disordered solids that lack long-range periodicity but behave mechanically like solids (Debenedetti and Stillinger, 2001).

Figure 1.2 shows as an example the amorphous arrangement of silicon dioxide (SiO_2). This material can exist as a metastable solid and can be transformed into the amorphous phase, known as silica glass. It can be observed that although some resemblance between the crystalline and the amorphous phases remains, the crystal represents a state of higher order.

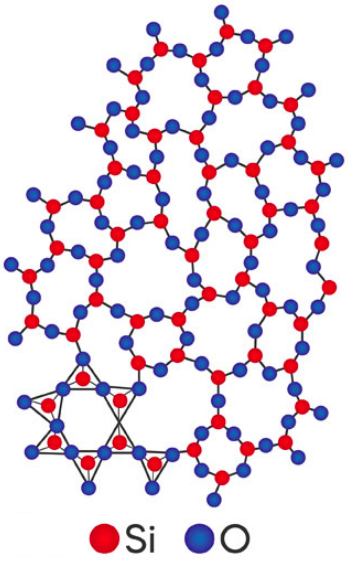

FIGURE 1.2: Schematic representation of the periodic arrangement observed in a SiO_2 amorphous phase. Red dots represent Si atoms whereas blue ones stand for O.

The most common way of obtaining a glass is by cooling a viscous liquid fast enough to avoid crystallization (Debenedetti and Stillinger, 2001). When a liquid

substance is cooled below its melting point, T_m, without crystallization it is identified as a supercooled liquid. Many systems may be supercooled, without acquiring translational and orientational order. When temperature is lowered below the melting point molecular motions slow down. Eventually, if the cooling rate is fast enough, the molecules rearrange so slowly compared to the cooling rate that they are not able to reach the crystalline structure and become arrested in a state between the liquid and the crystalline phase, the glass. The material appears *frozen* on the laboratory timescale (for example minutes), meaning that its molecules still flow, but in a time scale that cannot be appreciated by naked eye, contrary to what is observed in liquids.

As schematically shown in figure 1.3 different types of solids combining glass and crystal characteristics can be formed. If a supercooled liquid is cooled further down, it transforms into a structural glass. These phases maintain the orientational and translational disorder of the liquid from which they derive, and do not shown long range order or periodicity (Brand, Lunkenheimer, and Loidl, 2002). Glassy materials studied along this thesis are structural glasses (SG).

As explained the first section of this chapter, for most substances when the liquid phase is cooled below T_m the ordered crystal is formed. This case is illustrated in the black pattern of figure 1.3.

A different type of glass may be formed when the system is periodically arranged as regards the location of each particle within the lattice, but orientation of the components is not fixed. This is to say, atoms, molecules or unit cells are arranged within a periodical matrix, but from an orientation point of view they are still disordered and can change orientation while keeping their lattice positions. This type of material is called plastic crystal (ODIC: orientationally disordered crystals). In general, they resemble waxes and are easily deformed.

Figure 1.4 shows, as an example, a two-dimensional confocal microscopy image of a three-dimensional plastic crystal. On the left hand side a snapshot of the particles can be seen. The right-hand image is averaged over a longer period of time. The fact that some periodic order can be observed but each position presents a diffuse image produced by the change in orientation over a long period of time, shows that the particles are positioned on a 3D lattice whereas the rods can freely rotate. In these images, g indicates the direction of gravity (the gravity points forwards out of the image). E indicates the direction of the electric field (Image taken from Fundamental

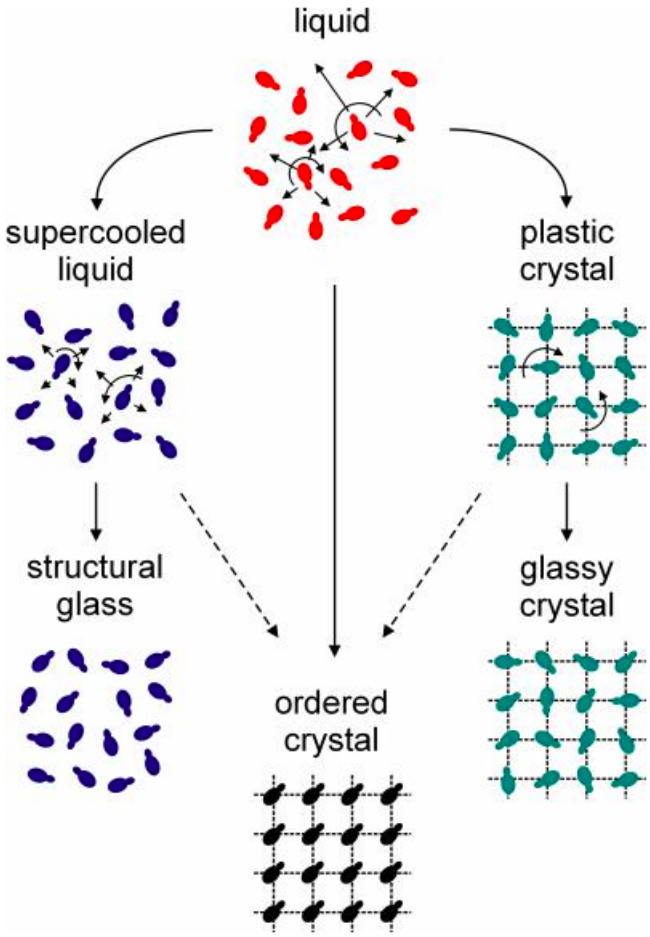

FIGURE 1.3: Schematic representation of the possible transitions from the liquid state of dipolar molecules into a structural glass (SG), an ordered crystal or glassy crystal phase (Brand, Lunkenheimer, and Loidl, 2002).

Research on Matter (FOM), Institute of the Netherlands).

If a plastic crystal is cooled further down, the orientational degrees of freedom can be dramatically reduced, yielding a glassy crystal or an orientational glass, as indicated in figure 1.3 (Brand, Lunkenheimer, and Loidl, 2002). This is to say, plastic crystals and glassy crystals are connected through a glass transition, and have positionally speaking the same structure, but plastics crystals have rotational freedom whereas glassy ones lack this capacity.

1.2 The comparison between glasses and crystals

The temperature at which the transition between the liquid and the amorphous (glassy) phase takes place, depends on the cooling/heating rate, and is called the

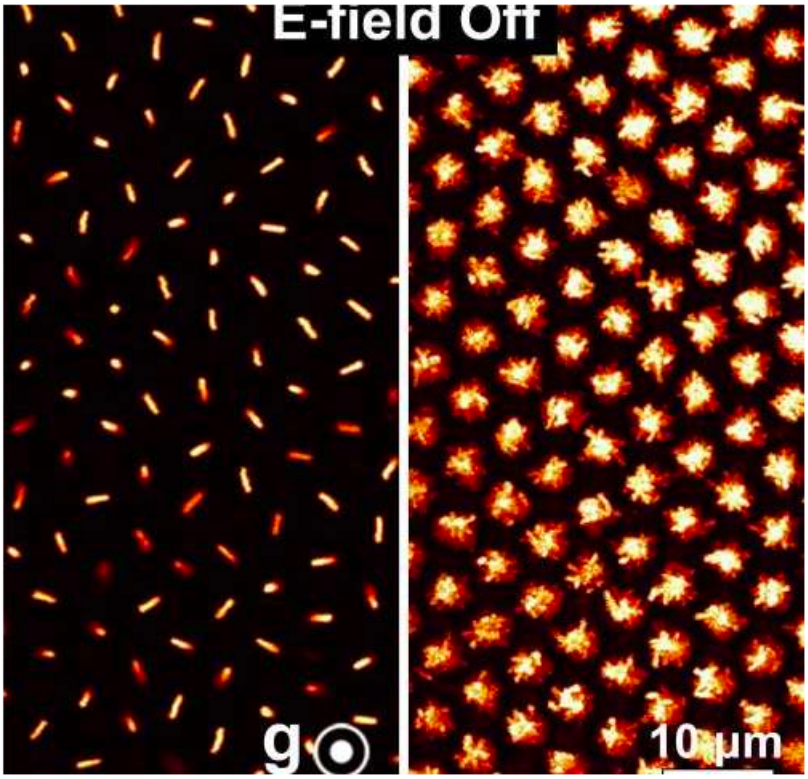

FIGURE 1.4: Two-dimensional confocal microscopy image of a three-dimensional plastic crystal. Left: snapshot of the particles. Right: Image is averaged over a longer period of time. The particles are positioned on a 3D lattice whereas the rods can freely rotate. In these images, g indicates the direction of gravity (the gravity points forwards out of the image). E indicates the direction of the electric field. (Image taken from Fundamental Research on Matter (FOM), Institute of the Netherlands.

glass transition temperature, T_g. The slower a liquid is cooled, the longer the time available for configurational sampling so that a higher level of packing can be achieved in the glass state. The viscosity, η, of a material is its ability to resist flow, where flow is defined as a gradual deformation by shear or tensile stress. Glassy materials have a viscosity value of 10^{13} poise. The temperature at which η reaches this value is the glass transition temperature.

Transforming from liquid to crystal phase upon isobaric cooling entails a first order change in volume (V) and enthalpy (H), meaning that both these properties change discontinuously, as portrayed by the blue trace in figure 1.5. This implies there is a discrete change in volume, and as the liquid forms a crystalline phase different degrees of freedom are lost with respect to the liquid structure.

Transitioning from liquid into glass, on the other hand, involves a continuous decrease both in volume and enthalpy, as portrayed by the light blue $\rightarrow$ violet traces

in Figure 1.5. The intersection of the liquid and vitreous portions of the volume versus temperature curve, provides one definition of T_g. It is generally the case that the glass transition temperature is found in many materials at around $2T_m/3$ (Debenedetti and Stillinger, 2001).

As observed in figure 1.5, upon cooling the glass formed with a slower cooling rate (a) adopts a more compact glassy structure than another glass achieved with a more rapid cooling rate (b). At the same time, upon heating, the glass transition temperatures observed will be different: T_{ga} for the slow cooling rate and T_{gb} for the fast one. The properties of a glass, therefore, depend on the process by which it is formed. Nevertheless although cooling/heating rates affect the properties of the glass formed, in practice the dependence of T_g is weak, as it changes from 3 to 5 °C when the cooling rate changes by an order of magnitude (Ediger, Angell, and Nagel, 1996).

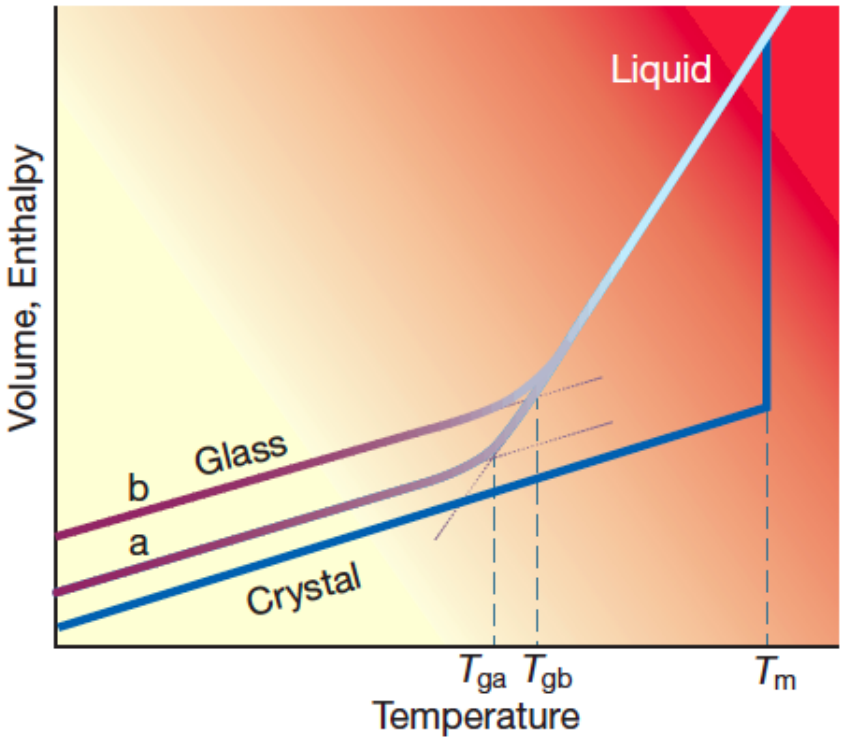

FIGURE 1.5: Temperature dependence of a liquid's volume V or enthalpy h at constant pressure upon cooling. T_m is the melting temperature. A slow cooling rate produces a glass transition at T_{ga}; a faster cooling rate leads to a glass transition at T_{gb}. Figure adapted from Debenedetti and Stillinger, 2001.

The heat capacity C_p of a material is a measurable physical quantity equal to the ratio of the heat added to (or removed from) an object to the resulting temperature

change at constant pressure. One way of defining C_p is

$$C_p = \frac{\partial h}{\partial T}\Big|_p \tag{1.1}$$

where ∂h denotes the change in enthalpy of the material experienced within the change in temperature ∂T at constant pressure. During the glass transition the heat capacity of the material, C_p, decreases abruptly (decreases upon cooling, increases upon heating). This effect corresponds to a jamming of several degrees of freedom. Another way of accounting for this change in volume and enthalpy is defined by the thermal expansion coefficient α_p, which can be derived as

$$\alpha_p = \frac{\partial V}{\partial T}\Big|_p \tag{1.2}$$

The change in enthalpy defined by C_p along the glass transition is analogous to the change in volume described by α_p along the process.
Figure 1.6 shows a schematic energy landscape where the crystal phase represents the absolute energy minimum and hence an equilibrated phase. The glass, on the other hand, is a local energy minimum, meaning that although its structure is somewhat stable, it is still flowing at very slow time scales and is more prone to transforming into a stable state upon small perturbations of the system.

1.3 Crystals and the crystallization process

As explained at the beginning of the present chapter, crystalline solids are characterized by long-range order (as portrayed by figure 1.1). Figure 1.6 shows a schematic illustration of an energy landscape. The x-axis represents all configurational coordinates whereas the y-axis stands for the potential energy. It can be observed that the crystalline state corresponds to a stable and absolute minimum of potential energy. Supercooled liquids on the other hand, represent a metastable equilibrium, which would be a local minimum in figure 1.6. Changes in the P-T parameters or the presence of a seed crystal or nucleus of growth can trigger the transition from the supercooled state to the crystalline one. Lacking any such nuclei, the liquid phase can be maintained all the way down to the temperature at which crystal homogeneous nucleation occurs.
Crystals can be formed in several ways: precipitating from a solution, freezing, or

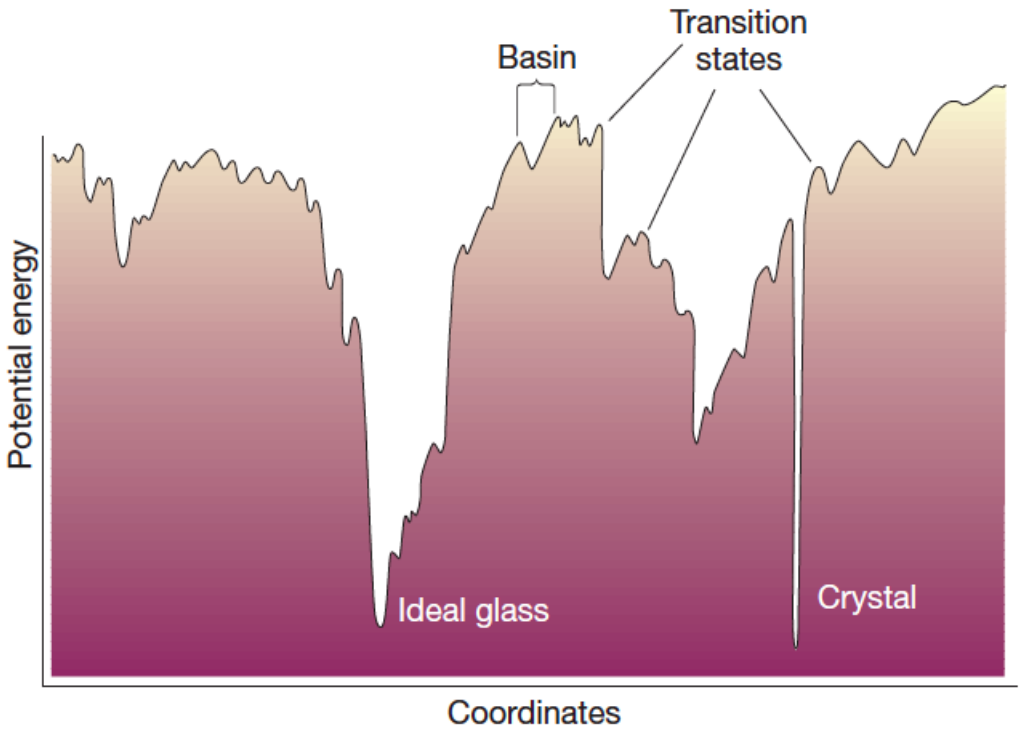

FIGURE 1.6: Schematic illustration of an energy landscape. The x-axis represents all configurational coordinates. Adapted from reference Stillinger, 1995.

more rarely deposition directly from a gas, for example. Attributes of the resulting crystal depend largely on factors such as temperature, air pressure, and in the case of liquid crystals, time of fluid evaporation. Normally, when a liquid is cooled at isobaric conditions at a rate such that vitrification is not possible, the molecules start to pack into a periodic array.

Many minerals and organic molecules crystallize easily in crystalline structures that do not present defects. However, larger biochemical particles, like proteins, are often difficult to crystallize. The ease with which molecules will crystallize strongly depends on the intensity of either atomic forces (in the case of mineral substances), intermolecular forces (organic and biochemical substances) or intramolecular forces (biochemical substances).

1.3.1 Nucleation and growth

Crystallization occurs in two major steps: nucleation and growth. Nucleation is the process by which a crystalline seed arises either from a supercooled liquid or a supersaturated solvent. Figure 1.7 *a* shows a schematic representation of this situation.

The nucleation time is defined as how long an observer has to wait before the new self-assembled structure appears.

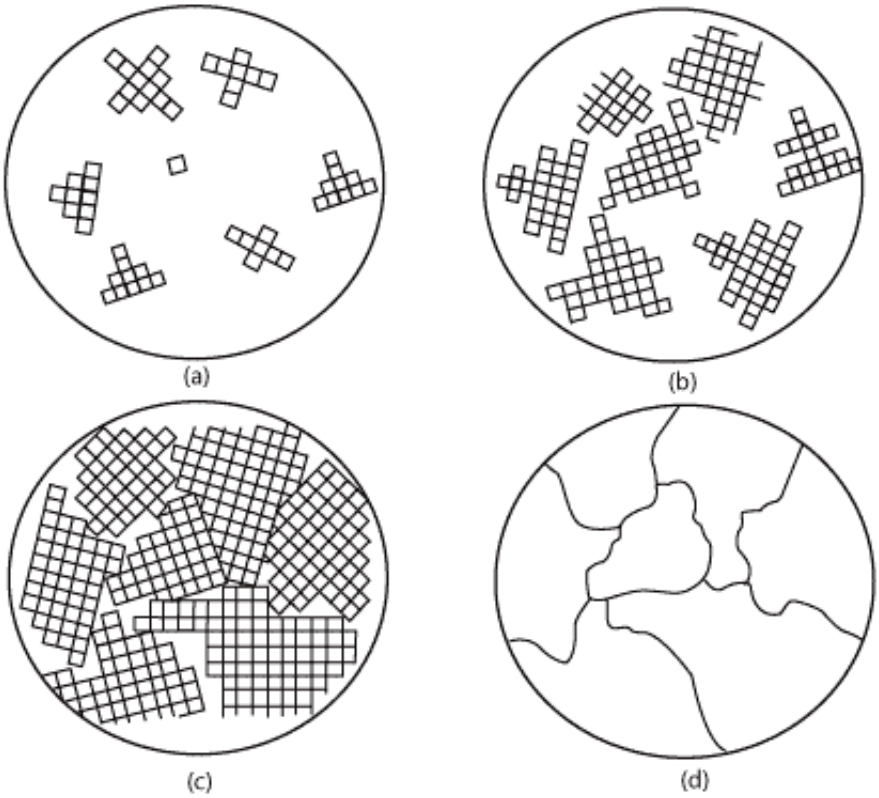

FIGURE 1.7: Schematic figure. a) Nucleation of crystals, b) crystal growth, c) irregular grains form as crystals grow together, d) grain boundaries as seen in a microscope.

As nucleation implies the formation of an initial seed from which the crystal will grow, this process is often found to be very sensitive to impurities in the system. If a material has impurities, these may act as nucleation sites that might trigger nucleation and growth of a crystalline phase, or increase its rate, when suitable thermodynamical conditions are achieved. It can be distinguished between heterogeneous and homogeneous nucleation. Heterogeneous nucleation begins at impurities or surfaces in the system while homogeneous nucleation takes place without the influence of foreign particles, well within the bulk substance.

Crystal growth entails the increase in size of the formed nuclei, as schematized in panel *b* of figure 1.7. As crystalline materials are ordered phases, the crystal growth differs from the condensation of a liquid droplet form vapor phase in that each molecule or ion must fall into the correct place in the crystal lattice. The crystals

increase in size by the progressive addition of atoms to existing crystalline domains (panel *c* of figure 1.7), until the various domains merge together (panel *d* of figure 1.7). The places where different sections of growing crystals overlap, are called the grain boundaries. These boundaries are sometimes large enough to be visible under an ordinary light microscope or even to the unaided eye.
When the entire solid grows from a unique nucleation site and without any impurities it is called a single crystal or monocrystal. On the contrary, when many nucleation sites are present the crystal phase grows forming a polycrystalline sample, where grain boundaries can be found.

1.3.2 The Avrami Law

Several models aiming at describing the crystallization process of materials have been proposed. A relevant one that describes how materials transform from one phase into another under isothermal conditions was proposed by Avrami (Avrami, 1939; Avrami, 1940). The Avrami Law describes the kinetics of crystallization making, in its simplest form, the following assumptions and simplifications (Jena and Chaturvedi, 1992):

- Nucleation occurs randomly and homogeneously over the entire untransformed portion of the material.
- The growth rate does not depend on the extent of transformation.
- Growth occurs at the same rate in all directions.

Frequently, the extent of phase transformation from liquid to crystal follows a characteristic s-shape or sigmoidal profile with respect to time, as portrayed by figure 1.8 *a*. This implies that the formation of an initial nucleating site and the first steps of crystal growth take place at a relatively slow pace. It takes a time t_0 for the substance to form a significant number of nuclei of the new phase and to begin the growth process. After this time, crystallization accelerates and the crystal grows at a very rapid rate. The transformation is rapid as the nuclei grow into particles at the expense of the old phase, while nuclei continue to form in the remaining parent phase. Finally, the transformation rate decelerates when almost all the material has completely transformed. Grain boundaries are more commonly formed at this stage of the process.

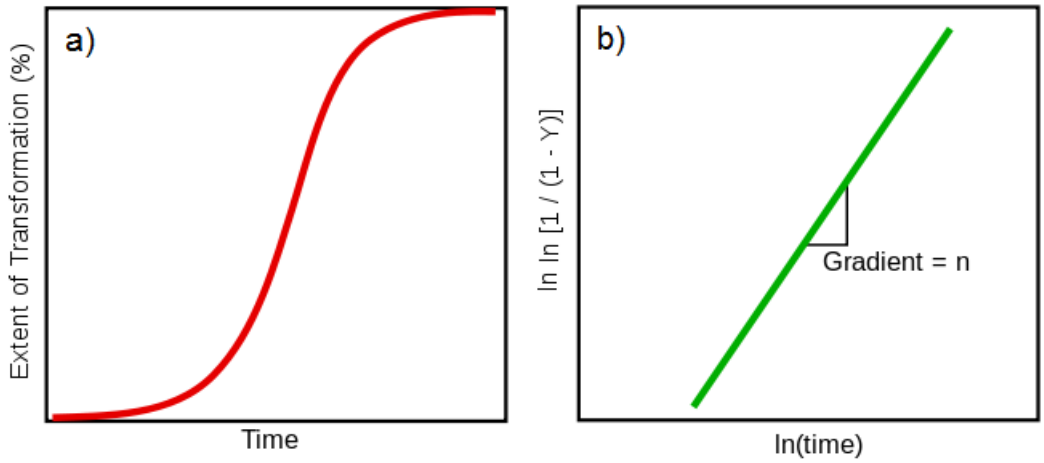

FIGURE 1.8: Schematic figure. a) Typical isothermal transformation plot (top). b) The transformation can be described using the Avrami equation as a plot of ln [ln(1/(1-Y))] vs ln(t) yields a straight line.

The parameter Y is defined as the ratio of the volume of the material that has crystallized V_c, over the total volume V: $Y = V_c/V$. The Avrami Law states that the parameter Y can be expressed as (Avrami, 1939; Avrami, 1940)

$$Y(t) = 1 - exp(-K(t - t_0)^n) \tag{1.3}$$

where K is the temperature-dependent crystallization rate and n is the Avrami exponent. The latter value should be a constant that depends exclusively on the crystalline morphology and crystallization mechanism (Wunderlich, 1976).
The equation 1.3 can be rewritten as

$$Ln(-Ln(1 - Y(t))) = Ln(K) + nLn(t) \tag{1.4}$$

This way, by plotting $Ln(Ln(1/1 - Y))$ vs $Ln(t)$ a straight line is obtained, which allows the determination of the constants n and k. If the transformation follows the Avrami equation, panel b of figure 1.8 is obtained.

1.4 Properties of glass-forming liquids

1.4.1 Relaxation time and viscosity

The viscosity of a material is a macroscopic property that measures how much its particles oppose flow by shear stress or tensile stress. This is to say, it is the property

of a fluid by virtue of which the material offers resistance against the flow. In the case of gases, momentum transfer is the parameter that affects the most the viscosity of the substance. In the case of liquids, viscosity is mainly dependent on intermolecular attraction forces. Higher viscosity of a liquid generally refers to the informal concept of 'thickness', meaning for example that honey has higher viscosity than water (Symon, 1971).

Shear viscosity, or dynamic viscosity η, expresses the resistance of a material to shearing flows, where adjacent layers move parallel to each other with different speeds. This magnitude is particularly relevant for glass forming materials, as it provides an alternative definition of the glass transition temperature, T_g. As previously mentioned, the temperature at which η reaches a magnitude of 10^{13} poise is defined as the glass transition temperature, since this viscosity value identifies glass materials.

Equivalently, the molecular relaxation time τ of a material is defined as the time it takes for its molecules to return from a perturbed state into equilibrium. Within a liquid, the relative position of a molecule with respect to its neighbors varies on a characteristic time τ. The temperature at which it takes 100 s for the molecules to recover their original state ($\tau = 100s$) is also defined as the glass transition temperature T_g. This is to say, the glass is defined as the phase at which the material needs 100 s to relax into its original state after a perturbation, or equivalently, when the viscosity reaches a value of 10^{13} poise.

Another useful parameter to characterize glass forming materials is the shear modulus, or modulus of rigidity, G. It is defined as the ratio of shear stress to the shear strain and is a quantity that measures the stiffness of materials (IUPAC, 2006).

A commonly used model to describe viscoelastic materials was introduced by Maxwell in 1866 which models them as a combination of spring with shear modulus G and dash pot with shear viscosity η, arranged in series. If the material is sheared, stress will arise as the elongation of the spring. Relaxation of the substance takes then place via the viscous flow of the dashpot at high temperatures. This model relates the viscosity η of the material and its characteristic relaxation time τ in the following manner:

$$\tau = \frac{\eta}{G} \tag{1.5}$$

Although this is a very simplified model that cannot predict the behavior of all glass-forming materials it serves as bridge between two very closely related properties, η and τ, that can be used almost equivalently to study the glass transition.

Temperature dependence of the relaxation time: Arrhenius and VFT behavior

When approaching T_g the relaxation time becomes very sensitive to temperature, as illustrated schematically in figure 1.9. Some materials present a dependence of η (and τ) with respect to temperature T that is well described by the Arrhenius functionality (red line in figure 1.9):

$$\eta = \eta_\infty exp[E/k_b T] \tag{1.6}$$

where k_b is the Boltzmann constant, η_∞ is the relaxation rate in the high temperature limit ($\eta_\infty = (2\pi\tau_\infty)^{-1}$), and E is the activation energy per molecule respectively. Silica, for instance, shows this kind of behavior. By plotting these parameters in a $Ln(1/T) - Ln(\eta)$ scale, the activation energy of the transition can be found as the slope of the line divided by k_b.

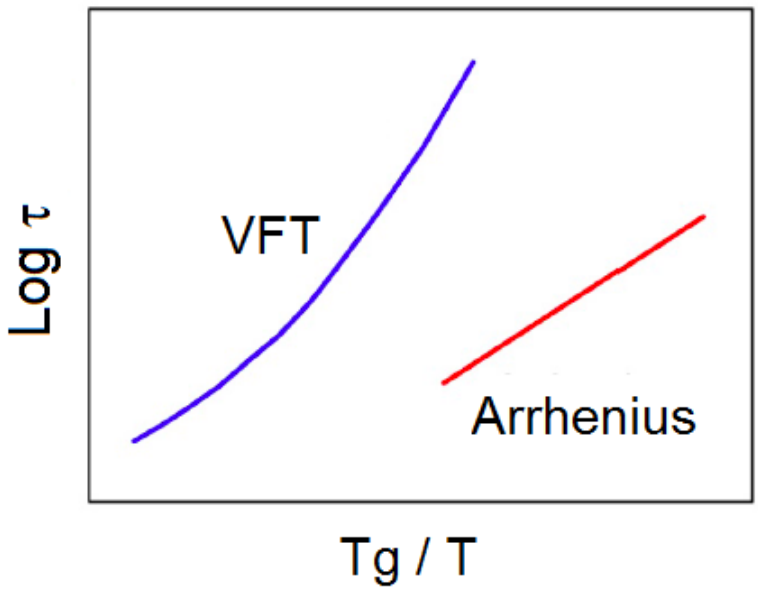

FIGURE 1.9: Tg-scaled Arrhenius and VFT dependence of relaxation time τ. Schematic figure.

Other liquids, such as toluene or chlorobenzene, exhibit an even more pronounced

viscous slow-down close to T_g. This behavior is represented over 2-4 orders of magnitude in η and τ with reasonable accuracy by the Vogel-Tammann-Fulcher (VFT) equation (blue trace in figure 1.9). The mathematical expression of it for relaxation time τ_α is expressed as

$$\tau_\alpha = \tau_0 exp\left(\frac{D \cdot T_{VF}}{T - T_{VF}}\right) \tag{1.7}$$

were the prefactor τ_0, the strength parameter D, and the Vogel - Fulcher temperature T_{VF} are phenomenological constants.
In the case of VFT behavior in figure 1.9 the activation energy of the transition can be found as well as the slope of the line divided by k_b, provided the slope is considered as the upper part of the curve, close to the glass transition temperature, T_g.

The strong and fragile classification

The discovery of the fact that some materials present VFT behavior in their viscosity or relaxation times with respect to temperature while others show Arrhenius type, motivated the classification proposed by Austen Angell between strong and fragile glass formers (Angell, 1988; Angell, 1985b).
A good glass former is one for which the cooling rate needed to avoid crystal formation is low. The extent to which the shear viscosity η (or τ_α equivalently) deviates from Arrhenius behavior is the basis of the distinction between strong and fragile liquids. Strong glass formers show linear Arrhenius behavior on their viscosity and relaxation times. Fragile liquids on the other hand, present marked deviations from this trend and follow the VFT equation (1.7).
Figure 1.10 shows a T_g- scaled Arrhenius representation of liquid viscosities. The clear distinction between strong and fragile glass formers can be observed. Silica (SiO_2), for instance, is the prototypical strong liquid, whereas o-terphenyl (OTP) is the canonical fragile glass-former.

In glass physics the term *fragility* indicates how rapidly the dynamics of a material slow down as it is cooled towards the glass transition. In general, the fragility of a material is measured by calculating its kinetic fragility index, m. This parameter characterizes the slope of the relaxation time (or viscosity) of a material with temperature, as it approaches the glass transition temperature from above. One way of mathematically describing m is the following

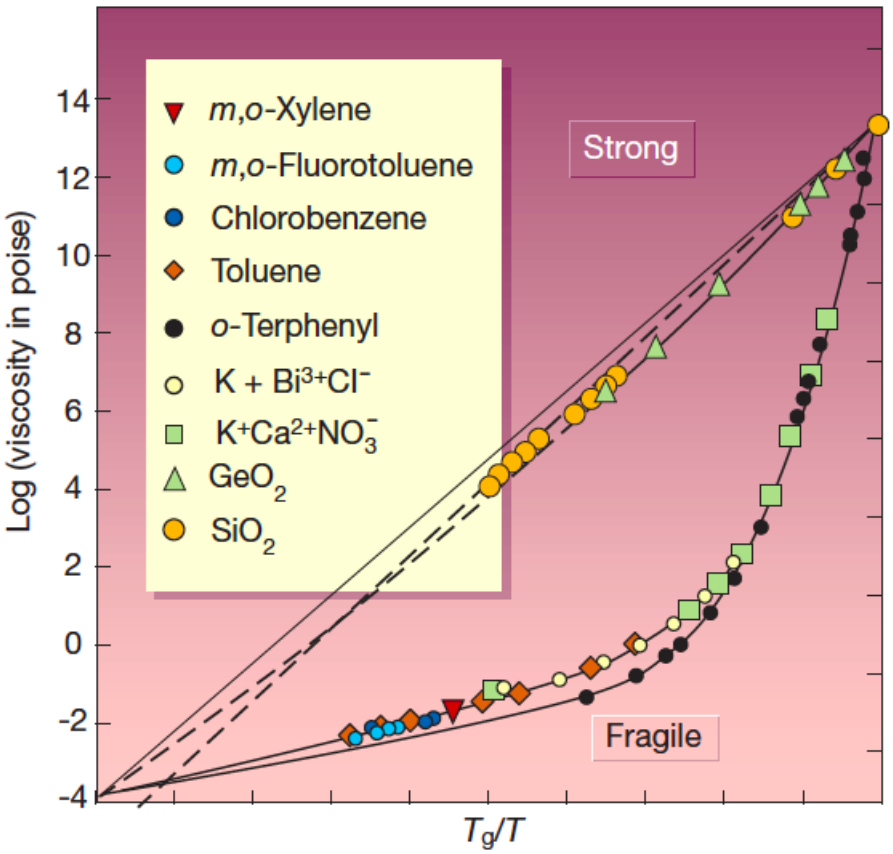

FIGURE 1.10: T_g-scaled Arrhenius representation of liquid viscosities showing Angell's strong-fragile pattern. Strong liquids exhibit approximate linearity (Arrhenius behavior) indicative of a temperature-independent activation energy. Fragile liquids exhibit super-Arrhenius behavior, their effective activation energy increasing as temperature decreases. Figure adapted from Debenedetti and Stillinger, 2001.

$$m = \frac{\partial log(\eta)}{\partial(T_g/T)}\Big|_{T=T_g} \tag{1.8}$$

A fragility m equal to 16 is the upper limit for strong liquids, whereas larger values of m indicate that the liquid is fragile. Only a few glass formers have fragility below 25; most are therefore fragile. The plot shown in figure 1.10 is known as *Angell plot* and the coefficient m of a substance can be derived by calculating the slope of its curve close to the glass transition temperature.

Although there are critics of the practice of using an internal liquid property, namely, a particular viscosity or relaxation time, as the basis for scaling, there really is no satisfactory alternative. The use of a thermodynamic transition point such as the melting point has of course been proposed, but quickly abandoned because of the

tremendous range of viscosities that different substances exhibit at their melting points. No helpful ordering of complex behavior patterns is gained thereby. Indeed, it is only the liquids that have high viscosities at their melting points that can successfully be supercooled to the glassy state (Angell, 2002).

1.4.2 Pressure dependence of the relaxation time

Lowering temperature is not the only way in which the glass transition can take place. As becoming a glass entails a change in specific volume, in many cases by exerting pressure at isothermal conditions into a glass forming liquid, can the glass transition (and of course the corresponding glassy phase) be achieved as well.
The pressure at which the transformation into the glassy material is observed, is named glass transition pressure P_g. While an isobaric change of temperature affects both the volume and the thermal energy of a system, an isothermal change of pressure only affects its volume. This property makes high-pressure measurements a very powerful tool, since it allows the user to be able to tell apart effects that are derived from volume, from those that actually arise from the kinetic/thermal energy of the system.
As mentioned in section 1.4.1, near the glass transition the temperature dependence of the structural relaxation time τ can be described by the phenomenological VFT equation (eq. 1.7). The pressure dependence of τ can be described in an analogous way as (Paluch et al., 1996; Corezzi et al., 1999)

$$\tau_\alpha(T,P) = \tau_0(T,0)exp\left(\frac{CP}{P_0 - P}\right) \tag{1.9}$$

where τ_0 is the relaxation time at ambient pressure, which can be estimated directly from the experimental measurements. C and P_0 are empirical parameters that depend on T only. In general, the parameter C has been found be constant along extensive experiments over a wide range of pressure and temperature (Paluch et al., 1998; Paluch, 2001; Paluch, Roland, and Pawlus, 2002; Paluch, Pawlus, and Roland, 2002; Paluch et al., 2002).
Equation 1.9 is obtained by observing that, from a dynamic point of view, both decreasing the temperature and increasing pressure have the same effect: to slow down the dynamics of the molecular rearrangements. For this reason, dynamically speaking, T and P can be regarded as 'equivalent' thermodynamic variables ($P \leftrightarrow T^{-1}$).

Chapter 2

Dielectrics under the presence of an electric field

2.1 Polarization of dielectric materials

A dielectric (or dielectric material) is an electrical insulator that can be polarized by an applied electric field. This is to say, in the presence of an electric field the bound atomic and/or molecular charges shift only slightly from their average equilibrium positions.

The positive bound charges move in the direction of the electric field and the negative ones against it. At the same time permanent dipoles reorient with the field, causing the polarization of the material and the formation of a macroscopic dipole moment (Jackson, 1998). The polarization $\mathbf{P}$ is defined as the average dipole moment, $\mathbf{p}$, per unit volume and quantifies how the material reacts to an applied electric field. The polarization is usually linearly proportional to the electric field:

$$\mathbf{P} = \chi \epsilon_0 \mathbf{E} \tag{2.1}$$

where χ is the dielectric susceptibility of the material under the influence of a macroscopic electric field $\mathbf{E}$ and ϵ_0 is the permittivity of vacuum (Kremer and Schönals, 2002).

Permanent molecular dipole moments occur when two covalently linked atoms in a molecule have substantially different electronegativity. This is to say, one atom attracts electrons more than the other, hence becoming more negative, while the other atom becomes more positive. This results in a permanent dipole moment of the molecule as a whole which can be oriented by an electrical field.

When a dielectric material with permanent dipoles is subject to an electric field, the

orientation of the molecules lags behind the field. This means when exposed to this kind of electric stimulus, the molecules or units try to reorient their dipole moments accordingly, but have at the same time to overcome the inertia of the molecule as a whole and steric interactions of several molecules at once.

Induced dipole moments on the other hand, appear only when a local electric field $\mathbf{E}_{Loc}$ is present, and are always parallel and proportional to it. In the case of a system composed of permanent or induced molecular dipole moments, the macroscopic polarization $\mathbf{P}$ is related to the microscopic dipole moments $\mathbf{p}_i$ of the individual molecules within a volume V by

$$\mathbf{P} = \frac{1}{V}\Sigma\mathbf{p}_i \tag{2.2}$$

where i counts all dipole moments $\mathbf{p}$ in the volume V (Kremer and Schönals, 2002).

2.1.1 Measuring the Total Polarization

Polarization evidenced through dielectric permittivity

The interaction between the external field and the dielectric material is generally expressed by permittivity ϵ (also know as complex dielectric constant), and is measured by registering the complex dielectric permittivity $\epsilon^*(\omega) = \epsilon'(\omega) - i\epsilon''(\omega)$, where ω denotes the radial frequency with the unit $[rads^{-1}]$. ϵ' and ϵ'' are the real and imaginary components of permittivity, respectively (Kremer and Schönals, 2002).

ϵ' is also identified as relative dielectric constant, and it determines the maximum energy that can be stored in the material. On the other hand, its imaginary counterpart, ϵ'', is called the relative loss factor, as it evaluates the absorption of electrical energy by a dielectric material that is subject to an alternating electric field (Barsoum, 1997; Hench and West, 1990).

The permittivity is often represented by a dimensionless quantity resulting from the ratio of the absolute permittivity, ϵ, and the vacuum permittivity, ϵ_0, called relative permittivity or dielectric constant:

$$\epsilon_r = \frac{\epsilon}{\epsilon_0} \tag{2.3}$$

Relative permittivity is directly related to the electric susceptibility (χ), as

$$\epsilon = \epsilon_r \epsilon_0 = (1 + \chi)\epsilon_0 \tag{2.4}$$

When a dielectric material is perturbed by an electric field, the response of the system can be described by a linear equation. If the perturbation is a time-dependent external electrical field E(t), the response is represented by a time-varying polarization P(t). In Linear Response Theory, the relationship between these quantities is(Böttcher and Bordewijk, 1978):

$$P(t) = P_\infty + \epsilon_0 \int_{-\infty}^{t} \epsilon(t - t') \frac{dE(t')}{dt'} dt' \tag{2.5}$$

where $\epsilon(t)$ is the time dependent dielectric function and P_∞ is the contribution to the polarization of induced dipole moments, that is, the sum of the electronic and ionic polarizations, which are assumed to be established on a very short timescale compared to that of the orientational polarization. $\epsilon(t)$ arises as the response of the material to the outer field.

As an example, figure 2.1 shows the typical response of a dielectric to a step-like change of the applied field (panel (a)). Turning on the field results in a polarization that takes a finite time to reach its equilibrium value (panel (b)).

If the disturbance applied to the dielectric material is a harmonic field, it can be written as $E(t, w) = E_0 exp(-i\omega t)$, where ω is the angular frequency. The expression for the polarization given in Eq. 2.5 can be transformed to

$$P(t, \omega) = \epsilon_0(\epsilon^*(\omega) - 1)E(t, \omega) \tag{2.6}$$

where $\epsilon^*(\omega)$ is the complex dielectric function presented in section 2.1.1: $\epsilon^*(\omega) = \epsilon'(\omega) - i\epsilon''(\omega)$. The real part of this parameter is proportional to the energy stored reversibly in the system. The imaginary part is proportional to the energy dissipated by internal friction. The Fluctuation-Dissipation Theorem states that the response of a system in thermodynamic equilibrium to a small applied force is the same as the effect of a spontaneous fluctuation.

By performing a one-sided Fourier or full imaginary Laplace transformation, the relationship between $\epsilon^*(\omega)$ and $\epsilon(t)$ is obtained as

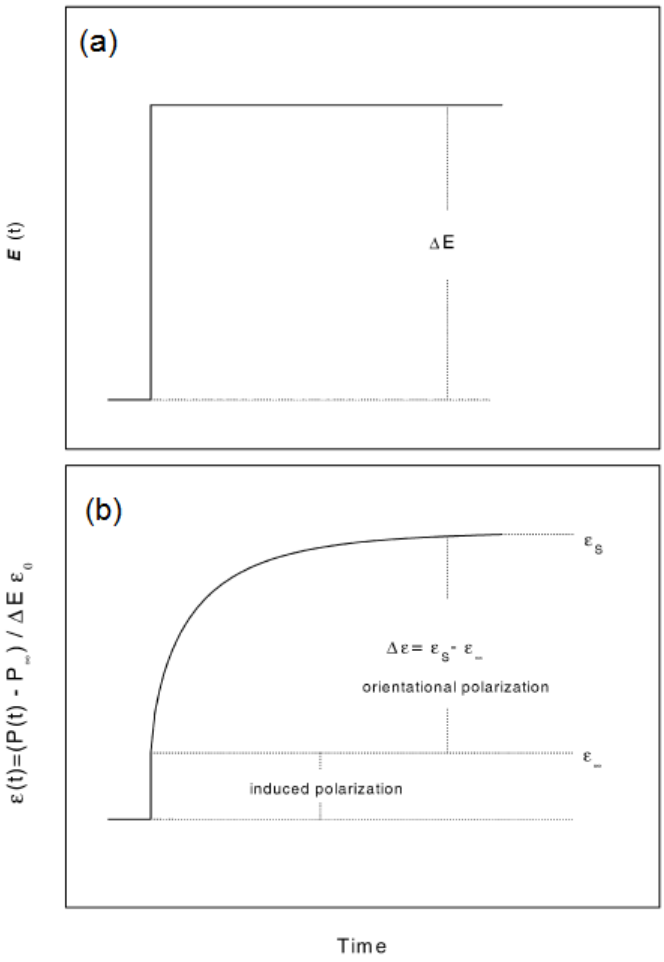

FIGURE 2.1: (a) Schematic relationship of the time dependence of the electric field ΔE (small solid line). (b) Schematic relationship of the time dependence of the relaxation function $\epsilon(t)$ (heavy solid line). The vector sign is omitted for sake of simplicity in the figure. The symbols denote the norm of the corresponding vectors. Changes in permittivity caused by induced and orientational polarization have been indicated with dashed lines. Figure adapted from Kremer and Schönals, 2002.

$$\epsilon^*(\omega) = \epsilon'(\omega) - i\epsilon''(\omega) = \epsilon_\infty - \int_0^\infty \frac{d\epsilon(t)}{dt} exp(-i\omega t)dt \tag{2.7}$$

Hence there is a direct connection between the frequency dependent-permittivity and the response in the time domain.

Like for all one-sided Fourier transformations of a causal function the real and the imaginary part of $\epsilon^*(\omega)$ are related to each other by the Kramers/Kronig relations (Böttcher and Bordewijk, 1978). From an experimental point of view, the fact that both components can be obtained from one another implies, experimentally, they both carry the same information. However, because of the limited frequency range

and conductivity contributions including Maxwell/Wagner or electrode polarization the practical applicability of the Kramers/Kronig transformations is limited for dielectric experiments.

Total Polarization

Generally, the mean value of the total polarization **P** of the system is the sum of all contributions of dipole moments $\mathbf{p}_i$ (both permanent and induced), as evidenced in equation 2.2. Four main types of induced polarization may be observed when a dielectric material is placed in the presence of an electric field: electronic, ionic, space-charge and orientation polarization. All polarization mechanisms contribute to the complex permittivity. The characteristic times, or equivalently the characteristic frequency of the electronic, ionic, orientational and space charge polarization contributions to the dielectric permitivitty under an alternating field are different, as schematically shown in figure 2.2. Figure 2.2 differs from the former figure 2.1 because in 2.2 the electronic and ionic contributions show up explicitly at high frequencies.

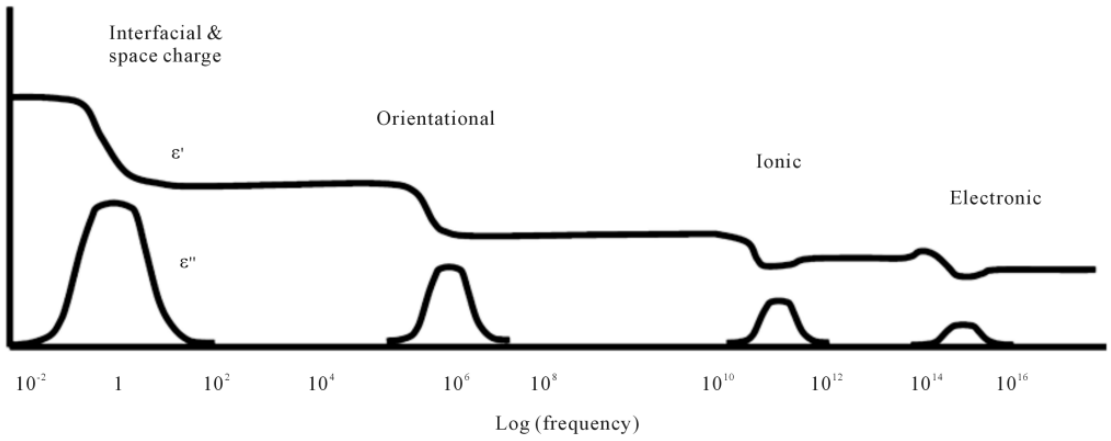

FIGURE 2.2: The frequency dependencies of the electronic, ionic, orientational and space charge polarization contributions to the dielectric permitivitty. Upper and lower traces show schematic behavior of ϵ' and ϵ'' respectively. Figure adapted from Raihan et al., 2015.

Depending on the bonding and structure of the dielectric material, they exhibit at least one of these polarization categories (Badr, Elshaikh, and Ashraf, 2011).

2.1.2 Electronic Polarization

Electronic polarization takes place when the electron cloud of an atom is displaced with respect to its nucleus in the presence of an external field. This creates an atomic/molecular dipole moment that does not depend on temperature, as shown in figure 2.3.

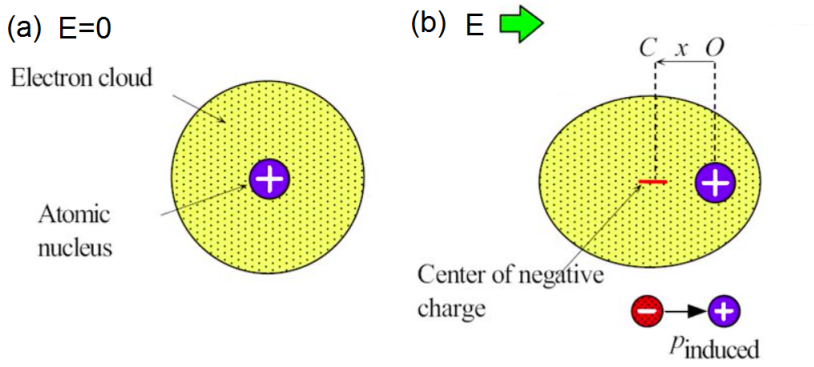

FIGURE 2.3: Electronic polarization of an atom. (a) Neutral atom in the absence of external field. (b) Polarized atom in the presence of field **E**.

Monoatomic gases, for instance, exhibit this kind of polarization. The time in which electronic polarization is established goes from 10^{-16} to 10^{-14} s (Raihan et al., 2015). It is a very rapid process, due to the low mass of the electron.

2.1.3 Ionic Polarization

Ionic polarization is observed in ionic crystals, formed by anions and cations, held together by an ionic bond, as exemplified in figure 2.4 for a binary salt. The total polarization of a given volume, is exactly zero because the charge distribution around a given ion is symmetric (panel (a)). When an external field is applied, the positively and negatively charged ions are pulled in opposite directions, generating a net polarization (panel (b)). The dipole moments between adjacent Na^+Cl^- pairs in field direction are now different (p' and p'') and there is a net dipole moment in a finite volume. This displacement does not dependend on temperature and takes place in a time scale between 10^{-10} and 10^{-12} s (Raihan et al., 2015).

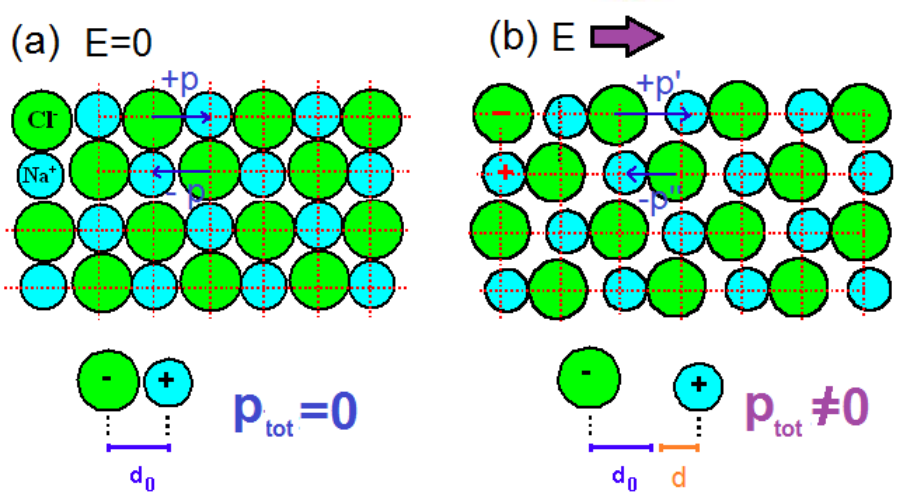

FIGURE 2.4: Ionic polarization. (a) Ionic crystal lattice in the absence of external field. Total polarization **P** is zero. (b) Ionic crystal lattice in the presence of field **E**.Total polarization **P** is non zero.

2.1.4 Space-charge Polarization

Space-charge or interfacial polarization occurs when, because of an external field, there is an accumulation of charge at an interface between two materials or between two heterogeneous regions within a material, as shown in figure 2.5. In panel (a) the dielectric material is placed in between two electrodes, charged with Q^+ and Q^-. When the dielectric field **E** is turned on (panel (b)), charges of the opposite polarity accumulate on the surfaces creating the so-called interfacial polarization. This generally happens when two electrodes are in contact with a dielectric material, as regularly done in Broadband Dielectric Spectroscopy (see Chapter 3). This type of polarization stems not only from bound charges (responsible for the ionic, electronic and orientational polarization), but also from free charges.

There are two different types of space-charge relaxations: those that arise from electrode polarization and those that are caused by internal interfaces. In the latter case, they can be described by the Maxwell-Wagner-Sillar model if the material under study has mesoscopic regions with different permittivity and σ_{DC} (Raihan et al., 2015). If only σ_{DC} varies in different portions of the material, then the Barton-Nakajama-Namikawa (BNN) model suffices to describe the observed response (Garcia-Belmonte, Henn, and Bisquert, 2006).

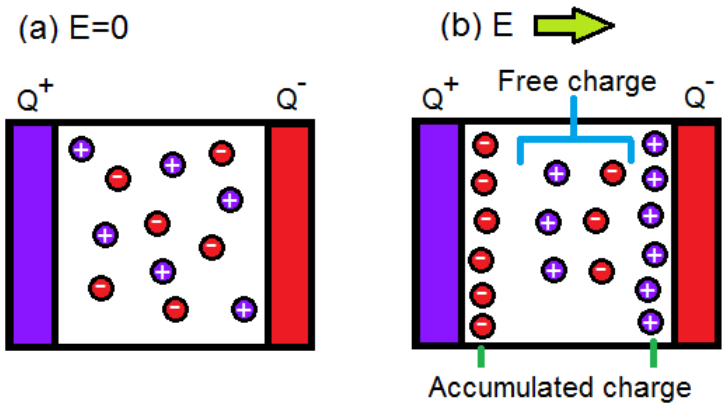

FIGURE 2.5: Interfacial polarization. Dielectric material between two electrodes. (a) No electric field. (b) Accumulated charges because of the effect of **E**.

In both cases the charges in the material tend to separate over a considerable distance, with respect to the atomic and molecular sizes. This build-up of charges generates a large contribution to dielectric loss. The electrode polarization effect is observed at frequencies lower than the σ_{DC} plateau because at these low frequencies the charges have enough time to accumulate on the electrodes before the direction of the field is reverted. In the case of Maxwell-Wagner-Sillars polarization and BNN the effect is observed at frequencies higher than the σ_{DC} plateau. Interfacial polarization is typically dependent on temperature (Raihan et al., 2015; Martin, Yao, and Berg, 2009).

2.1.5 Orientation Polarization

If the atoms or molecules in a material are weakly bonded, they can partially align their dipolar moment to the field (Lunkenheimer et al., 2000; Evain et al., 1993; Griffiths and Haseth, 2007; Skoog, Holler, and Nieman, 1998; Kremer and Schönals, 2002). This process is called orientational polarization and is experimented by molecules that have a permanent dipole moment, like the water molecules shown in figure 2.6. Dipolar molecules in glass formers can rotate usually in a constrained manner, so that they are only partially aligned with the field, in sharp contrast to ionic polarization, where dipole moments are induced by the field and are always parallel to it.

Since the molecules move, the vector **p** is constantly changing its direction. Figure 2.6 shows an instant snapshot of what could be an arrangement of water molecules

or other polar molecules. If one were to add up the contribution of these dipoles with no interacting field, the total dipole moment of the system would be zero, as portrayed in panel (a). When the electric field is turned on (panel (b)) dipoles have a tendency to turn into the field, since this is energetically beneficial. Nevertheless, a perfect orientation with the field is generally not observed, since this polarization effect is at the same time counteracted by random collisions with other dipoles which is boosted by the thermal energy.

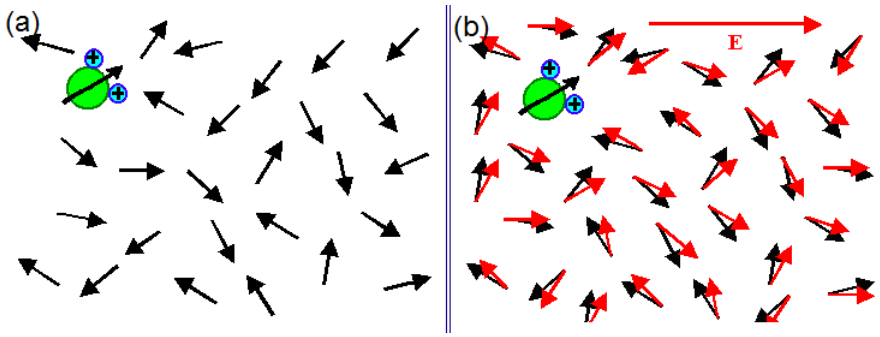

FIGURE 2.6: (a) Water molecules randomly arranged. Black arrows indicate their dipole moments. (b) Water molecules in the presence of electric field **E**. Dipoles tend to shift towards alignment to **E**. Red arrows represent the new orientation of the dipole moments **p**.

When an alternating electric field as $E(t) = E_0 exp(i\omega t)$ of angular frequency $\omega = 2\pi\nu$ is applied onto a dielectric material, two processes take place. Firstly, the redistribution of electric charges that gives way to induced polarization: electronic, ionic or interfacial, as previously explained. Secondly, orientation polarization.

In liquid water, for instance, every molecule is a small dipole. Even though the total charge of the molecule is zero, the nature of the chemical bonds is such that the positive and negative charges do not completely overlap. In fact, in water molecules the H atoms form an angle of around $105°$, creating an asymmetry of charge and hence a permanent electric dipole. The polar nature of water molecules and the fact that the hydrogen nuclei (protons) are quite labile, allows them to bond to each other in groups and is associated, among several other effects, with the high surface tension of water.

While the ionic and electronic polarization is a very rapid process and changes instantaneously with the field, the orientational polarization is much slower. It spans between over a broad frequency range between $10^{-2} - 10^{9}$ s. and is highly dependent on temperature (Raihan et al., 2015).

2.2 Types of Relaxations

2.2.1 The primary α relaxation

Glass-forming materials are characterized by a number of dynamic properties, common to different materials such as glass-forming alcohols, polymers, or metallic glasses (Ediger, Angell, and Nagel, 1996; Angell et al., 2000; Dyre, 2006). In the study of glass forming systems the most important dynamic process is the so-called primary α-relaxation process, which is related to the structural and cooperative rearrangement of the molecules within the material, that arises from the process of orientational polarization. τ_α is directly related with viscosity, and hence to the glass transition. Glassy materials show a $\tau_\alpha = 100s$, which coincides with a viscosity value of 10^{13} poise, as previously stated (see 1.4.1).

The decrease of viscosity experimented by a glass forming material at its glass transition temperature, T_g, is evidenced by a peak in the complex dielectric function called the primary α relaxation, as shown in figure 2.7. When the electric field is applied onto the dielectric material all dipoles align with it. This process takes a slightly different amount of time to different regions or units that may have heterogeneous dielectric properties and mechanic inertia. The time taken for a region to relax in this scenario is known as the dielectric relaxation time, and is identified as τ. These differences in the time response of the different domains cause the relaxation peak to broaden.

If the material shows a maximum in the ϵ'' peak upon a forcing frequency of 10^{-2} Hz., this implies most dipole moments reorient within 100 s., as frequency and period are related by inverse proportionality. As previously stated, glassy materials are defined by an α relaxation time τ_α of 100 s. which implies a viscosity of 10^{13} poise. For this reason, the glass transition temperature can be identified as well, as the temperature at which the maximum of the ϵ'' peak is located at a frequency of $((2\pi\tau_\alpha)^{-1})$.

Since the α relaxation implies an overall tumbling of the material, and this is at the same time closely linked to the kinetic and thermal energy of the molecule, the α relaxation is highly dependent on temperature and shifts to higher frequencies as temperature grows. The higher the thermal energy of a domain, the faster it will reorient in order to be aligned with the forcing electric field.

In general, the relaxation times τ depend mainly on temperature, but other factors

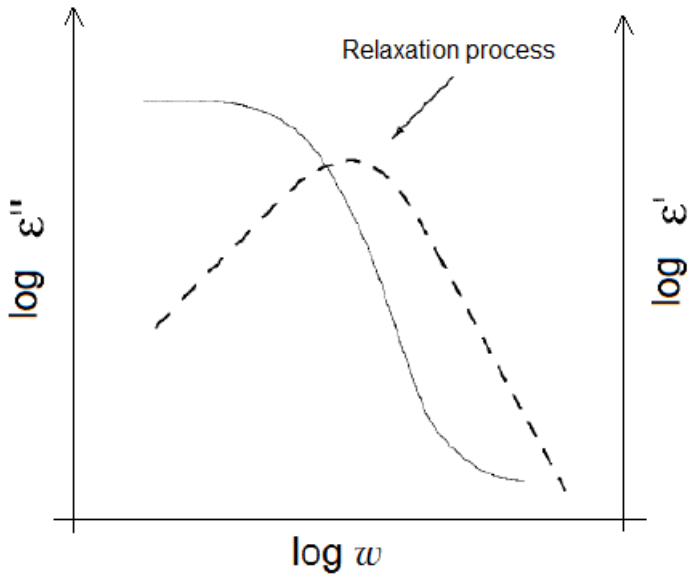

FIGURE 2.7: Schematic representation of the frequency dependence of $\epsilon^*(\omega)$. Dashed and full lines represent the imaginary (ϵ'') and real (ϵ') parts of the permittivity, respectively. Figure adapted from Kremer and Schönals, 2002.

may play a role as well. The structural loss peak (α peak) observed in figure 2.7 differs from a simple Debye relaxation function (see section 3.2.1). The Debye behavior describes a process where the density of relaxation times depends exclusively on thermal agitation. Other fitting functions have been proposed to account for the spreading of the relaxation times produced by other factors, as will be see in Chapter 3.

2.2.2 Dynamic processes beyond the primary α relaxation

Besides the primary α relaxation, other dynamic processes can be generally detected in glassy materials, taking place at time scales significantly shorter. Finding an explanation for the nature of all these phenomena is a prerequisite for the understanding of the glass transition, and it has been a matter of lively debate within the experimental and theoretical community.

The slow β relaxation

Figure 2.8 provides a schematic view of the frequency dependence of the dielectric loss in glass-forming materials near the glass transition temperature T_g. As mentioned in section 2.2.1, the intense peak on the left corresponds to the primary α

relaxation.

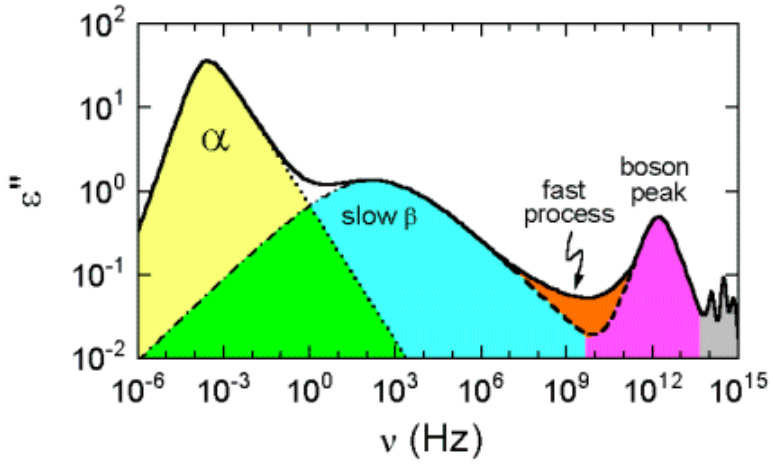

FIGURE 2.8: Schematic view of the frequency dependent dielectric loss in glass-forming materials as observed in extremely broadband measurements (Lunkenheimer et al., 2000). Figure adapted from reference Kremer and Schönals, 2002.

In many glass-forming materials a slow β secondary relaxation shows up, as indicated in light blue in figure 2.8. Depending on temperature, it is mostly observed in the Hz-MHz range, at frequencies beyond that of the α peak. In general, this kind of relaxations show a smaller strength than that of the α peak, symmetric loss profiles and an Arrhenius temperature dependence of their corresponding relaxation time.

In general, slow secondary processes show an Arrhenius temperature dependence of the relaxation time, and wide and symmetric loss profiles frequently described by the Cole-Cole function (see Chapter 3). Slow β processes are frequently adduced to an internal change of the molecular conformation, as would be the movement of a molecular side group. Despite of this, Johari and Goldstein (Johari and Goldstein, 1970; Tarjus, Kivelson, and Kivelson, 1976) have demonstrated that the β relaxation is a rather universal property of glass formers and it shows up even in rigid molecules where internal modes are absent, and in some polymers where there are no rotable side groups (McCrum, Read, and Williams, 1991). For this reason, the term Johari Goldstein β relaxation has been coined to identify these processes related to the glassy state of the material, in order to tell them apart from those due to internal motions. The fact that this relaxation is present even in rigid molecules lacking flexibility, suggested its universal nature in glasses and other disordered materials. On the other hand, some small molecular glass-formers give no indication

that JG relaxation is present, despite numerous investigations using a variety of experimental techniques. These exceptions cast doubt on universality and fundamental importance (Thayyil et al., 2008). However, the microscopic processes behind it are still controversially discussed and there is no accepted physical theory able to explain its origin(Kudlik et al., 1999).

The fast β relaxation

A different type of β relaxation is the fast β relaxation, which is observed in the GHz-THz range. This contribution is generally attributed to the " rattling" movement of a particle in the transient confinement formed by its neighbors Bengtzelius, Götze, and Sjölander, 1984; Leutheuser, 1984; Götze, 1985; Götze and Sjögren, 1992. It is stable on a short time scale and produces the additional contributions indicated as "fast process" in figure 2.8.
It should be noted that the fast β process is not identical with the JG β relaxation.

The boson peak

At frequencies ranging the THz domain a second loss peak shows up, as portrayed by the pink peak in both panels of figure 2.8. This feature is known from neutron and light scattering and is called the boson peak (Petry and Wuttke, 1995; Rössler, Novikov, and Sokolov, 1997). It is a universal feature of glassy materials and although it seems to be linked to the inter-atomic vibrational mode, there are no satisfactory explanations to its origin. Several models have been proposed to explain its existence, as soft potential models (Karpov, Klinger, and Ignatiev, 1983; Buchenau et al., 1992), phonon localization models (Elliott, 1992; Malinovsky, Novikov, and Sokolov, 1987), coupled harmonic oscillators with a distribution of force constant model (Schirmacher, Diezemann, and Ganter, 1998) or the MCT model (Götze and Mayr, 2000). Nevertheless this matter is still being discussed.

2.2.3 The temperature dependence of dielectric relaxations

As all the formerly mentioned dynamic processes show a distinctive dependence with temperature, it is useful to plot the temperature dependence of the characteristic relaxation time of the dielectric loss of each process.

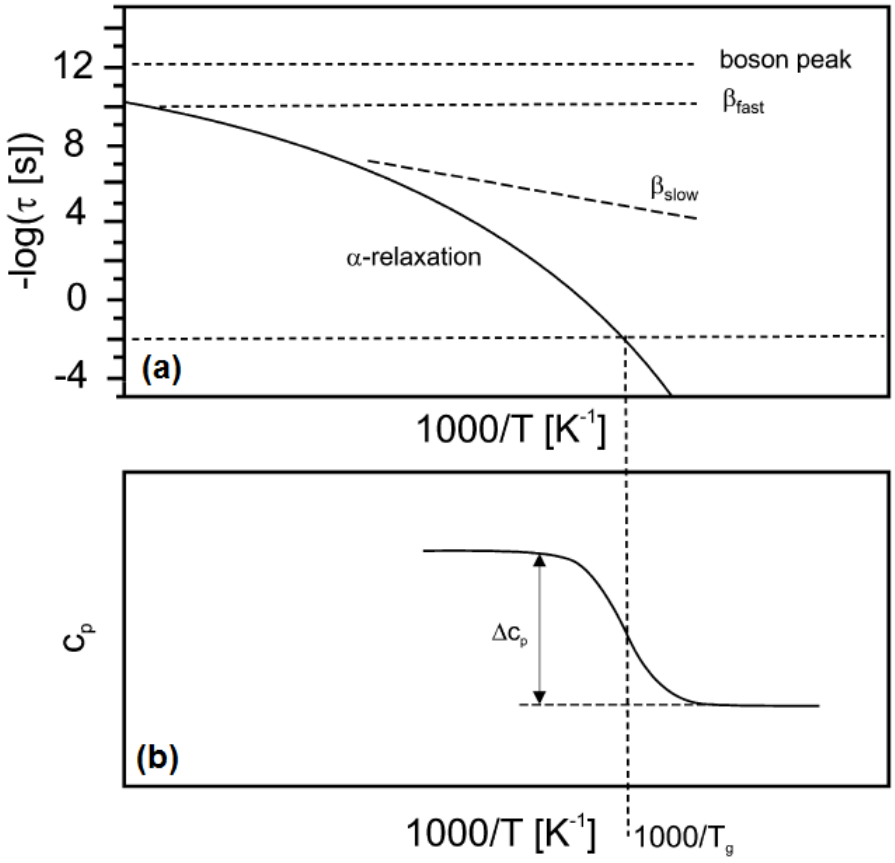

FIGURE 2.9: Schematic view of the dynamics taking place in glass forming liquids. (a) Activation plot (relaxation rate vs inverse temperature) on the loss processes shown in figure 2.8. (b) Calorimetric determination of the glass transition temperature (specific heat at constant pressure) c_p vs inverse temperature for a certain cooling rate. Figure adapted from reference Kremer and Schönals, 2002.

Figure 2.9 (panel (a)) represents a schematic view of the activation plot (relaxation rate vs inverse temperature) on the loss processes shown in figure 2.8. The primary α relaxation marks the collective rearrangement of dipoles and can be used to identify the glass transition temperature T_g. As seen on the previous chapter (section 1.4.1) even though every molecular system has its own signature in the temperature dependence of dynamics, the α relaxation generally shows a VFT behavior with respect to temperature, as can be seen on the curvature of the corresponding trace in figure 2.9. As mentioned on the previous section, when the relaxation time τ is equal to 100 s (i.e $-log(\tau) = -2$) the corresponding temperature is identified as the glass transition temperature, T_g. For this reason, the horizontal dashed line marking this relaxation time intersects the VFT trace of the α relaxation at $T = T_g$. Panel (b) of figure 2.9 schematically shows the calorimetric determination of the

glass transition temperature (specific heat at constant pressure) c_p vs inverse temperature for a certain cooling rate. The dashed line connecting the two panels shows that the relaxation time at which the VFT curve of the α relaxation reaches a value of $-log(\tau) = -2$ identifies T_g, which can be obtained as well and naturally coincides with the midpoint of the calorimetric trace produced by the glass transition of a material when its heat capacity changes.

Secondary processes, on the other hand, show a different temperature dependence as portrayed on the figure (2.9). Whereas the slow β relaxation generally shows an Arrhenius dependence upon temperature, the β fast process and the boson peak do not change with this parameter, and hence are portrayed by the horizontal lines in panel (a).

Understanding the molecular origin of these processes is still a challenge and a matter of lively debate among the scientific community. The Coupling Model is, in this sense, a useful tool to investigate the origin of secondary relaxations.

2.2.4 The Coupling Model as a tool to investigate secondary relaxations

A secondary relaxation may relate either to intramolecular motions involving the displacement of polar side-groups, or else it may be a Johari-Goldstein relaxation. A Johari-Goldstein relaxation is, as mentioned in the previous section, a relaxation that is not internal. This type of process involves the whole molecule and can be interpreted as the single-molecule relaxation, precursor of the cooperative α-relaxation according to the Coupling model (Ngai and Paluch, 2004; Ngai, 1998; Ngai, 2011; Capaccioli et al., 2012a; Ngai, 2003).

The change in Arrhenius temperature dependence of τ_β at T_g is a characteristic feature that indicates the β relaxation is a Johari-Goldstein process (Ngai, 2007). As an example, red dots in figure 2.10 indicate the relaxation times of the β relaxation of the ternidazole drug (TDZ), where it can be observed that at the temperature corresponding to T_g, the behavior of β changes, indicating its Johari-Goldstein nature.

The Coupling Model generally states the relaxation time τ_{CM} of the Johari-Goldstein relaxation should be related to that of the primary process τ_α as:

$$\tau_{CM} = t_c^p \tau_\alpha^{(1-p)} \tag{2.8}$$

Here t_c's typical value is $2 \cdot 10^{-12}$ s and represents a cross-over time determined

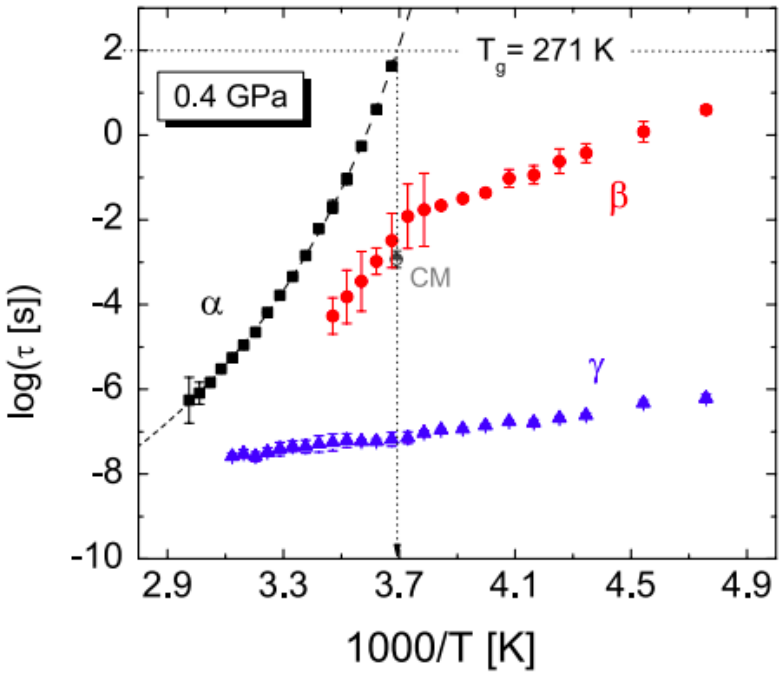

FIGURE 2.10: Arrhenius plot of the relaxation times for all three dynamic processes observed in TDZ in isobaric measurements at 0.4GPa. Error bars are smaller than markers except where they are indicated. The grey half-filled circle with error bar corresponds to the precursor relaxation time near T_g, calculated according to the Coupling Model. Figure adapted from reference Romanini et al., 2017.

by the intermolecular interaction and independent of temperature (Ngai, 2007; Alvarez, Alegria, and Colmenero, 1991). The parameter p is equal to $1 - \beta_{KWW}$, where β_{KWW} is the stretched exponent that describes the shape of the α-relaxation process in the time domain (Kohlrausch, 1854) (see section 3.2.4). Making use of all these parameters and through equation 2.8 the corresponding τ_{CM} can be calculated.

In the example shown in Figure 2.10 gray half filled circles show the relaxation time predicted by the Coupling Model for T_g. As they overlap with the experimental points (red markers) of the β relaxation, the Coupling Model indicates this process can be considered the precursor of the α process, being then a whole-molecule JG process. This means that the other secondary processes (i.e the observed γ process) must be intramolecular, linked to the dynamics of a subpart or side-group of the molecule. The Coupling Model then becomes a powerful tool to identify JG β relaxations and consequently shed some light into the nature of other secondary processes possibly observed.

2.3 Conductivity mechanisms and the dielectric modulus representation

2.3.1 Conductivity

As molecular relaxations are observed in the dielectric response when fixed (bound) charges are present in the studied material, conductivity appears when mobile charge carriers exist. These conductivity contributions lead to a divergence of $\epsilon^{''}$ for low frequecies. Their amplitude can vary greatly for different glass formers, and in some cases it can completely suppress other features in the spectra. Electric conductivity σ gives a measure for the magnitude of the current that flows under the application of an electric field **E**. According to Maxwell's equations the current density **j** satisfies the following relation

$$\mathbf{j} = \sigma^* \mathbf{E} \tag{2.9}$$

The unit most frequently used for σ is Siemens per centimeter (S/cm). σ^* is the complex conductivity given by

$$\sigma^*(\omega) = \sigma^{'}(\omega) + i\sigma^{''}(\omega) = -i\omega\epsilon_0(1-\epsilon^*) = -i\omega\epsilon_0\chi^* \tag{2.10}$$

being $\sigma^{'}(\omega)$ and $\sigma^{''}(\omega)$ the real and imaginary components respectively (Kremer and Schönals, 2002). These components are, at the same time, defined as

$$\sigma^{'}(\omega) = \omega\epsilon_0\epsilon^{''}(\omega) \tag{2.11}$$

and

$$\sigma^{''}(\omega) = \omega\epsilon_0(\epsilon^{'}(\omega) -) \tag{2.12}$$

The real part of conductivity, $\sigma^{'}$, is called σ_{AC} conductivity, and it is the electric conductivity originated from an electric potential dependent of time (or equivalently, frequency). This is to say, the conductivity of a material under the application of an AC current. σ_{DC}, on the other hand, does not depend on time (nor frequency), and is normally determined as the plateau value of $\sigma^{'}$ as a function of frequency ν, as depicted in figure 2.11. The red vertical line indicates the σ_{DC} value of each measurement where it intersects with the $\sigma^{'}$ value.

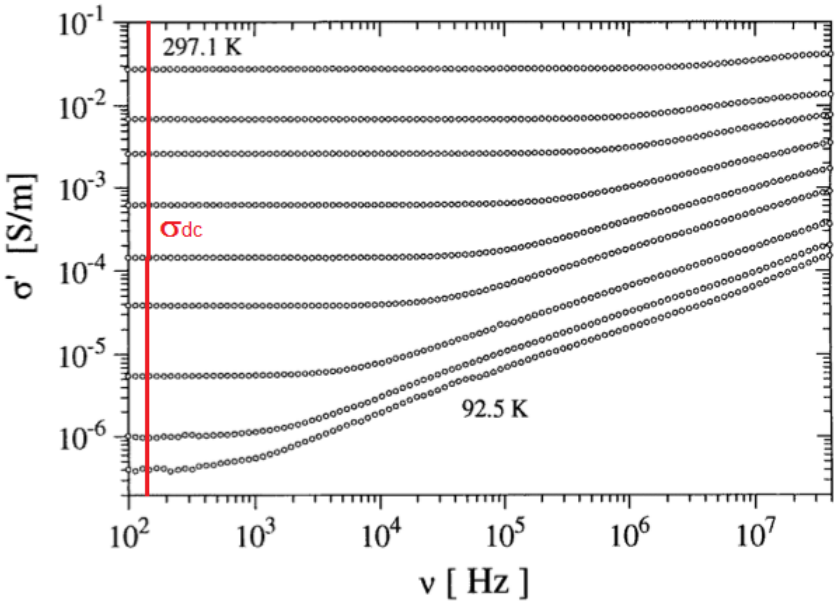

FIGURE 2.11: Real part of the conductivity as a function of frequency of a conjugated polymer (poly(3n-decylpyrrole). The red vertical line indicates the σ_{DC} value of each measurement where it intersects with the $\sigma^{'}$ value.

Materials are generally classified with respect to their capability of conducting current by transport of electronic charge carriers (i.e their electronic σ_{DC}). Those which present a σ_{DC} higher than $10^2 S/cm$ at room temperature are called conductors. The ones lower than $10^{-8} S/cm$ are insulators, and those in the middle are called semiconductors, as represented in figure 2.12. However, one should bare in mind that the majority charge carriers can also be ions or protons.

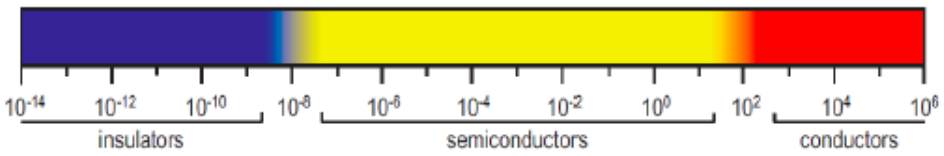

FIGURE 2.12: Division of materials according to their conductivity levels at room temperature. The conductivities are given in S/cm. The division in conductivity levels is only rough; the real distinction between insulators, semiconductors, and conductors/metals is based on the theory of electronic bands.

Transport mechanisms and charge carriers

The conduction mechanisms (or charge transport) in a system depend on the charge carrier. In general, charge carriers may be electrons, ions or protons.

Electrons are generally transported either through band-like conduction or electron/hole hopping. The first mechanism is typical in crystalline solids, which are solid materials whose constituents (such as atoms, molecules, or ions) are arranged in a highly ordered microscopic structure, forming a crystal lattice that extends in all directions. In these systems conduction takes place via the propagation of delocalized electrons through the conduction band, which is depicted in band theory as half-filled or partially filled.

Bloch waves represent the solution to the Schroedinger equation in a periodic potential, and propagate with no resistance in a perfect periodic arrangement with no defects or atoms displaced from their crystallographic position. Vibrations (phonons) cause the atoms to be slightly shifted from their equilibrium sites on the crystalline net. When temperature increases, impurities and phonons in a metal increase as well, blocking and hence diminishing the resulting conductivity of the material. This is to say, conductivity in crystalline solids diminishes with increasing temperature, since lattice vibrations become larger with increasing temperature. Electron or hole hoping, on the other hand, generally occurs in disordered systems and molecular solids where the electronic states are localized in small regions or molecules.

Transport of ions (except for H^+) happens through diffusion or hopping between empty sites. The latter mechanism is typical in solid ionic conductors (for example, ionic solids with a large fraction of missing ions or 'vacancies', or ionic solids made of small cations and large anions) where the thermal energy is enough so as to make the mobile ions dissociate of their site and diffuse across the interstitial sites. Solid-state ionic conductivity is important not only in applications such as batteries for portable devices, rechargeable batteries or fuel cells, but also for electrical insulation, as it worsens the insulating properties of electronic insulators. For example, in SiO_2 glass insulation, the presence of impurities, such as alkali oxides, lowers the material's resistance. Inversely, the presence of heavier-metal oxides such as BaO or PbO increases it. Diffusion of ions, on the other hand, is commonly observed in liquid electrolyte solutions, where all ions are mobile and transport charge, as opposed to solid electrolytes where usually only one type of ion is mobile.

Finally, proton H^+ conductivity takes place either as vehicle mechanism or Grotthus

shuttling, as is the case in systems with extended H-bond networks. The conductivity of proton charge carriers is important in fuel cells and in some hydrogen-bonded liquids and solids such as water, ice and phosphoric acid.

In order to be able to distinguish between the electronic or ionic nature of the transport mechanism in a disordered material, the temperature dependence of σ_{DC} can be of help. As schematically shown in figure 2.13, each type of charge carrier presents a distinct behavior as a function of temperature. A sub-Arrhenius behavior is typical of electronic conduction (as in disordered semiconductors), whereas a super-Arrhenius dependence implies ion charge carriers (as observed in disordered electrolytes). In order to be able to distinguish between ionic and protonic conductivity, a measurement of σ as a function of relative humidity is generally carried out.

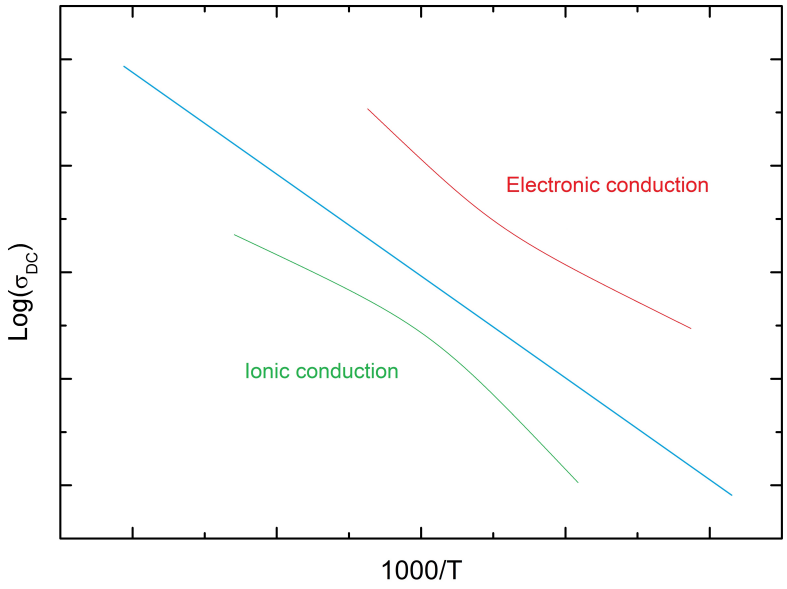

FIGURE 2.13: Schematic dependence of σ_{DC} as a function of temperature, indicating the ionic (green) or electronic (red) nature of the charge carrier producing the conductivity.

Conductivity in disordered systems

In disordered systems without long-range order the charge conduction can be either electronic or ionic in nature. In both cases, however, lattice vibrations provide the energy for hopping transport, and thus, this type of conduction is phonon-assisted and the electric conductivity increases with increasing temperature (Staveren, Brom, and Jongh, 1991). Whether the charge carrier is an electron or an ion, in order to

have a successful charge transport, a simultaneous change in the local polarization is required.

In disordered systems a charge (positive or negative) is surrounded by (bound, i.e., polarization) counter charges. When charge transport takes place, one of these mobile charge carriers jumps (hops) into a new site. If the polarization charge follows the hopping charge, then charge transport will be successful. If it doesn't, then the carrier will eventually jump back to its original location (Kremer and Schönals, 2002). This mutual movement of the charge carrier and the surrounding polarization cloud requires an electrical relaxation time τ_σ. If the frequency of the outer electric field is higher than $1/\tau_\sigma$ its effect on the charge transport averages out, whereas if it is lower, then the relaxation of the polarization cloud will be in phase with the dielectric field. This is to say, when the fluctuations of the electric field are too rapid for the electron cloud to follow (i.e high frequencies) charge transport is not succesfully achieved, since the electron cloud does not have enough time to follow the hopping of the charged particle. On the other hand, when the electric field has a lower frequency, the electron cloud can manage to be in phase with the external input, and so the charged particle can be successfully transfered with its polarization cloud following. At low frequencies of the alternating field, charges have time to accumulate on the electrode surface before the field is altered, resulting in high conductivity. In the high frequency region this time is generally not enough for charges to accumulate and the electron cloud to follow, resulting in a lower conductivity profile.

Space-charge polarization (generally observed as electrode polarization in BDS) frequently gives rise to very high values of the dielectric constant towards low frequencies. Apart from this contribution, the variation of the real part of the conductivity with frequency can be empirically expressed as

$$\sigma^{'}(\omega) = \sigma_{DC} + A\omega^{s} \tag{2.13}$$

which is known as Jonscher's Universal dielectric response (UDR) (Jonscher, 1977). In eq. 2.13 σ_{DC} is the DC conductivity, A is constant for a particular temperature, and s is the dimensionless frequency exponent. The ac response in the high frequency limit is considered in this model as the sum of the individual (not correlated) responses of pairs of sites randomly distributed through the material. This behavior is described by the pair approximation model introduced by Pollak and

Geballe (Pollak and Geballe, 1961). Typically, charge carriers which are free to move through the material (delocalized) are represented by an s value close to zero, while values between 0.5 and 0.8 indicate more density of fixed or nearly fixed charges.
Generally, whereas the imaginary part of permittivity ϵ'' experiences an increase at low frequencies for most materials, the real counter part ϵ' remains constant. In electrolites (ionic conductors) a different thing happens and ϵ' increases at low frequency due to electrode polarization (Kremer and Schönals, 2002).
An empirical rule suggested by *P. Walden* concerning ions in solutions is know as the Walden Rule. It states that the product of the molar conductivity σ_{DC} and the viscosity η is approximately constant (c) for the same ions in different solvents (Walden, 1906):

$$\sigma\nu \approx c \tag{2.14}$$

This relation is generally satisfied in solutions of big ions and of low coordination with unspecific ion-solvent interactions. Given a certain electrolite studied in different solvents, the obtained conductivity for each solvent with respect to its viscosity, should fall within a line of slope 1, as portrayed in figure 2.14.

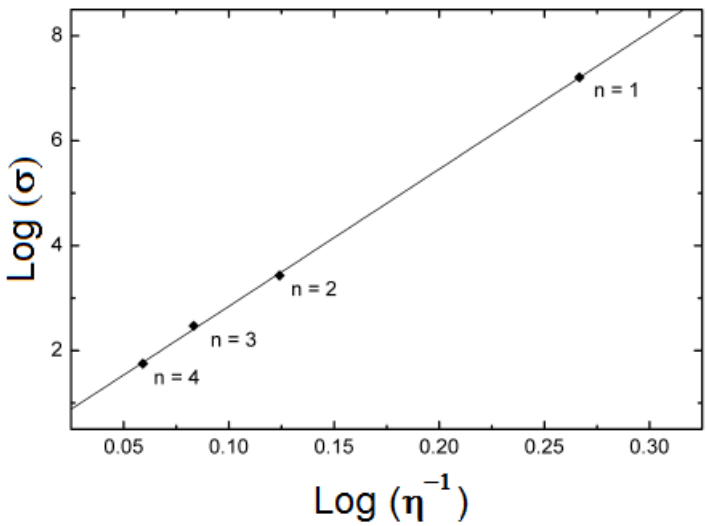

FIGURE 2.14: Conductivity of 1 M $LiAsF_6$ in sulfolane/glyme mixtures (1:1) for glymes (Dimethoxyethane) n=1 to n=4. Figure adapted from reference Walden, 1906.

2.3.2 The modulus

As previously mentioned, conductivity contributions can vary greatly for different glass formers, and in some cases they can completely suppress other features in the spectra. When this is the case, dielectric spectra is generally studied in terms of σ or M'', which represent the conductivity and the dielectric modulus respectively (Kremer and Schönals, 2002).

The complex modulus can be defined as $M^* = 1/\epsilon^*$. As the modulus M can be described either in the frequency or time domain, it is called electric modulus $M(t)$ in the latter, and complex electric modulus ($M^*(\omega) = M'(\omega) + iM''(\omega)$) in the former domain (Kremer and Schönals, 2002). It is related to the relaxation of the electric field within the material (Macedo, Moynihan, and Bose, 1972).

Although the modulus was originally introduced by *Macedo* (Macedo, Moynihan, and Bose, 1972) to study space charge relaxation phenomena, this representation is now widely used to analyze ionic conductivities (Angell, 1990). When a pure conduction process takes place, a relaxation peak is observed in the imaginary component of the modulus (M''), whereas no peak appears in the corresponding plot of the imaginary dielectric permittivity ϵ''. On the other hand, when a dielectric relaxation process takes place, a peak can be observed both in the M^* and ϵ^* representation. This allows one to use both pictures to tell apart localized dielectric relaxation processes from long-range conductivity (Hodge, Ingram, and West, 1976; Gerhardt, 1994).

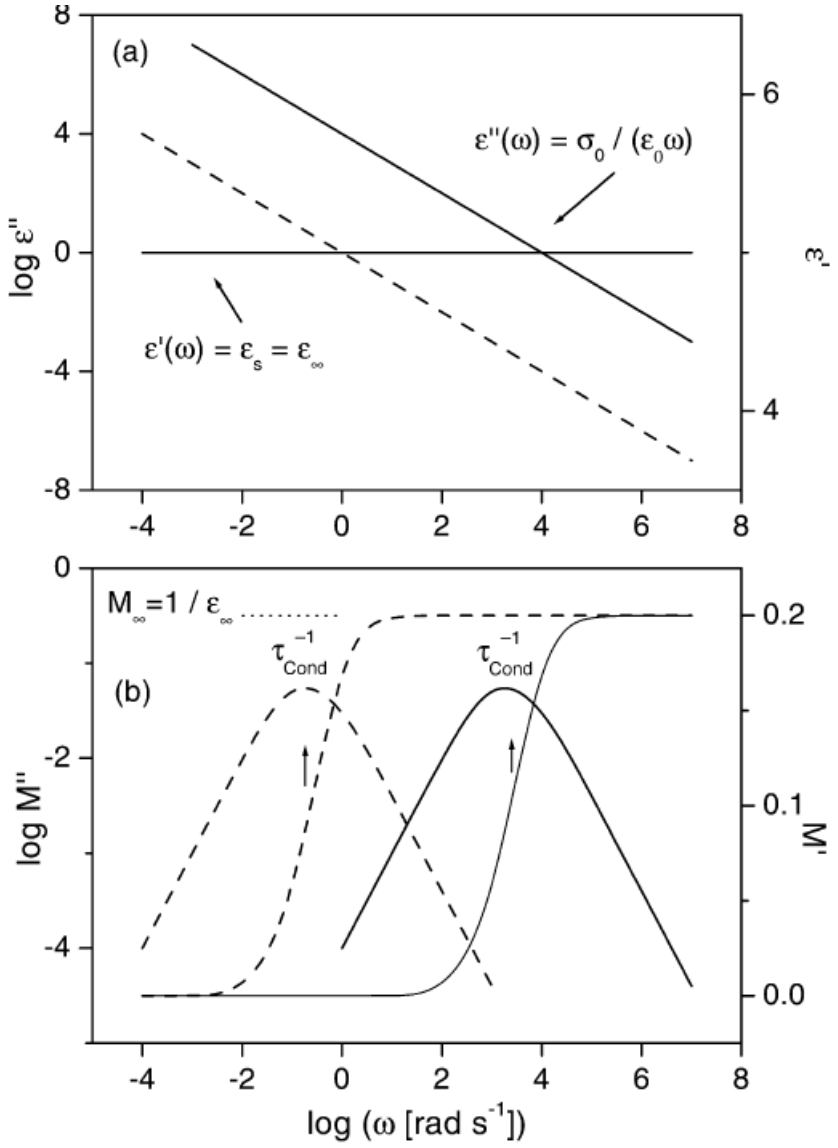

FIGURE 2.15: (a) Theoretical example for a complex dielectric function with a pure ohmic contribution: $\sigma_0/\epsilon_0 = 1$ (dashed line), $\sigma_0/\epsilon_0 = 104$ (solid line), $\epsilon^{'} = 5$. (b) Real part M' and imaginary part M'' of the complex electric modulus according to the complex dielectric function given in (a): $\sigma_0/\epsilon_0 = 1$ (dashed line), $\sigma_0/\epsilon_0 = 104$ (solid line). Figure adapted from Kremer and Schönals, 2002.

Figure 2.15 illustrates a theoretical example for a complex dielectric function with purely ohmic conductivity contribution. When this is the case, no contribution of conductivity arises in the real part of permittivity, whereas $\epsilon^{''}(\omega) = \frac{\sigma_0}{\epsilon_0 \omega}$ increases linearly with decreasing frequency, as observed in panel (a) (σ_0 is the DC conductivity). As previously explained, as this is a pure conduction process, panel (b) shows that while a relaxation peak is observed in the imaginary component of the modulus

M'', no peak appears in the corresponding plot of the imaginary dielectric permittivity ϵ''.

Chapter 3

Experimental Techniques

3.1 Broadband Dielectric Spectroscopy

Dielectric spectroscopy is an experimental technique that measures the dielectric resistance of a medium to the flow of an alternating current (AC) as a function of frequency (Lunkenheimer et al., 2000; Evain et al., 1993; Griffiths and Haseth, 2007; Skoog, Holler, and Nieman, 1998; Kremer and Schönals, 2002). When an external field is applied onto a dielectric material it interacts with its dipole moment causing dielectric polarization. If the dielectric is composed of weakly bonded molecules, those molecules not only become polarized, but also reorient in order for their symmetry axes to align to the field experimenting orientational polarization (Jackson, 1998), as explained in Chapter 2.

This interaction between the external alternating field and the dielectric material is generally expressed by permittivity ϵ, and is measured by registering the complex dielectric permittivity $\epsilon^*(\omega) = \epsilon'(\omega) - i\epsilon''(\omega)$ (Kremer and Schönals, 2002, see **??**). This magnitude can be measured in the broad frequency range from 10^{-6} Hz up to 10^{15} Hz, which makes BDS a truly powerful tool to study processes with very different relaxation times in a wide variety of scientific fields such as fuel cell testing, biomolecular interaction, microstructural characterization and, of course, glassy systems. The slowing down of the alpha relaxation that characterizes a glassy material (see 2.2.1) can be followed during the transition from the liquid to the solid glass state or, equivalently when heating, the alpha's relaxation may be observed throughout the softening produced along the glass to liquid transition (Kremer and Schönals, 2002; Lunkenheimer et al., 2000; Lunkenheimer and Loidl, 2002). Since the study by BDS spans over a wide range of frequencies, measurements are carried out differently depending on the frequency domain.

In this thesis measurements were done in the low frequency range between 10^{-2} Hz and 10^7 Hz, and two different setups where used for temperature and pressure-temperature dependent experiments, respectively. In both apparatus a Novocontrol Alpha Analizer was used, and the sample was placed in a capacitor cell. The measured quantity is the complex impedance $Z^*(\omega)$ of the sample, from which the complex dielectric permittivity ($\epsilon^*(\omega)$) is obtained as:

$$\epsilon^*(\omega) = \frac{1}{i\omega Z^*(\omega) C_0} \tag{3.1}$$

where C_0 is the vacuum capacitance of the capacitor where the sample is placed.

3.1.1 Temperature dependent measurements

Temperature dependent measurements were carried out using an *Alpha-analyzer* parallel plate capacitor, connected to the setup shown in figure 3.1. A *Quatro controller* is connected to the computer and by using the *WinDETA* software provided by the company the data is registered.

The sample cell is placed inside a cryostat and connected to the impedance analyzer. At the same time, a PT 100 temperature sensor is placed inside the cryostat in thermal contact with one of the capacitor plates, in order to register its temperature by connecting it to the Quatro controller. A dewar full of liquid nitrogen is connected to the cryostat and by placing a liquid nitrogen evaporator with a vaporizing module one can inject a flow of liquid nitrogen inside the cryostat. The temperature and pressure inside the dewar are monitored with sensors connected to the controller and both parameters can be regulated by means of a heater and vacuum pump respectively in order to create the desired P-T conditions and extract the desired amount of nitrogen. The gas goes then into a different cavity where its heated to the desired temperature and then injected into the cryostat, in order to thermallize the sample. All sections of the setup are connected to a vacuum pump so as to avoid heat loss. The system can work in the temperature range between 116 K and 773 K with a precision of 0.01 K.
Figure 3.2 shows a picture of the sample holder with a scheme of the capacitor used for liquid samples.

Two stainless steel electrodes in the shape of coaxial cylinders are used to analyze liquid samples. In the case of measurements presenting low dielectric loss, as

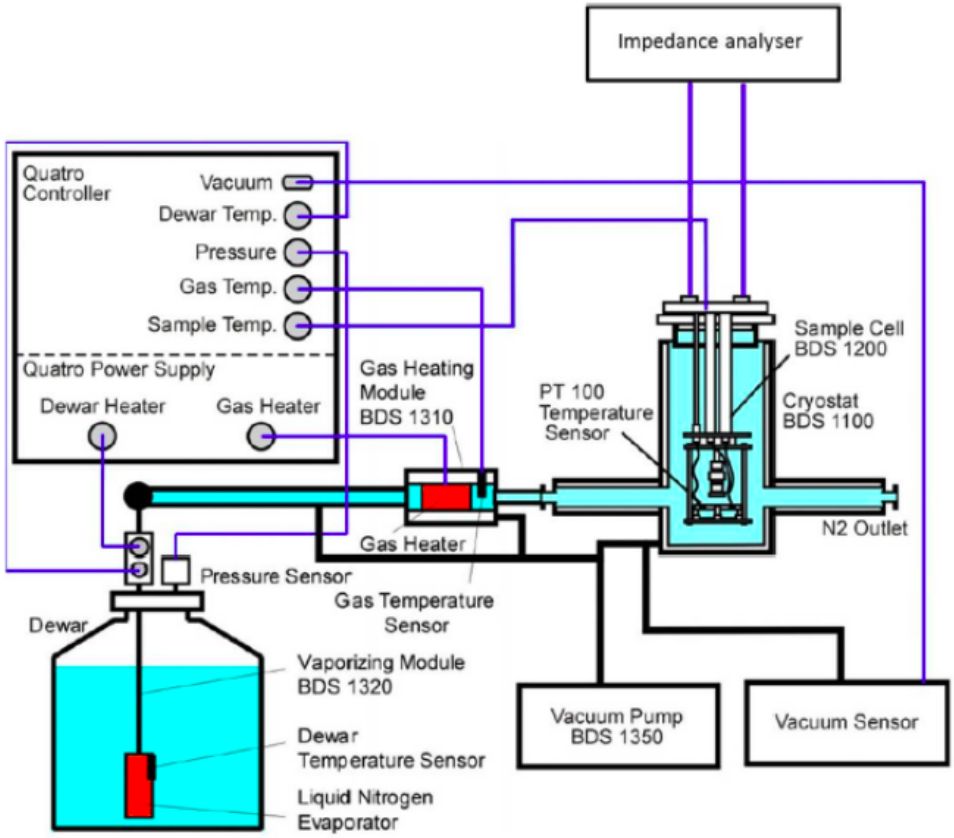

FIGURE 3.1: Experimental setup for temperature broadband dielectric measurements. Image taken from *http://www.novocontrol.de/*.

generally observed at low temperatures, using short distances between electrodes and a large plate area results in a higher strength of the acquired signal. For this reason, glass fiber cylinder spacers of 50 or 100 nm diameter are used to fix the distance between the electrodes. Electrode 1, placed on top, counts with a hole in the middle that allows the surplus liquid to exit the sampling volume, in order to have its height fixed by the diameter of the spacers and not the amount of sample contained between the electrodes. A Teflon ring in placed between the electrodes so as to avoid short-circuits. The capacitor filled with the sample is then placed in the sample holder shown in the photograph, and pressed against plates by tightening the screw on top. The whole line is subsequently inserted inside the cryostat for measuring.

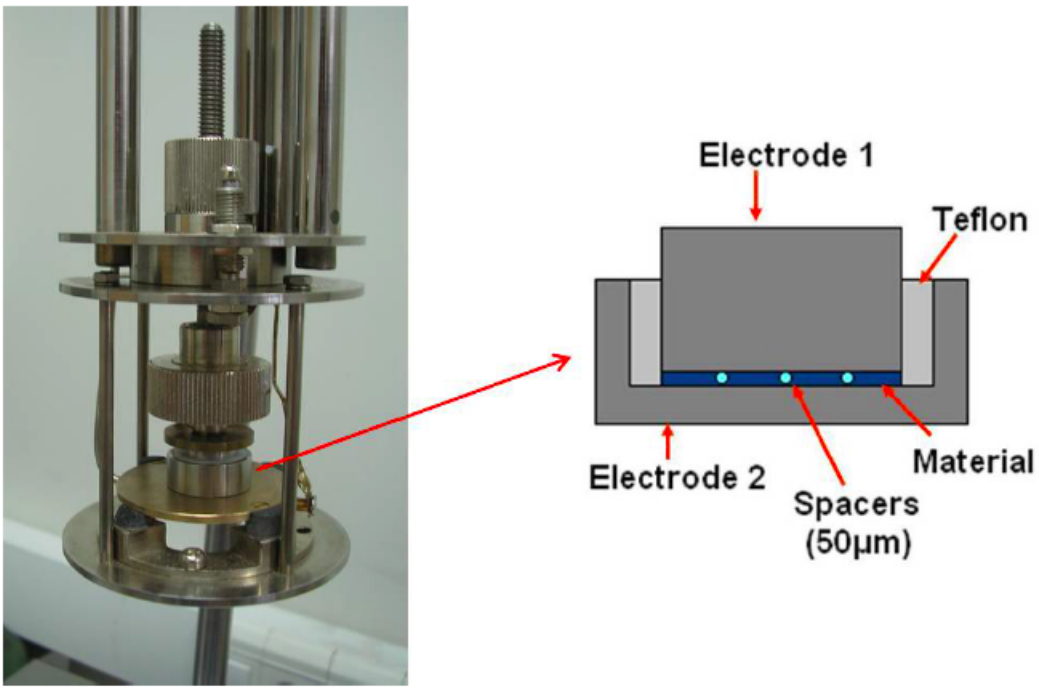

FIGURE 3.2: Picture of the sample holder with a scheme of a transversal cut of the capacitor used for liquid samples.

3.1.2 Pressure-Temperature (PT) dependent measurements

Pressure-Temperature dependent measurements were performed between ambient pressure and 5000 bar and in the (203-393) K range using a *Novocontrol Alpha Analyzer* as the one described in the latter subsection. Figure 3.3 illustrates a scheme of the setup used. A copper beryllium high pressure chamber (by *Unipress*) (1) surrounded with a thermal insulator material is used as container for the stainless steel dielectric cell (2) that is connected to the Novocontrol Alpha Analyzer (3). A thermal bath *(Lauda Proline RP1290)* (4) linked to the chamber by a thermally insulated hose allows the thermal liquid to flow inside the walls of the chamber allowing one to modify its temperature. In order to control this parameter a PT 100 (5) is located inside its wall and connected to a multimeter. The chamber is filled with *Huber* oil, which permits pressure and temperature transference to the sample. The working range of the bath is between 185 and 473 K and is controlled with an accuracy of 0.02 K. A thermocouple (6) is placed inside the chamber and next to the dielectric cell with the purpose of measuring the temperature as close as possible to the sample itself. The high pressure chamber is connected to a pipe line where *Huber* oil stored in a container (7) can be injected or removed by making use of an hydraulic manual

pump (8). Opening or closing the valves delimiting the different sections of the pipe line (9-11). A pressure sensor (12) is positioned at the entrance of the chamber, and by closing valve (10) and opening valve (11) one can measure the pressure at which the dielectric cell is subjected. Pressure can be applied with an accuracy of 0.5%.

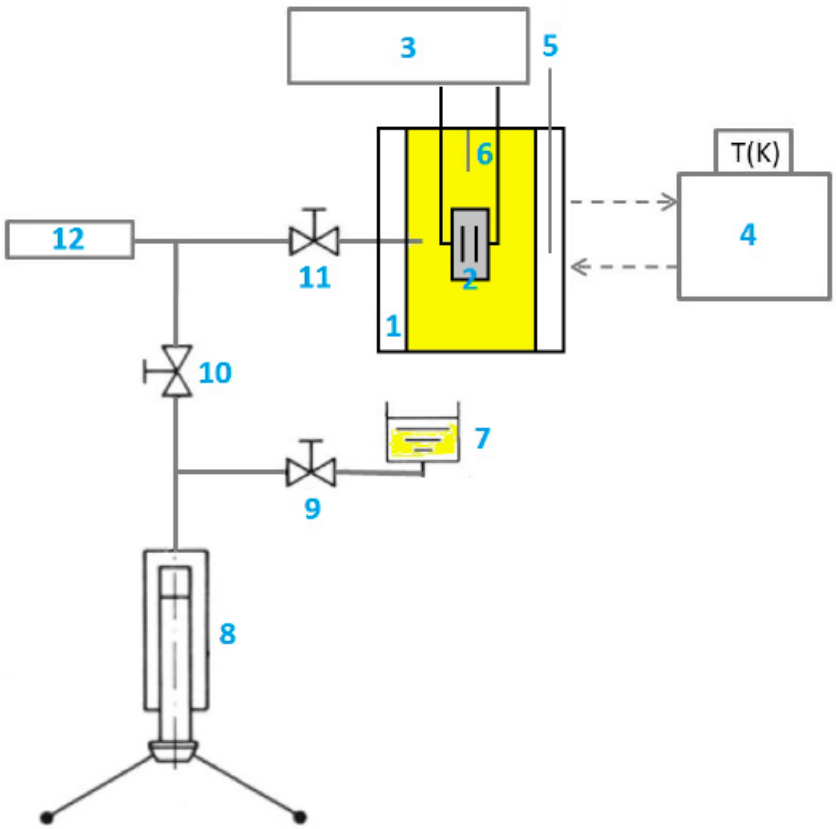

FIGURE 3.3: Experimental setup for the high-pressure dielectric measurements. (1) high pressure chamber, (2) dielectric cell, (3) Novocontrol Alpha Analyzer, (4) Lauda Proline thermal bath, (5) PT100, (6) thermocouple, (7) Huber oil container, (8) hydraulic manual pump, (9-11) valves, (12) pressure sensor.

The dielectric cell consists of two parallel plate cylinders made of stainless steel. A Teflon ring spacer is placed between the electrodes in order to keep constant the distance among them. With the aim of preventing a possible contamination with the pressurizing fluid the capacitor is covered with a Teflon membrane and latex wrapping. Both electrodes are connected with contacts screwed onto them and subsequently connected to the impedance analyzer.

3.2 Phenomenological relaxation models

As explained in Chapter 2 the complex dielectric function $\epsilon^*(\omega)$ and its dependence on frequency of the outer field and temperature originates from different processes. Each of these processes has specific features in the frequency and temperature dependence of the real and imaginary part of the complex dielectric function (Kremer and Schönals, 2002) (see sections 2.2.1 and 2.2.2).

Figure 3.4 shows a schematic representation of the frequency dependence of $\epsilon^*(\omega)$, where the imaginary (ϵ'') and real (ϵ') parts of the permittivity are plotted with dashed and full lines respectively. In general, relaxation processes portray a step-like decrease of (ϵ') accompanied by a peak in (ϵ'') with increasing frequency ω. At low frequency, the imaginary part of the permittivity (loss spectrum) shows a background proportional to inverse frequency (slope -1 in fig 3.4), that arises from electrical conductivity processes (see 2.3.1).

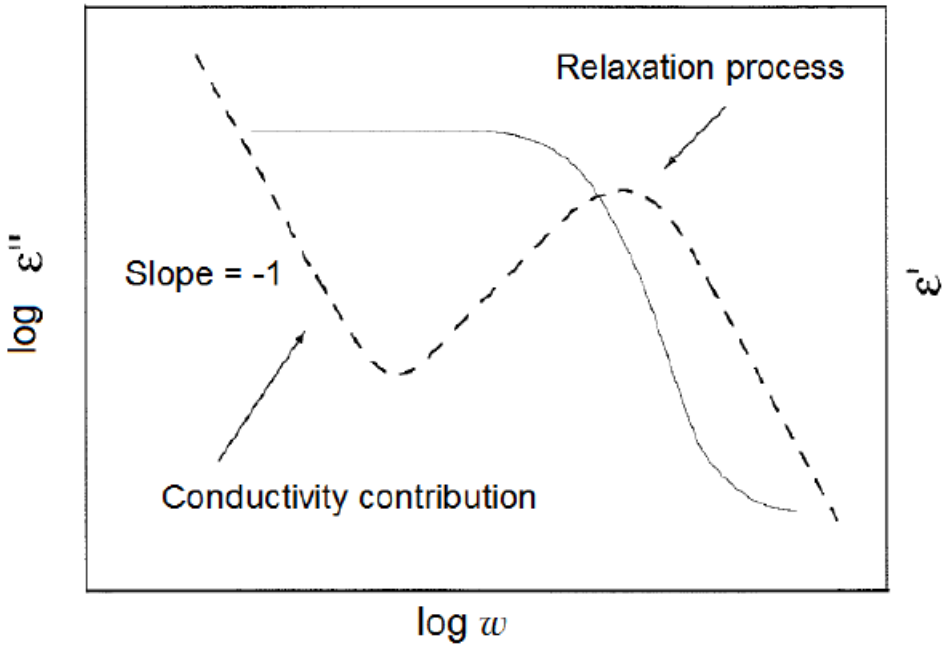

FIGURE 3.4: Schematic representation of the frequency dependence of $\epsilon^*(\omega)$. Dashed and full lines represent the imaginary (ϵ'') and real (ϵ') parts of the permittivity, respectively. Figure adapted from Kremer and Schönals, 2002.

The information about the dipolar dynamics governing the sample under study can then be extracted from the loss peak of the dielectric measurement by means of fitting different models. Since the extent of the interactions taking place between the dipoles of the test substance modify the shape of the ϵ'' peak, the models used have

to be carefully chosen so as to describe and fit the observed behavior of the loss peak. The functions and models used along the analysis of the dielectric spectra shown in this thesis will be discussed in the following subsections.

3.2.1 The Debye model

Relaxation processes due to rotational fluctuations of molecular dipoles analyzed by dielectric spectroscopy provide important information about the dynamics of a molecular ensemble, since these processes are related to the dynamics of characteristic parts of a molecule (functional groups, etc.) or to the molecule as a whole. When the frequency of the applied outer electric field coincides with the reorientational times τ of molecular dipoles, the dielectric loss shows a characteristic peak, as can be seen in figure 3.5. The frequency of the applied field at which the maximal loss is observed is shown as ν_p. This parameter is related to the relaxation time of the fluctuating dipoles, τ_p, by $\tau_p = 1/\omega_p$ where $\omega_p = 2\pi\nu_p$. The distribution of relaxation times for the material under study can be consequently obtained by analyzing the shape of the dielectric loss peak. At the same time, this behavior in the imaginary part of $\epsilon^*(\omega)$ is accompanied by a step-like decrease in the real component, with increasing frequency ω, as shown in figure 3.5. The maximum intensity of the real permitivitty (i.e $\lim_{\omega\tau\ll 1}\epsilon'(\omega)$) is denoted by ϵ_s, whereas its minimum value (i.e $\lim_{\omega\tau\gg 1}\epsilon'(\omega)$) is indicated as ϵ_∞. The strength $\Delta\epsilon$, can be determined either as the area under the dielectric loss peak or as the height of the $\epsilon'(\omega)$ step, since both magnitudes are interrelated by the Kramers/Kronig relations (Bobrov, Trigger, and Heijstand P.P.J.M. Schram, 2010). The relative amount of dipoles contributing to the dielectric relaxation can be determined by looking at its strength.

In 1929, Debye proposed a simple way to calculate the time dependence of the dielectric behaviour by assuming the fluctuation in polarization (P) is proportional to its actual value (Debye, 1929). This translates into the following first order differential equation

$$\frac{d\mathbf{P}(t)}{dt} = \frac{-\mathbf{P}(t)}{\tau_p} \tag{3.2}$$

Solving of equation 3.2 leads to the correlation function $\Phi(\tau)$ for polarization between the parameters t and the relaxation time of the fluctuating dipoles, τ_p

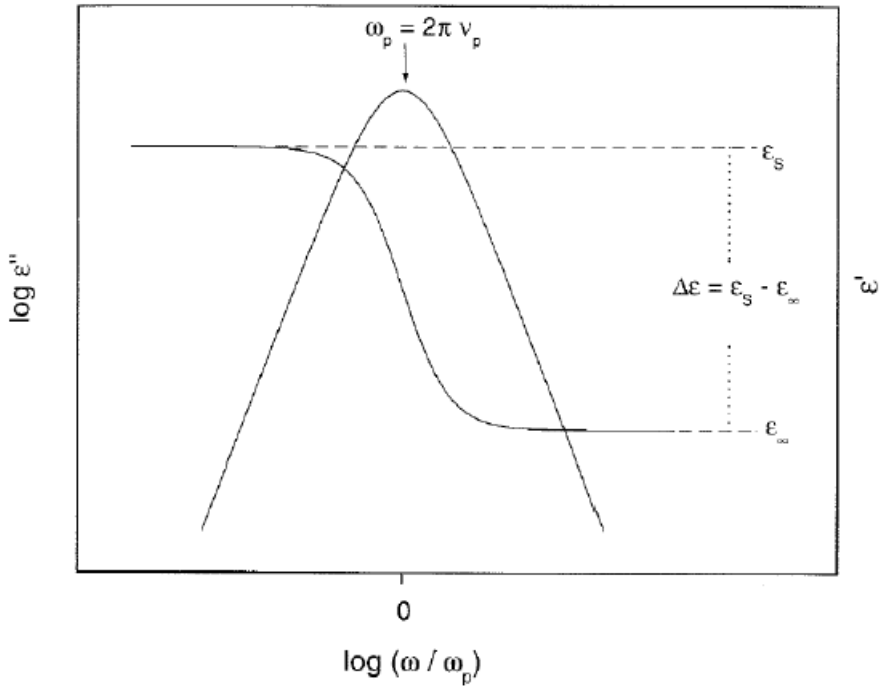

FIGURE 3.5: Real ϵ' and imaginary part ϵ'' of the complex dielectric function vs normalized frequency for a Debye relaxation process. Figure adapted from Kremer and Schönals, 2002.

$$\Phi(\tau) = exp(\frac{-t}{\tau_p}) \tag{3.3}$$

This solution is valid only under the simultaneous conditions of having noninteracting dipoles that relax at only one characteristic time (τ_p) and that equilibrium has to be reached by means of solely one type of process.
The Debye function for the frequency dependence of the complex dielectric function is given by

$$\epsilon_D(\omega) = \epsilon_\infty + \frac{\Delta\epsilon}{1 + i\omega\tau_p} \tag{3.4}$$

The mathematical expressions of its real and imaginary components are given later on in table 3.1). The loss peak obtained by a Debye model is symmetric, with a half width ω_D of 1.14 decades, as shown in figure 3.5. In most experimental cases, as happens in glass-forming liquids, the full width of measured loss peaks is much broader than that predicted by this model, while their shape is many times asymmetrical with a high frequency tail. This type of behaviour is called non-Debye or non-ideal. Some important empirical model functions generalized from the Debye

model have been developed and tested to describe this kind of dielectric response. In the following subsections some of them will be described.

3.2.2 The Cole-Cole and Cole-Davidson function

The Cole-Cole function is used for describing processes that show a broader distribution than that described by the Debye model, as evidenced by the red traces in figure 3.6). This kind of behavior is frequently observed in polymer materials.

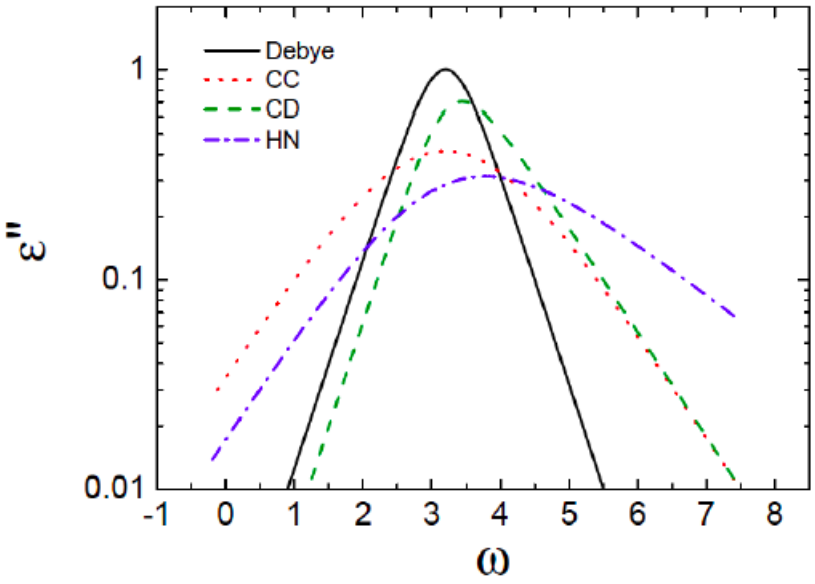

FIGURE 3.6: Immaginary part of the dielectric permittivity for Debye (full black line), Cole-Cole (dotted red trace), Cole-Davidson (dashed green trace) and Havriliak-Negami (dash dotted blue trace) functions. Figure adapted from Kremer and Schönals, 2002.

The mathematical expression of the Cole-Cole function goes as follows (Cole and Cole, 1941):

$$\epsilon_{CC}(\omega) = \epsilon_\infty + \frac{\Delta\epsilon}{1 + (i\omega\tau_{CC})^\alpha} \tag{3.5}$$

where τ_{CC} is the relaxation time linked to the frequency of maximal dielectric loss as $\tau_{CC} = \frac{1}{\omega_p}$. The parameter α lies in the interval $(0;1]$ and produces a symmetric broadening of the peak. The smaller α is, the broader the resulting peak. For $\alpha = 1$ the Debye function is re-obtained. Table 3.1 shows the real and imaginary components of the Cole-Cole function.

It is many times the case, as happens in liquids or low-molecular glass-forming materials, that the dielectric loss peak shows an asymmetrical broadening. This behavior can be described by using the Cole-Davidson function, which introduces the parameter β, a new broadening coefficient. The mathematical expression of the Cole-Davidson function is (Davidson and Cole, 1950; Davidson and Cole, 1951)

$$\epsilon_{CD}(\omega) = \epsilon_\infty + \frac{\Delta\epsilon}{1 + (i\omega\tau_{CD})^\beta} \tag{3.6}$$

where $\beta \in (0;1]$ and τ_{CD} is the relaxation time. As seen in the green dashed trace of figure 3.6) the Cole-Davidson function shows asymmetrical broadening of its complex part, with respect to the Debye function: the low frequency side is broadened following a power law proportional to ω, whereas the high frequency side is proportional to $\omega^{-\beta}$. When $\beta = 1$ the Debye function is reobtained. At the same time, there is a shift on the frequency of the maximum dielectric loss, which is located at

$$\omega_{max} = \frac{1}{\tau_{CD}} tan\left(\frac{\pi}{2\beta + 2}\right) \tag{3.7}$$

The Cole-Davidson function is illustrated with the dashed green line in figure 3.6) and its real and complex parts are specified in table 3.1.

3.2.3 The Havriliak - Negami function

A more general distribution function that includes the previously mentioned symmetric and asymmetric broadenings from Debye behaviour, results from the combination of the Cole-Cole and Cole-Davidson functions. This function was formulated by Havriliak and Negami and can be stated as

$$\epsilon_{HN}(\omega) = \epsilon_\infty + \frac{\Delta\epsilon}{[1 + (i\omega\tau_{HN})^\alpha]^\beta} \tag{3.8}$$

with the same domains for α and β as previously stated. When $\beta = 1$ one recovers the Cole-Cole function, for $\alpha = 1$ the Cole-Davidson expression is obtained, and if both conditions are satisfied simultaneously, then the Debye behaviour is reobtained. As happens with the Cole-Davidson function, the frequency of maximal dielectric loss is shifted with respect to the Debye case. It position depends on the

shape parameters, α and β, in the following manner (Havriliak and Negami, 1966; Havriliak and Negami, 1967):

$$\omega_{max} = \frac{1}{\tau_{HN}} \left(sin\left(\frac{\alpha\pi}{2+2\beta} \right) \right)^{1/\alpha} \left(sin\left(\frac{\alpha\beta\pi}{2+2\beta} \right) \right)^{-1/\alpha} \tag{3.9}$$

The function's behavior can be observed in the dash-dotted blue line in figure 3.6). Its real and imaginary components are specified in table 3.1.

	ϵ^*	Real part (ϵ')	Imaginary part (ϵ'')
D	$\epsilon_\infty + \frac{\Delta\epsilon}{1+i\omega\tau_D}$	$\epsilon_\infty + \frac{\Delta\epsilon}{1+(\omega\tau_D)^2}$	$\frac{\Delta\epsilon\omega\tau_D}{1+(\omega\tau_D)^2}$
CC	$\epsilon_\infty + \frac{\Delta\epsilon}{1+(i\omega\tau_{CC})^\alpha}$	$\epsilon_\infty + \frac{\Delta\epsilon(1+\omega\tau_{CC})^\alpha cos(\alpha\pi/2))}{1+2(\omega\tau_{CC})^\alpha cos(\alpha\pi/2)(\omega\tau_{CC})^{2\alpha}}$	$\frac{\Delta\epsilon(\omega\tau_{CC})^\alpha sin(\alpha\pi/2))}{1+2(\omega\tau_{CC})^\alpha cos(\alpha\pi/2)(\omega\tau_{CC})^{2\alpha}}$
CD (*)	$\epsilon_\infty + \frac{\Delta\epsilon}{(1+i\omega\tau_{CD})^\beta}$	$\epsilon_\infty + \Delta\epsilon cos^\beta(\phi)cos(\beta\phi)$	$\Delta\epsilon cos^\beta(\phi)sin(\beta\phi)$
HN	$\epsilon_\infty + \frac{\Delta\epsilon}{[1+(i\omega\tau_{HN})^\alpha]^\beta}$	$\epsilon_\infty + \Delta\epsilon[1 + 2(\omega\tau_{HN})^\alpha cos(\frac{\alpha\pi}{2}) + (\omega\tau_{HN})^{2\alpha}]^{-\beta/2} cos[\beta arctan(\frac{sin(\alpha\pi/2)}{(\omega\tau_{HN})^{-\alpha}+cos(\beta\pi/2)})]$	$\Delta\epsilon[1 + 2(\omega\tau_{HN})^\alpha cos(\frac{\alpha\pi}{2}) + (\omega\tau_{HN})^{2\alpha}]^{-\beta/2} sin[\beta arctan(\frac{sin(\alpha\pi/2)}{(\omega\tau_{HN})^{-\alpha}+cos(\beta\pi/2)})]$

TABLE 3.1: Compilation of the different model functions described in this section. (*) In this case, $tan(\phi) = \omega\tau_{CD}$.

The Havriliak-Negami (HN) relaxation was firstly used to describe the dielectric relaxation of some polymers (Havriliak and Negami, 1967), but it is now widely used along a scope of several glass forming materials. It is then sufficient with a set of four parameters to describe a dielectric relaxation process. If more than one process takes place in the material simultaneously, a set of HN functions may be used to describe its dielectric behavior. In the case where the different relaxation regions are independent, the final dielectric response is described by the addition of each of the components.

3.2.4 The Kohlrausch - Williams - Watts function

In many areas of physics, in particular when studying disordered systems, It is often the case that a non-Debye relaxation behavior in the time domain can be described by the empirical Kohlraush/Williams/Watts (KWW) function. Its mathematical expression is obtained by inserting a fractional power law into the exponential function (Kohlrausch, 1847; Williams and Watts, 1970). This results in the following dependence of permittivity in the time domain:

$$\epsilon_{KWW}(t) = \epsilon_\infty + \Delta\epsilon[1 - exp(-\frac{t}{\tau_{KWW}})^{\beta_{KWW}}] \tag{3.10}$$

where β_{KWW} is the so-called stretching exponent, which lies in the (0:1] domain and τ_{KWW} is the corresponding relaxation time. In contrast with a basic exponential decay (β_{KWW}=1), the stretched exponential parameter leads to an asymmetric broadening of $\epsilon(t)$ at short times (i.e high frequencies). Although there is no analytic Fourier transform in the frequency domain of the KWW function, an approximate connection between the HN and the KWW expressions can be stated through the β_{KWW}, the relaxation times of both functions, and the shape parameters of the HN function. An initial relationship between the Cole-Davidson function and the KWW formula was derived by Lindsay and Patterson (Lindsay and Patterson, 1980), and this work was later on extended by Colmenero et. al (Alvarez, Alegria, and Colmenero, 1991). The mathematical approximations linking both phenomenological descriptions are

$$\beta_{KWW} \approx (\alpha\beta)^{1/1.23} \tag{3.11}$$

$$ln\left(\frac{\tau_{HN}}{\tau_{KWW}}\right) \approx 2.6(1 - \beta_{KWW})^{1/2} exp(-3\beta_{KWW}) \tag{3.12}$$

The α-relaxation can then be studied either through the time domain by the transient currents method (Hedvig, 1977; McCrum, Read, and Williams, 1991), or in the frequency domain via broadband dielectric spectroscopy. Nevertheless, since the KWW function has only one shape parameter (β_{KWW}) and the HN function has two (α and β), information is lost when using the former, given that in general no correlation can be stated between α and β parameters (Schönals, 1997).

3.3 Differential Scanning Calorimetry

Thermal analysis refers to several techniques by which a physical property of a sample is measured as a function of temperature. Differential Scanning Calorimetry (DSC) is the experimental technique by which the amount of energy required to maintain a sample and a known reference at the same temperature is measured Hoehne and Flammersheim, 1996; Stanley, 1971. For this purpose, two separate microfurnances with a platinum thermometer and heat sensor are disposed inside of the instrument (Figure 3.7).

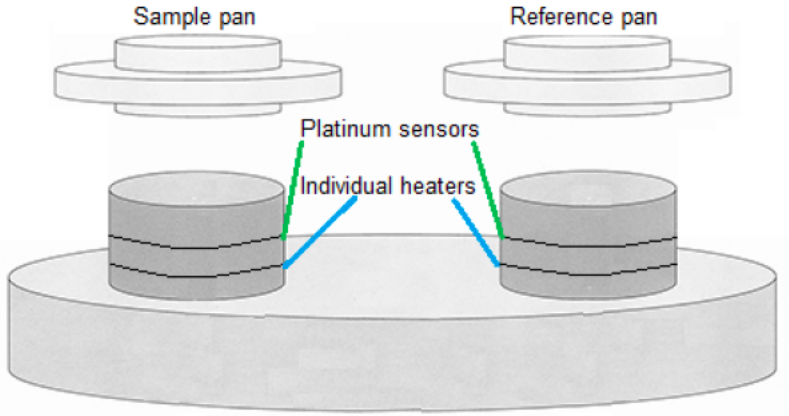

FIGURE 3.7: Sketch of a power compensation DSC.

The sample is placed in an aluminum capsule on top of one of them, and a second empty capsule of known weight is placed over the second microfurnance and serves as reference. Indium is normally used as a standard for calibration of temperature and enthalpy changes within the system. Both capsules are then subjected to the same cooling/heating ramps while a circuit tries to compensate the heat flow rate by a proportional control.

Given that phase transitions such as melting and crystallization are associated with the generation or absorption of heat, whenever a phase transition takes place in the sample the system allows an extra flow of heat into the material in order to keep its temperature equal to the reference (Skoog, Holler, and Nieman, 1998; Pungor, 1995). A differential heat flux signal is then produced with respect to the empty reference and as a function of temperature, resulting in characteristic features as the ones portrayed in figure 3.8. As the compensating heating power ΔP needed to equilibrate

temperature on both, sample and reference, is proportional to temperature difference (ΔT), it can be mathematically represented as:

$$\Delta P \propto \Phi_T \propto \Delta T \tag{3.13}$$

where Φ_T represents the differential heat flow rate given in mJ/s. That is to say, the output signal in figure 3.8 shows Φ_T as a function of temperature.

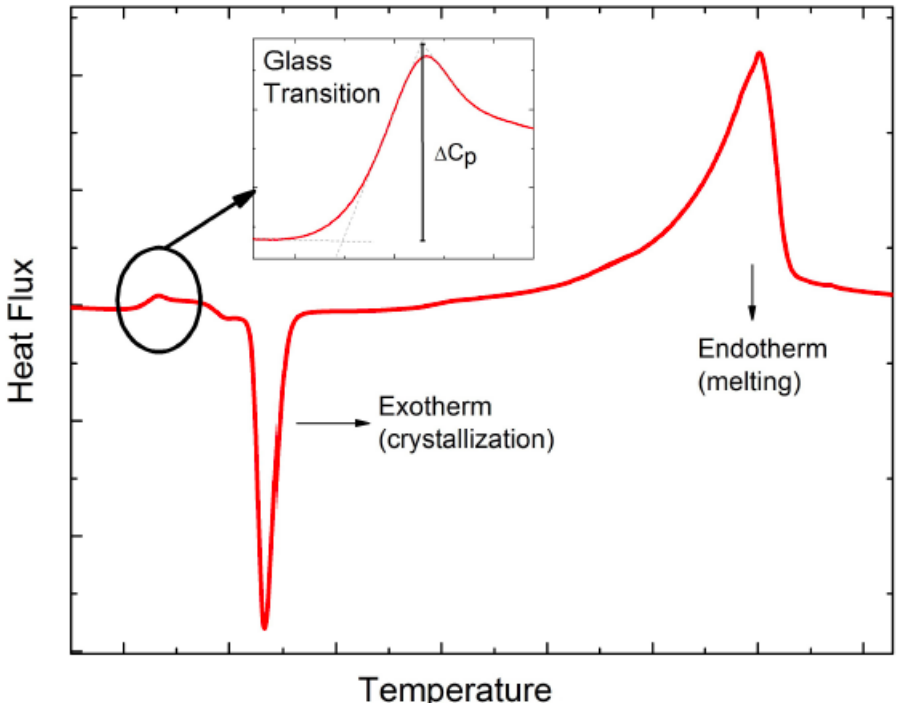

FIGURE 3.8: Illustrative example of a DSC scan.

In this thesis the convention of plotting endotherms as positive peaks and exotherms as negative ones has been adopted. Whereas melting transitions are hereby featured as positive peaks, crystallization processes are negative ones. Glass transitions, on the other hand, involve a change in the heat capacity of the material at constant pressure (ΔC_p) and give rise to step like features in the thermograms, as can be observed in figure 3.8.

DSC thermograms carried out in this thesis were acquired using a *Q100* calorimeter from *TA-Instruments* equipped with a refrigerated cooling systems yielding an operating range from 183 to 823 K, with cooling/heating rates between 2 and 10 K/min. During DSC experiments the sample and reference's atmosphere is controlled by connecting nitrogen or helium purge gases to the system. At the same time, a mass flow controller is used to regulate the flow rate of the gas.

Chapter 4

Prilocaine-H_2O bulk system

4.1 Introduction

When it comes to live organisms, not only glassy systems are relevant, but also water and aqueous solutions play a fundamental role in almost every mechanism. In an adult human approximately 60% of the body is composed by water, whereas in babies this percentage goes up to 78% (Mitchell et al., 1945). Having a thorough understanding of the mechanisms governing the interaction of water with the substances that are absorbed by our bodies is a fundamental question that needs to be addressed in order to develop better, non toxic and more effective products, such as in foods or pharmaceutical ingredients.

In this sense, the effective formulation of pharmaceutical products represents a major challenge. The effect of water on the behavior of these substances is of paramount importance, since not only absorption of water from the environment may change the drug's properties while its being stored, but also because assimilation of the substance in the human body is mediated by the dilution in water of the drug itself (Ewing et al., 2016).

Shelf-life is the term that defines how long a pharmaceutical product may endure without drastically changing its physiochemical properties. Whereas in general a drug formulated in crystalline phase is more stable and has a longer shelf-life, this aggregation state has low energy has a relatively poor temporal dissolution profile, which is a problem for the many drugs which display low solubility in water. The glassy state on the other hand, has a faster dissolution profile due to its higher internal energy, leading to a higher bioavailability. Nevertheless, the glassy state is as well a metastable phase, which means it presents less endurance against the

change of thermodynamical parameters without experimenting phase transformation (Yoshioka and V.J.Stella, 2002).
In the case of drugs, avoiding phase transformation or change in physico-chemical properties is of paramount importance, is providing a drug formulated in a phase that can be easily absorbed by the human body and is compatible with an aqueous medium. The molecule of water is relatively small in size, it has a permanent dipolar moment and a high dielectric constant. These properties make it an excellent solvent for many substances. It has unique hydration properties towards biological macromolecules (particularly proteins and nucleic acids) that determine their three-dimensional structures, and hence their functions in solution. From a conductivity point of view, water ionizes and allows easy proton exchange between molecules. Through this mechanism it contributes to the richness of the ionic interactions and proton reactions in biology. Understanding the structure and the molecular dynamics of bulk and confined water in organic systems is of uttermost importance to the investigation of macromolecular function in cellular and other biochemical systems, as well as the study of food texture and quality, and the stability of biotechnology and pharmaceutical products (Levy and Onuchic, 2006).

4.1.1 H- Bonding

H-bonds are a vital part of every hydrated system. One of the most relevant and outstanding properties of water is the high cohesion between its molecules, known as the Hydrogen bond (H bond). The H bond keeps the water molecule tightly bonded, causing, besides many other effects, the relatively high boiling point of water (100 °C) (Sabin, 1971). Because of its extensive hydrogen bonding, water is liquid over a far greater range of temperatures that would be expected for a molecule of its size.
An H-bond is the partially electrostatic interaction that arises between an H atom from a molecule or a molecular fragment X-H, bound to a more electronegative atom (such as nitrogen (N), oxygen (O) or Fluorine (F)). The most electronegative atom is then covalently bonded to an H atom (-FN, -NH, or -OH), whose electrons it shares unequally. This means that the high tendency of attracting electrons of the electronegative atoms causes the hydrogen to become slightly positively charged. The H atom giving away its electron is called the H-bond donor, whereas the electronegative atom attracting the electron of the H is called the bond acceptor (see figure 4.1 (*a*)).

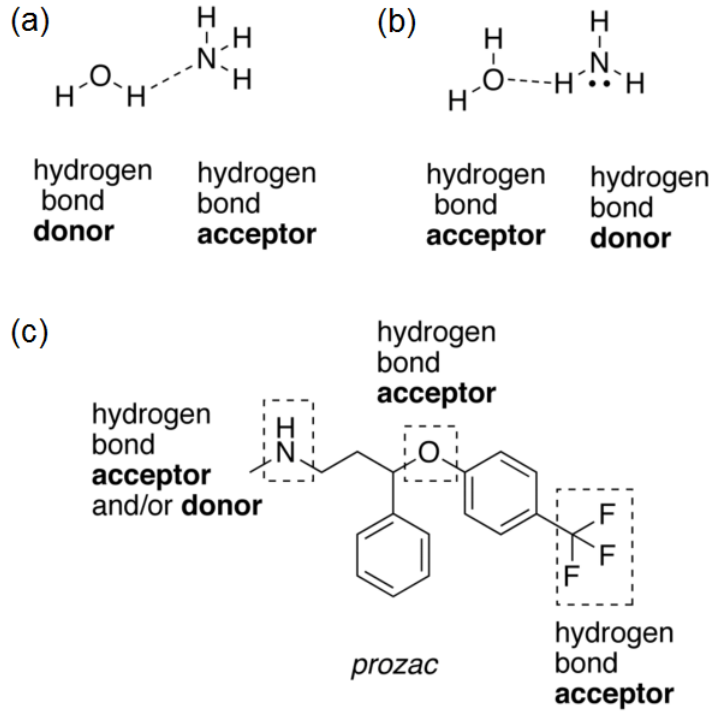

FIGURE 4.1: Examples of hydrogen bond donating (donors) and hydrogen bond accepting groups (acceptors).

At the same time, it may happen that a molecule with an electronegative atom (also typically F, N, or O) with a lonely pair of electrons, gets a slightly negative charge, and 'gives away' one of its electrons, in the form of a H-bond between one of its H and a more electronegative atom from another molecule (see figure 4.1 (*b*)). H-bonds can take place between atoms of the same molecule (intramolecular) or between atoms in different molecules (intermolecular), as seen in panel (*c*) of figure 4.1. Depending on the nature of the donor and acceptor atoms which constitute the bond, their geometry, and environment, the energy of a hydrogen bond can vary in strength from weak ($1 - 2$ kJ mol^{-1}) to strong (161.5 kJ mol^{-1} in the ion HF-2) (Larson and McMahon, 1984; Emsley, 1980). Typical enthalpies in vapor include:

- $F - H \cdots F$ (161.5 kJ/mol or 38.6 kcal/mol), illustrated uniquely by HF2-, bifluoride
- $O - H \cdots : N$ (29 kJ/mol or 6.9 kcal/mol), illustrated water-ammonia
- $O - H \cdots : O$ (21 kJ/mol or 5.0 kcal/mol), illustrated water-water, alcohol-alcohol
- $N - H \cdots : N$ (13 kJ/mol or 3.1 kcal/mol), illustrated by ammonia-ammonia

- $N - H \cdots : O$ (8 kJ/mol or 1.9 kcal/mol), illustrated water-amide
- $HO - H \cdots : OH^+3$ (18 kJ/mol or 4.3 kcal/mol)

This makes these interactions somewhat stronger than a van der Waals interaction, and weaker than fully covalent or ionic bonds.
Figure 4.2 illustrates the H-bonding between pure water molecules. It may be observed that in the liquid phase, each molecule is bonded to 3 or 4 other water molecules, by means of directional hydrogen bonds. Since the molecules within a liquid are constantly changing their positions, the H-bonds are permanently breaking and reforming.

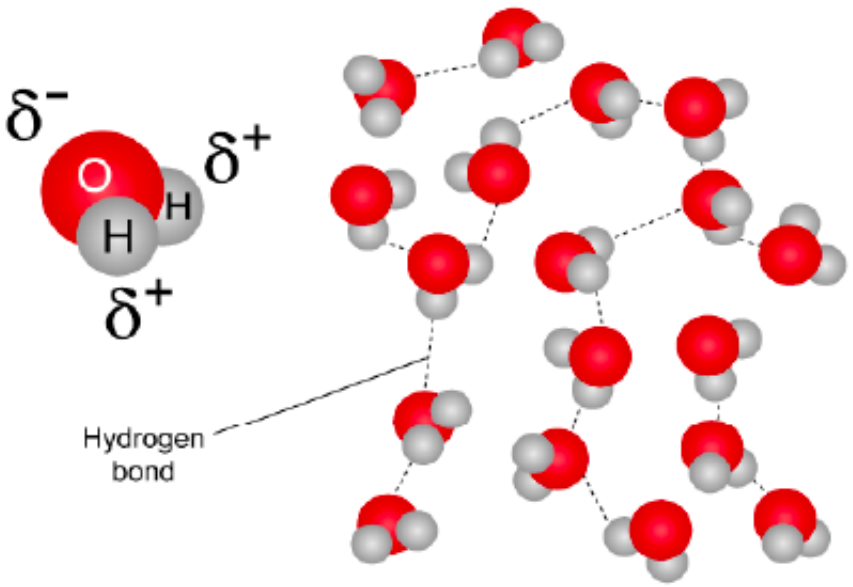

FIGURE 4.2: H-bonding between pure water molecules. The water dipole and the (dynamically disordered) hydrogen bond network between water molecules. (M.Chaplin, 2014)

Hydrogen bonding occurs in many different types of systems in inorganic molecules such as water, and in organic molecules, such as DNA or proteins. Given the fact that water readily forms H-bond with other substances, water becomes then the natural solvent for many ionic compounds. Studying these h-bonds in an intra and inter molecular approach is fundamental for understanding the behavior of many relevant aqueous systems.

4.1.2 Water as a plasticizer

Water is the universal biological solvent, key to the formation of biological structures as well as many other biological processes (Mallamace et al., 2016; Ball, 2008). Aqueous solutions have important implications for the food, cosmetic, and pharmaceutical industries. Water has been long regarded as a universal plasticizer of foods and pharmaceutical products, in the sense that it serves to soften or make less brittle a hydrophilic or hygroscopic specimen (Levine and Slade, 1988; Slade, Levine, and Reid, 1991; Abiad, Carvajal, and Campanella, 2009; Roos and Karel, 1991).

The addition of water has a clear plasticizing effect also in glass-forming organic materials, where it leads to a decrease in viscosity upon hydration, or equivalently, an increase of molecular mobility, which results in a lower glass-transition temperature T_g (the higher the water content the lower the T_g) (Surana et al., 2003; Peleg, 1994; Peleg, 1995; Hancock and Zografi, 1994). In this sense, water is regarded as the most important plasticizer of food components and almost all biological materials, and it is also one of the lowest molecular weight plasticizers to exhibit extremely low T_g (Roos, 1995). In this respect, it is natural that water should have a plasticizing effect on the molecular mobility and thus on T_g, because the glass transition temperature of larger organic molecules is usually higher than that of water (the mobility of large molecules is lower than that of water) and it is expected that the glass transition temperature of binary mixtures is intermediate between those of the pure substances (Katkov and Levine, 2004). The plasticizing effect of water in glass-forming solutions is so ubiquitous and consistent that a recent survey has suggested that aqueous solutions may display a universal dependence of T_g on water content, with a relatively steep decrease of the glass transition temperature upon addition of water (Zhao, Cao, and Wang, 2015a). In fact, it has even been suggested that the hydration water content can be quantitatively determined from the T_g value of the liquid mixtures (Wang et al., 2016).

The phrasing *plasticizing effect* is often used to indicate only a change in the macroscopic mechanical properties of a sample. Perhaps the most dramatic and familiar example of the plasticizing effect of water is that of syrups and honey, which behave as fluids, while non-hydrated sugars form stable crystalline phases, characterized by a extremely high viscosity. It should be pointed out that, in terms of the mechanical resistance of a sample, hydration can also have the opposite effect, at

least in a limited water content or humidity range: namely, a number of studies reported that, when some dried solid food matrices are re-humidified, small amounts of adsorbed water led to increased rigidity and firmness, i.e., to stiffer mechanical properties (Vrentas, Duda, and Ling, 1988; Seow, Nair, and Lee, 1995; Seow, Cheah, and Chang, 1999; Roudaut, Dacremont, and Meste, 1998; Li, Kloeppel, and Hsieh, 1998; Konopacka, Plocharsky, and Beveridge, 2002; Spackman and Schmidt, 2009). This behavior is similar to the effect observed in synthetic glassy polymers, where, at temperatures below T_g, an increase in the concentration of some diluents, usually behaving as plasticizers, leads to a harder and tougher structure despite the T_g decrease (Lazaridou, Biliaderis, and Kontogiorgos, 2003). This effect has been termed 'anti-plasticizing effect' despite the fact that the T_g actually decreases with addition of water (Hancock and Zografi, 1994; Pittia and Sacchetti, 2008; Halek, Paik, and Chang, 1989; Fontanet et al., 1997; Marzec and Lewicki, 2006; Gondek and Lewicki, 2006). The studies reporting an increased mechanical rigidity upon water sorption deal either with complex systems containing several components and/or large biomolecules of size much larger than that of a water molecule. The complexity of such samples hinders the identification of the mechanisms responsible for the increased stiffness (a change in mechanical stiffness may be ascribable, for example, to spurious effects due to texture heterogeneity). Indeed, the fact that in all these systems T_g decreases with increasing water content indicates that the rigidity increases despite the simultaneous increase in the molecular mobility.

Concerning the universality of the plasticizing effect of water on the glass transition temperature, there are indeed very few studies where the opposite effect, namely, an increase of T_g upon hydration, has been observed or suggested. To the best of our knowledge, only three claims have appeared in the scientific literature about a possible anti-plasticizing effect of water, on T_g, two of which were observed in rather complex samples, with one observation being controversial. In 2005, Schumann and LeBoef reported (Schaumann and LeBoeuf, 2005) a moisture-induced increase of the glass transition temperature in a peat sample. These authors argued that the antiplasticizing effect on T_g is caused by a reduction of side chain mobility due to the formation of hydrogen bond-based cross-links between water molecules and polymer side chains. In 2009 an analogous phenomenon was reported (J.Perdomo et al., 2009) for cassava starch at low moisture content. At higher water content the effect was opposite, with water inducing a decrease in T_g. Other research groups were

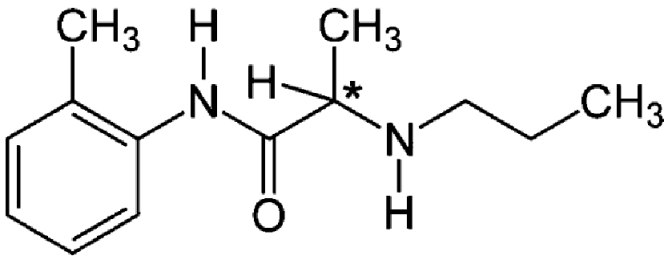

FIGURE 4.3: The molecular structure of the prilocaine drug.

however unable to find any anti-plasticizing effect of water on cassava starch. The discrepancy was tentatively ascribed to the different cassava genotypes employed in the different studies. (Aichayawanich et al., 2011; Chang, Cheah, and Seow, 2000; Zhu, 2015).

Finally, in 2014 an antiplasticizing effect of water on N-ethyl acetamide was reported (Li et al., 2014). This first observation of a genuine antiplasticizing effect of water on the molecular mobility of a simple glass former represents a serious challenge to the proposed universality of water as plasticizer. It could perhaps be argued that the glass transition temperature of N-ethyl acetamide is not far from that of water (Angell, 2008). The authors of Ref.Li et al., 2014 do not provide insight as to the possible origin of the observed effect.

4.1.3 Anti-plasticizing effect of water in the prilocaine drug

In the present chapter, a genuine anti-plasticizing effect of water on the molecular dynamics of a simple molecular system, the pharmaceutically active molecule prilocaine, is reported. Prilocaine, is a local anesthetic of the amino amide type often used in dentistry (Brodin et al., 1984; Nyqvist-Mayer, Brodin, and Franck, 1985; Nyqvist-Mayer, Brodin, and Franck, 1986). Figure 4.3 illustrates the drug's molecular structure.

The equilibrium phase diagram of the prilocaine-water system has been studied in a recent work (Rietveld et al., 2013a). For a water molar fraction greater than approximately x = 0.33, the system separates in two stable liquid phases: a prilocaine-rich liquid with minority water content (liquid $L_1, x = (0.33 \pm 0.02)$, with approximately 2 molecules of prilocaine for every H_2O), and a very dilute water-based solution of prilocaine (liquid $L_2, x = (0.98 \pm 0.01)$, with approximately 1 molecule of prilocaine for every 99 molecules of H_2O). The two have slightly different densities

and are thermodynamically stable at room conditions, which allows their separation by physical means.(Rietveld et al., 2013a). These phases can be distinguished at naked eye by their color: while the former presents a whitish color, the latter is transparent. Figure 4.4 shows the phase diagram of the binary system.

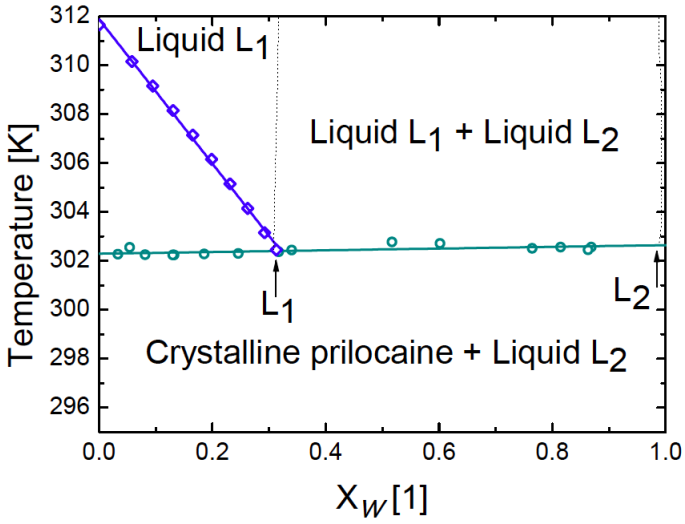

FIGURE 4.4: Temperature-composition (X_w: water mol fraction) phase diagram of the binary system prilocaine-water exhibiting a miscibility gap in the liquid phase. L_1 is the prilocaine-rich liquid, L_2 the water-rich liquid. Solid squares: eutectic equilibrium. Solid circles: monotectic equilibrium. Solid diamonds: liquidus related to the fusion of prilocaine. Figure adapted from Rietveld et al., 2013b.

Through these experiments prilocaine-rich homogeneous aqueous mixtures with water (molar fraction lower than 0.33) have been studied, both in the supercooled liquid and glass states. At the same time, the results have been contrasted with the case of anhydrous prilocaine. It has been found that water has an antiplasticizing effect on the relaxation dynamics and glass transition temperature of prilocaine. This change is observable and consistent over a large water concentration range, and it is even more dramatic than in the case of N-ethyl acetamide because the T_g of prilocaine is much higher (by 84 K) than that of water, so that the T_g of the binary mixtures may be expected to be significantly lower than that of the organic component (Katkov and Levine, 2004). Most likely the microscopic origin of the antiplasticizing effect is related to a tighter hydrogen-bond network resulting in the formation of water-prilocaine complexes such as water-bridged dimers. This study may have commercial implications, as the formation of equilibrium mixtures of water with prilocaine or similar active pharmaceutical ingredients is commonly used to obtain anesthetic formulations such as creams (Ceolin et al., 2010; Rietveld et al., 2013b).

4.2 Sample preparation and experiments

4.2.1 Differential Scanning Calorimetry (DSC)

Prilocaine hydrochloride was purchased from APIChem Technology Co. and purified to obtain pure prilocaine (N- (2 methylphenyl) - 2(propylamino) propanamide, chemical formula: $C_{13}H_{20}N_2O$). For DSC measurements, hydrated prilocaine with different water content was obtained by mixing pure prilocaine with water at relative H_2O molar fraction lower than 0.33. Since these concentrations require a very low volume of water, the capsules were prepared as follows: Hermetic aluminium pans were placed in a scale, powder prilocaine was placed inside and a drop of water was poured on top. Then, water was let to diffuse and evaporate until the desired concentration (total sample mass) was reached. At this point the pan was hermetically sealed with a press and placed inside the DSC apparatus. For all further experiments, the hydrated prilocaine was obtained by first dissolving the prilocaine powder in excess deionized water (molar fraction > 0.33) and then sonicating at 327 K. Under these conditions, the binary system above the monotectic equilibrium at 302.4 K is in a separated phase of two homogeneous liquids, one rich in prilocaine (L_1) and the other rich in water (L_2), which was observed to remain stable for at least two years at or slightly above room temperature (Céolin et al., 2010). The prilocaine-rich liquid L_1 was extracted from the gravity-separated biphasic mixture, obtaining saturation-concentration hydrated prilocaine.

4.2.2 Broadband Dielectric Spectroscopy (BDS)

Isothermal and isobaric BDS experiments were performed to gain insight into the dynamics of pristine and hydrated prilocaine. In order to achieve a homogeneous liquid solution of water-saturated hydrated prilocaine, a solution was prepared by mixing equal amounts of purified water and pure prilocaine. Then, the mixture was melted at 50 °C and was let to rest in a thermal bath at the same temperature for 2 days. This allowed the system to separate into the two liquid phases: a prilocaine-rich aqueous solution (hydrated prilocaine), and a water-rich prilocaine solution (Rietveld et al., 2013b). By making use of a warmed up syringe so as to avoid PLC crystallization, liquid hydrated prilocaine could be extracted. By making use of a warmed up syringe (so as to avoid PLC crystallization), liquid hydrated prilocaine could be extracted.

BDS was carried out both at ambient pressure (1 bar) and under an applied hydrostatic pressure of 1000 bar. All measurements were performed using parallel-plate capacitors, into which the samples were inserted in liquid form, and dielectric spectra were acquired between 10^{-2} and 10^{-6} Hz using the Novocontrol Alpha Analyzers described in Chaper 3. For the measurements at 1000 bar, in order to prevent a possible contamination with the pressurizing fluid (thermal oil from Huber) the capacitor was covered with a teflon membrane and latex wrapping. The insulated capacitor was then placed in a high-pressure chamber (Unipress) made of a Cu-Be alloy, which was filled with the thermal oil and connected to a manual pump that allowed applying hydrostatic pressure between ambient pressure and 0.6 GPa, as measured by means of a pressure transducer with an accuracy of $\pm$0.5%. The temperature was controlled by thermal baths (Lauda Proline RP 1290 and Huber Unistat) with a liquid flow circuit connected to the high-pressure setup.

4.2.3 Raman and Infrared Spectroscopy

Raman measurements were carried out using a confocal Raman imaging spectrometer (Alpha300 Access from WITec) and a liquid-nitrogen cryostat (Oxford Microstat Model N). An Olympus objective (MPLN plane achromatic lens) with a 10 X magnification was used to focus the laser (diode laser of 532 nm wavelength and 20 mW maximum power) onto the sample. Liquid samples of pure prilocaine, L_1 and L_2 were placed on a glass slide precooled to 180 K, which resulted in vitrification. The samples were placed in a low-vacuum cryostat (14 mbar) immediately after deposition, and characterized at 180 K. The spectra were recorded with a 600 cm^{-1} grid, by accumulation of three spectra integrated for 200 seconds each.
IR measurements were carried out using a Fourier transform infrared spectrometer with attenuated total reflectance, model Vertex 70 by Bruker. The hydrated prilocaine was loaded and measured right at ambient conditions, whereas pure prilocaine was melted at 313 K in situ to ensure that the liquid phase was measured.

4.3 Results and discussion

4.3.1 DSC

As mentioned in the introduction of this chapter, for a prilocaine aqueous solution of water molar fraction greater than approximately x = 0.33, the system separates in

two stable liquid phases: L_1 ($x = 0.33 \pm 0.02$) and L_2 ($x = 0.98 \pm 0.01$). Other less hydrated concentrations ($x < 0.33$) of the binary system can be obtained by mixing stoichiometric amounts of the two components, but special care has to be taken in this case since water may evaporate, leading to lower water content than desired. In this thesis I have focused on the prilocaine-rich liquid L_1, hereinafter referred to as 'hydrated prilocaine'. Such phase is interesting as it represents a thermodinamically stable homogeneous mixture of water and prilocaine that is richer in the prilocaine component, with water fraction up to x = 0.33 (throughout the chapter, x refers to the molar fraction of water).

Fig.4.5(a) shows the DSC thermograms of hydrated prilocaine (L_1) obtained by phase separation, and of less hydrated prilocaine (with x $\leq$ 0.33) obtained by stoichiometric mixture of prilocaine and water. In the latter case, prilocaine/water physical mixture of the desired stoichiometry was heated to 313.5 K for 5 minutes which allowed prilocaine to melt, and then the mixture was cooled to 203.15 K at a rate of 8 K/min. The thermal protocol followed was:

1. Equilibrate at 293.15 K
2. Isothermal for 1 min
3. Ramp 8 K/min to 313.15 K
4. Isothermal for 5 min
5. Ramp 8 K/min to 203.15 K
6. Isothermal for 1 min
7. Ramp 8 K/min to 215.15 K
8. Isothermal for 60 min
9. Ramp 8 K/min to 203.15 K
10. Isothermal for 1 min
11. Ramp 8 K/min to 323.15 K
12. Isothermal for 1 min
13. Equilibrate at 293.15 K

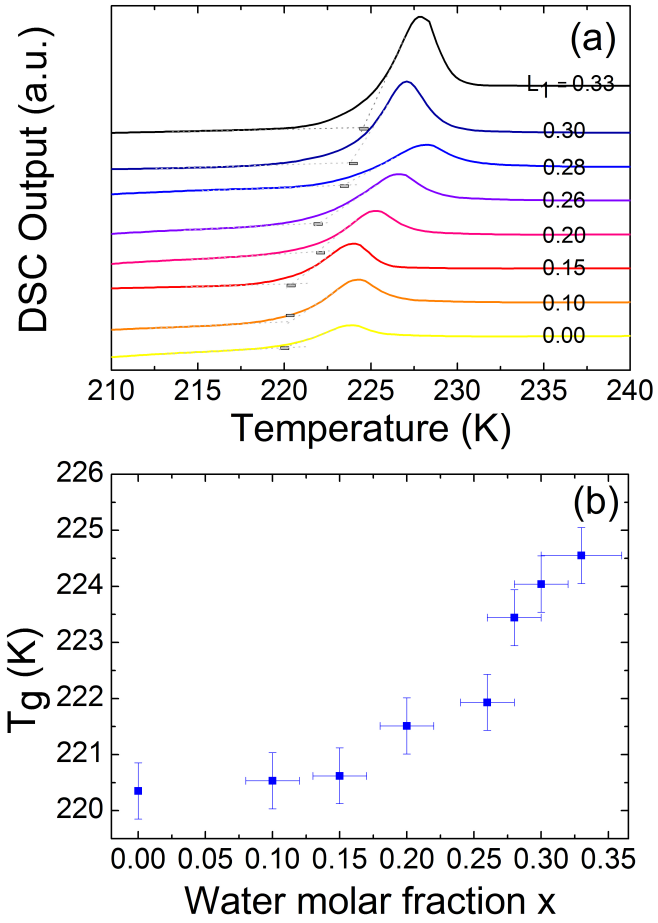

FIGURE 4.5: Effect of water on the glass transition temperature.(a) DSC scans for different water molar fractions x of binary prilocaine/water mixtures, measured upon heating at 8 K/min right after aging during 1 hour at 215.2 K. (b) Onset T_g values for prilocaine as a function of water concentration (data corresponding to the thermograms in (a)).

Steps 3 and 4 produce the isobaric melting of prilocaine, when heated to 313.5K, surpassing its melting point. When the crystalline drug turns into liquid, it melts with the water in the capsule. The solution is cooled in step 5, ramping at a pace of 8K/min to a temperature of 313.15 K. In step 6 the sample is heated to a temperature approximately 5 K below its glass transition, in order to allow its relaxation/annealing process by letting it rest for 60 min (step 8). This annealing generates a more relaxed sample, that results in a sharper glass transition feature, that can be observed when heating at 8K/min to 323.15 K (step 11). The heating scan corresponding to this step is shown in figure 4.5(a). The T_g, taken to be the onset of the glass-transition feature in the thermograms, is shown in Fig. 4.5 (b). T_g is found to increase with increasing water content, with an enhancement of more than 4 K at water saturation (x = 0.33) upon isobaric heating (step 11). The obtained T_g value upon heating for pure prilocaine is (220.4 $\pm$ 0.5) K, whereas for hydrated prilocaine (x=0.33) it goes up to (224.5 $\pm$ 0.5) K.

DSC cooling traces (step 5) and the corresponding T_g onsets are shown in Fig. 4.6. It can be observed that the increase in T_g is consistent throughout the whole concentration range. The glass transition increases from approximately 220.5 K at $x = 0.0$ to 227 K for $x = 0.33$, which means more than 6 K increase in T_g with the increase in water content. Such increase represents a clear antiplasticizing effect, which is surprising considering the almost universal plasticizing effect of water on T_g especially when mixed with small organic molecules (Zhao, Cao, and Wang, 2015b; Wang et al., 2016).

In order to be able to contextualize the behaviour of aqueous prilocaine's glass transition with respect to other substances, a model has been applied to experimental data reported in the literature. The glass transition temperature for mixtures (such as aqueous mixtures) can be modeled in many cases by means of the Gordon-Taylor equation (Gordon and Taylor, 1952):

$$T_g' = \frac{w_s T_g + K w_w T_w}{w_s + K w_w} \tag{4.1}$$

where w_s and w_w are the weight fractions of the solute and water, respectively, and similarly, T_g and $T_w = 134K$ are the glass transition temperatures of the anhydrous solute and water (Sugisaki, Suga, and Seki, 1968). The constant K is a measure of the extent of plasticization, where a higher K value corresponds to stronger

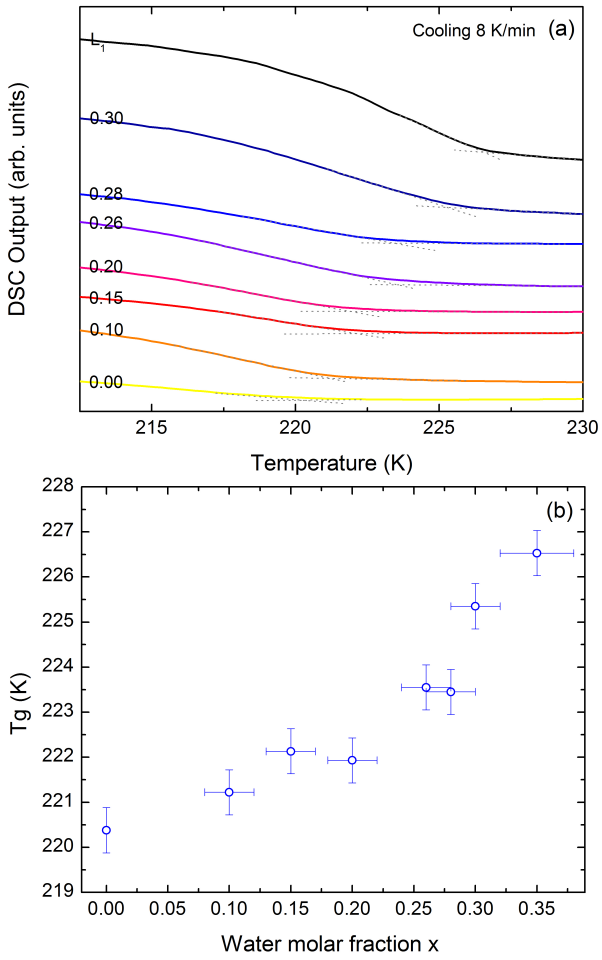

FIGURE 4.6: Effect of water on the glass transition temperature. (a) DSC scans for different water molar fractions x of binary prilocaine/water mixtures, measured upon cooling at 8 K/min. (b) Onset T_g values at cooling for prilocaine as a function of water concentration (data corresponding to the thermograms in (a)).

plasticization. For example, sugars are reported to have K values between 3.7 and 7.8 (Hancock and Zografi, 1994; Bellavia et al., 2009) [1], and proteins 1.3 to 5 (Contard and Ring, 1996; Orford et al., 1989; Kalichevsky, Blanshard, and Tokarczuk, 1993; Kalichevsky, Jaroszkiewicz, and Blanshard, 1992). In order to compare with a wide variety of systems covering a broad range of K values (1.4 to 8.8) the Gordon-Taylor equation (4.1) was applied to the cases of sorbitol (K=2.9) and the phospholipids DPPC (1,2-dipalmitoyl-sn-glycero-3-phosphocholine) (K=8.8) and DOPE (1,2-dioleoyl-sn-glycero-3-phosphatidylethanolamine), both in gel and inverted hexagonal phase (K=3.5 and 1.4 respectively). All K values were taken from the aforementioned references, and the corresponding glass transition temperatures calculated through equation 4.1 are shown in Table 4.1.

Solute	T_g (anhydrous) (K)	K parameter
Sorbitol	270.0	2.9
DPPC, lamellar gel phase	338.2	8.8
DOPE, lamellar gel phase	259.6	3.5
DOPE, inverted hexagonal phase	185.9	1.4

TABLE 4.1: Parameters of the Gordon-Taylor equation for systems covering a broad K range. Data were taken from the following references: sorbitol (Ewing et al., 2016; Talja and Roos, 2001), DPPD and DOPE inverted hexagonal phase (Shalaev and Steponkus, 2010) and DOPE lamellar gel phase (Contard and Ring, 1996).

The dependence of T_g of these substances on water content and compared to the prilocaine case is depicted in figure 4.7. It can be then observed, that although the increase in T_g shown in figure 4.5 is relatively modest, one would usually expect a much larger *decrease* in T_g for almost any material. For example, for sorbitol, addition of a similar amount of water (0.3 molar fraction) results in a decrease of T_g by approximately 13 K.

4.3.2 BDS

Ambient pressure measurements

In order to verify that the molecular dynamics of prilocaine is indeed slower in the presence of water, BDS measurements on both pure prilocaine and hydrated prilocaine close to saturation (i.e., on the L_1 liquid obtained by physical phase separation)

[1] Note that k values reported in Hancock and Zografi, 1994 are related to K values in the present work as $K = 1/k$.

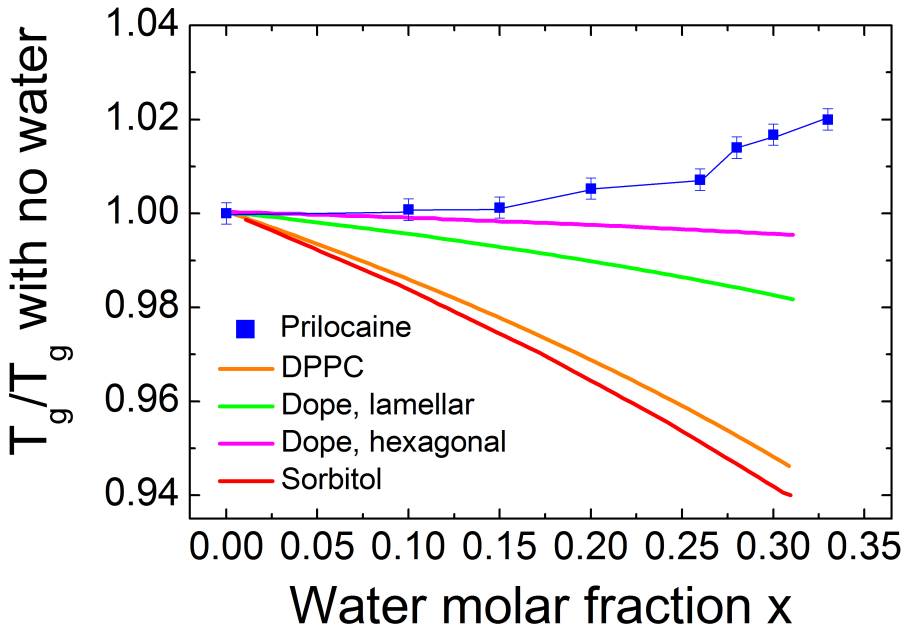

FIGURE 4.7: Effect of water on the glass transition temperature. Normalized glass transition temperatures for binary water-solute systems. Prilocaine: this work. T_g values for other systems are described with the Gordon-Taylor equation based on the T_g values reported in table 4.1.

were carried out. This was done by inserting the liquid samples into the Alpha Analyzer precooled to 120 K and acquiring spectra every 2 K up to room temperature. Fig. 4.8 (a) shows the comparison of the isothermal loss spectra $\epsilon''(f)$ of pure and hydrated prilocaine at the same temperature of 243 K. Both spectra are characterized by a prominent loss feature corresponding to the primary (α) relaxation dynamics associated with the glass transition. The dielectric loss spectra were fitted as the sum of a relaxation process, represented by a Havriliak-Negami profile, on top of a background proportional to reciprocal frequency representing the dc conductivity. It may be observed that the frequency of the α relaxation in hydrated prilocaine is lower than that of the pure compound indicating a lower mobility in the hydrated samples, in agreement with the DSC results.

The same behavior was observed at all temperatures, as visible in the Arrhenius plot (Fig. 4.8 (b)) of the relaxation times extracted by a fit of the α relaxation peak with an Havriliak-Negami function (see Chapter 3). The Arrhenius plots of both anhydrous and hydrated prilocaine follow a Vogel-Fulcher-Tammann dependence on temperature, given by eq 1.7. The T_g for pure prilocaine, estimated as the temperature at which the α relaxation time equals 100 s (dashed horizontal line in Fig.4.8 (b))

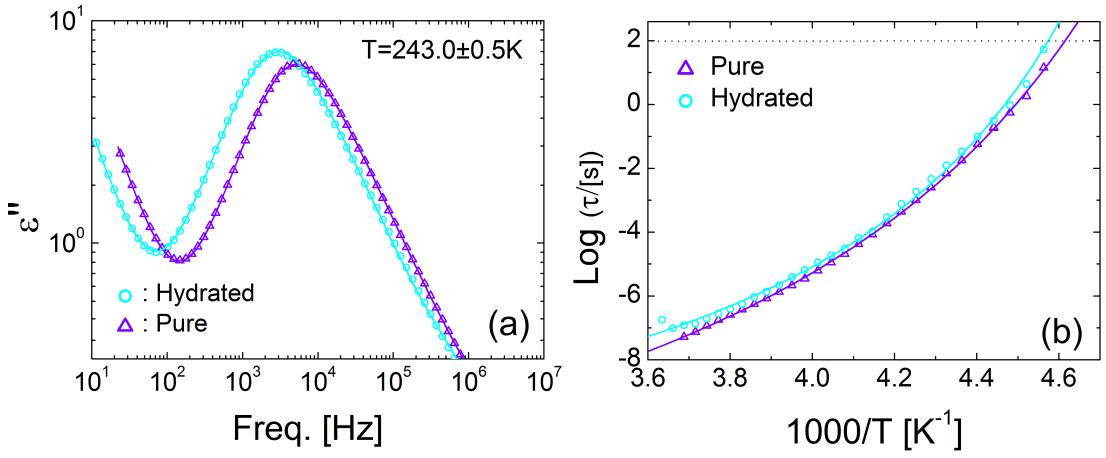

FIGURE 4.8: Effect of water on the temperature-dependent relaxation dynamics of prilocaine. (a) Comparison of the dielectric loss spectra of hydrated and pure prilocaine at 243 K. Continuous lines are fits. (b) Arrhenius plot of the primary relaxation times τ of pure and hydrated prilocaine at ambient pressure. Continuous lines are fits with the Vogel-Fulcher-Tammann Eq. 1.7.

is 216.5 K, in agreement with an earlier Broadband Dielectric Spectroscopy (BDS) study (Wojnarowska et al., 2015). For hydrated prilocaine the extrapolated T_g is 2 K higher, which according to our calorimetric study (Fig. 4.5) corresponds to a nominal water concentration just below 0.30, *i.e*, close to saturation.

High pressure measurements

In order to have insight into a more tightly packed structure of the PLC drug and with the aim of shedding light into the mechanisms affecting the glass transition, BDS experiments under pressure have been performed. The result of the dielectric characterization of pure prilocaine under an applied hydrostatic pressure of 1000 bar using the high pressure BDS equipment described in Chapter 3 is shown in panels (a) and (b) of Fig. 4.9. The dielectric loss spectra were fitted as the sum of a relaxation process, represented by a Havriliak-Negami profile, on top of a background proportional to reciprocal frequency representing the dc conductivity.

As visible in panel (a) for the temperature of 240 K, application of pressure shifts the α-relaxation frequency to smaller values, *i.e*, it slows down the molecular dynamics, as expected. The Arrhenius plot of the relaxation time of pure prilocaine at high pressure is shown in Fig. 4.9 (b). For the purpose of comparison, the ambient pressure curve of Fig. 4.8 (b) is also shown in the same figure.

The extrapolated T_g at 1000 bar is 220.9 K, roughly 4 K higher than that of pure prilocaine at ambient pressure. This increase is comparable with the highest increase of T_g due to mixing with water (Fig. 4.5). It can be observed in Fig.4.8 (b) that the curvature of the hydrated sample is higher than that of the pure compound. This entails a slightly higher kinetic fragility index (Angell, 1985a; Böhmer et al., 1993) (see chapter 1 section 1.4.1) m of hydrated prilocaine compared with the pure compound. At the same time, Fig.4.9 (b) shows that the curvature of the high-pressure data appears higher, which implies a higher fragility index. Table 4.2 shows the obtained values for the fragility parameters m in each case.

Substance	Pressure (bar)	Fragility m
Prilocaine	1	18 ± 2
Prilocaine	1000	20 ± 2
Hydrated prilocaine	1	21 ± 2

TABLE 4.2: Fragility m calculated for each of the studied systems.

In other words, the antiplasticizing effect of water on prilocaine is analogous to that of an applied hydrostatic pressure, namely, an increase of T_g by few degrees K and an increased kinetic fragility index.

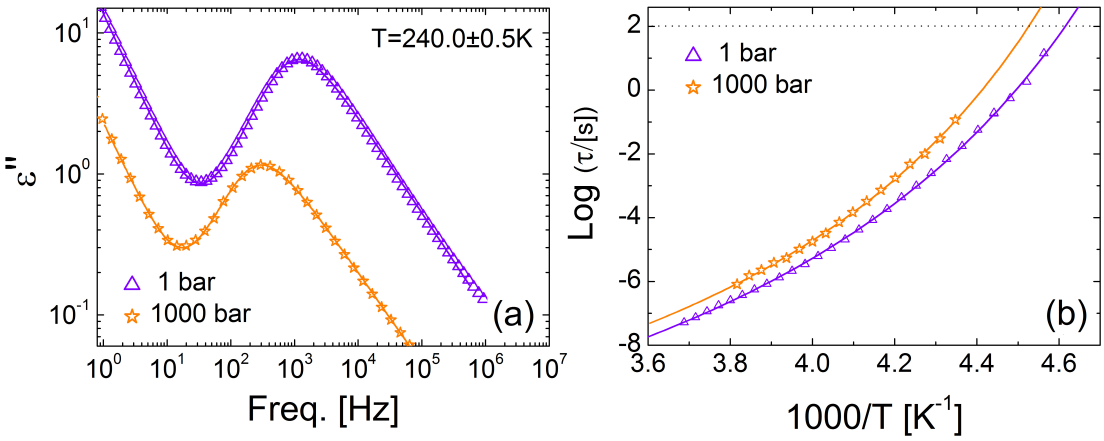

FIGURE 4.9: Effect of water and pressure on the temperature-dependent relaxation dynamics of prilocaine. (a) Comparison of the dielectric loss spectra at 240.0 K of pure prilocaine at ambient (1 bar) and high (1000 bar) pressure. Continuous lines are fits. (b) Arrhenius plot of the primary relaxation times τ of pure prilocaine at ambient pressure and at 1000 bar. Continuous lines are fits with the Vogel-Fulcher-Tammann Eq. 1.7.

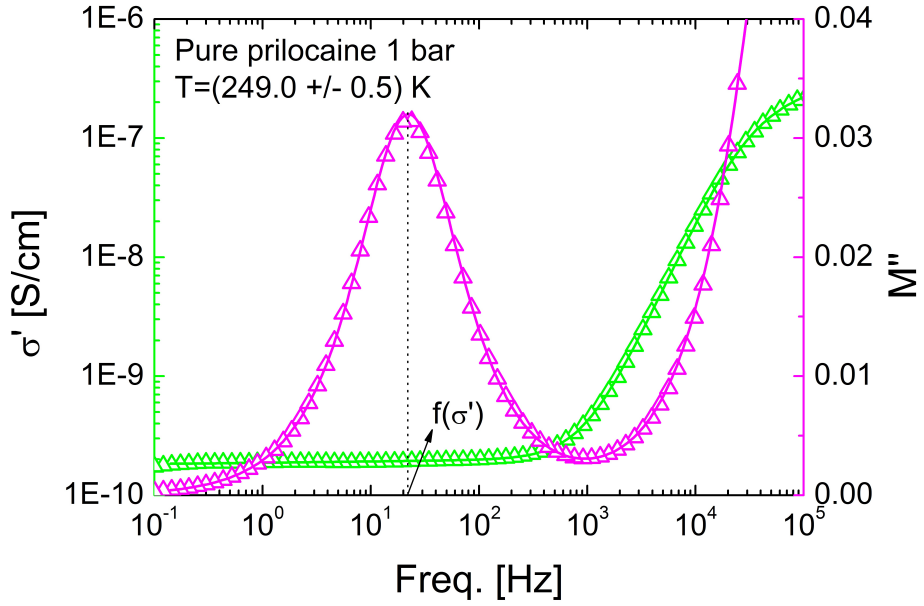

FIGURE 4.10: Comparison between the ac conductivity spectrum ($Log(\sigma'(f))$, green axis and trace) and the imaginary modulus spectrum ($M''(f)$, pink axis and trace) of pure prilocaine at 1 bar and 249 K. The latter exhibits a maximum at the (temperature-dependent) frequency $f(\sigma')$, indicated with a dotted line.

Conductivity mechanisms

With the aim of understanding the charge transport and conductivity mechanisms in the system, the ac conductivity and the dielectric modulus have been analyzed (see 2.3). Figure 4.10 shows the modulus (M'') and ac conductivity ($Log(\sigma')$) spectra of pure prilocaine at 1 bar and 249 K. It can be observed that the maximum of the modulus (the so-called *conductivity relaxation*, Contard and Ring, 1996; Sippel et al., 2015) occurs at a frequency $f(\sigma')$ that lies in the middle of the dc plateau of the conductivity spectrum; the same is observed in all experimental prilocaine spectra studied (also at high pressure, and also for hydrated prilocaine). To obtain a precise determination of the dc value of the conductivity, σ_{dc}, this was defined as the value of $\sigma'(f)$ at the frequency f_σ of the modulus maximum (Wojnarowska et al., 2013a).

Fig. 4.11 (a) shows the Arrhenius plot of the dc conductivity (σ_{dc}) determined as the low-frequency plateau value of the ac conductivity spectra $\sigma'(f) = 2\pi f \epsilon_0 \epsilon''(f)$, as explained in figure 4.10, of pure prilocaine at ambient and high pressure, as well as that of hydrated prilocaine at ambient pressure. In all three cases σ_{dc} exhibits a sub-Arrhenius temperature dependence, which is typical of ionic conduction in liquids and disordered solids. (Bauer et al., 2010; Do et al., 2013; Zachariah et al., 2015a;

Zachariah et al., 2015b).

An empirical rule suggested by *P. Walden* concerning ions in solutions is know as the Fractional Walden Rule (see 2.3.1), and it states that the product of the molar conductivity and the viscosity is approximately constant for the same ions in different solvents (Walden, 1906). The linear response between σ_{DC} and τ_α shown in Fig.4.11(b) indicates that all samples obey roughly the Walden rule, which is also a hallmark of ion diffusion in liquids and disordered systems (Walden, 1906; Barthel, Krienke, and Kunz, 1998).

The ionic nature of the conductivity is also confirmed by the pressure dependence of σ_{dc}: as visible in Fig. 4.11 (a), the dc conductivity is one order of magnitude lower at 1000 bar than at ambient pressure. Such decrease in conductivity with applied pressure is due to the fact that a higher density entails a smaller size of the intermolecular voids and thus a reduction of the ion percolation network.

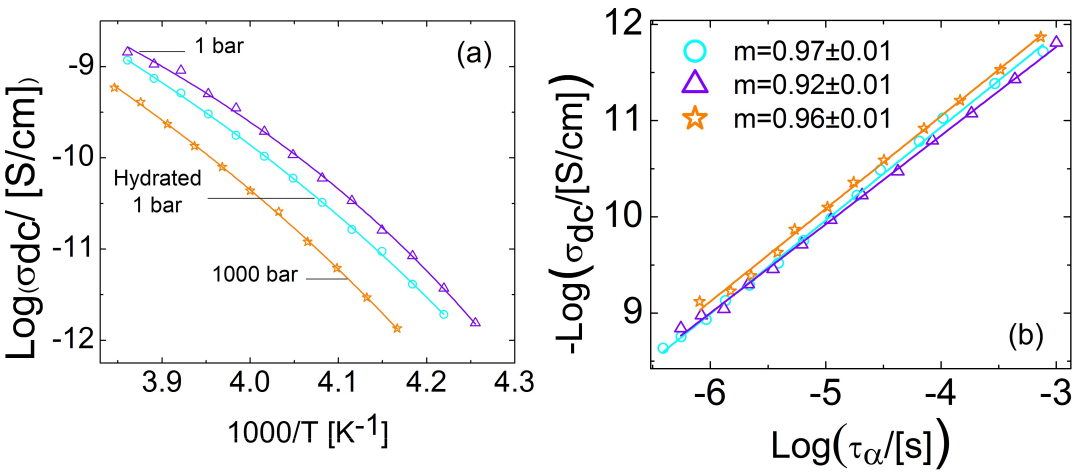

FIGURE 4.11: (a) Ionic dc conduction in pure and hydrated prilocaine. Arrhenius plots of the dc conductivity σ_{dc} for pure prilocaine at 1 and 1000 bars, together with that of hydrated prilocaine at 1 bar. (b) Logarithmic Walden plot (σ_{dc} vs τ) for the same three samples.

It is worth noticing that the conductivity of hydrated prilocaine is lower by a factor of two or three than that of the pure compound. This result is remarkable since the presence of water usually leads to an increase of σ_{dc} due to protonic charge transport (Knight and Voth, 2012; Zachariah et al., 2015c). Hence the effect of hydrating prilocaine is similar to that of an applied pressure also on σ_{dc}: the conductivity decreases in both cases, indicating a lower free volume available for ion drift. Similarly, the increase of relaxation time upon mixing with water suggests a lower free volume for molecular diffusion.

4.3.3 Infrared and Raman Spectroscopy

In order to gain insight about the microscopic origin of the observed anti-plastizicing effect, we have also performed some Raman and FTIR experiments to find out the most probable hydration of prilocaine. Fig. 4.12 shows the vibrational spectra of pure and hydrated prilocaine, in the wavenumber range between 1600 and 1750 cm^{-1}, both in the liquid (a) and glassy (b) states. Two bands are visible in this spectral range, namely the bending mode of water and the stretching vibration of the C=O double bond of the carbonyl oxygen of the propyl-alanine-amide chain of prilocaine (see Fig. 4.3). The H_2O bending mode (1640 cm^{-1}) is visible in the ATR FTIR spectrum of the dilute prilocaine aqueous solution (liquid L_2) while it is not visible in hydrated prilocaine (liquid L_1) due to its relatively low water content.

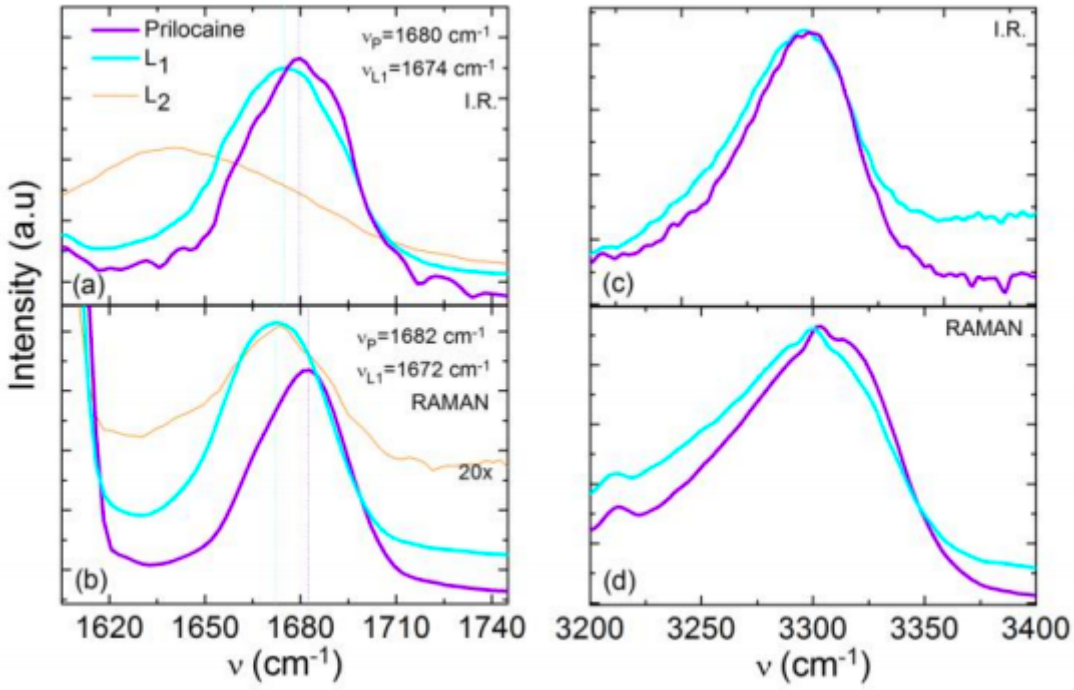

FIGURE 4.12: Vibrational spectra of pure and hydrated prilocaine. Attenuated total reflection infrared spectra measured at room temperature in the liquid phase (a) and Raman spectra acquired at 220 K on the glass (b), between 1605 and 1745 cm^{-1} (left panels) and between 3200 and 3400 cm^{-1} (right panels). Besides the spectra of pure and hydrated prilocaine, the spectra of a diluted prilocaine solution in water (liquid L_2) are also shown for comparison.

The presence of water has a dramatic effect on the stretching vibration of the C=O group: as evidenced by the vertical dotted lines in Fig. 4.12, a clear shift is observed in the spectral position of the main C=O band between the pure prilocaine and hydrated prilocaine (liquid L_1). The shift is visible in the liquid phase by ATR,

but is more pronounced in the Raman spectra of the glass phase, where the C=O bands of pristine and hydrated prilocaine are shifted by as much as 10 cm^{-1}.
The C=O stretching band is also visible in the Raman spectra of the glass phase of the water-rich liquid L_2, where it is also shifted compared with pure prilocaine (Fig. 4.12 (b)) by the same amount as in the L_1 liquid (in ATR, the same band is visible as a shoulder to the H_2O bending mode). On the other hand, virtually no change was observed in the region of the N-H vibrations, visible as a relatively broad band around 3300 cm^{-1}. The spectral position of such band was not affected by water in the liquid state ATR spectra (panel c), and it shifted only slightly in the Raman spectra of the glass (panel d; it should also be noted that the stretching bands of water may contribute to the overall intensity in the spectra of hydrated prilocaine). By comparison, hydrogen bonding of water to the N-H group of simple amides will lead to shifts of the N-H vibrations of tens of cm^{-1} (Myshakina, Ahmed, and Asher, 2008). This indicates that water binds mainly to the carbonyl oxygen. This is consistent with the results recently reported by some of us through the study of prilocaine by means of neutron diffraction and Empirical Potential Structure Refinement simulation (Silva-Santisteban et al., 2017).
H-bonding of water to prilocaine is energetically favored with respect to inter-prilocaine H-bonding, since hydrogen bonds with oxygen donors are stronger than with nitrogen donors. This is to say, in a matrix of pure prilocaine molecules, intermolecular bonds take place most likely through N-N bonds. N-N bonding in the case of pure prilocaine may be expected to be even weaker than in most cases, as they involve chain nitrogens. Water molecules on the other hand, might donate two H-bonds to a single prilocaine molecule, binding to the carbonyl oxygen and simultaneously to a chain nitrogen as depicted in Fig. 4.13 (for example Silva-Santisteban et al., 2017), or else bridge together two distinct prilocaine molecules. This prilocaine H-bonding is more energetic, and hence stronger,than the N-N one.

Given that the addition of water has little effect on the N-H vibration and a large on the C=O band (Fig. 4.12), it is possible that the addition of water leads to preferential formation of prilocaine dimers held together by hydrogen bonds between a water molecule and the carbonyl oxygen of each prilocaine. The saturation water content for hydrated prilocaine (liquid L_1) is between 0.3 and 0.35, corresponding to one water molecule every two prilocaine moieties, (Rietveld et al., 2013a) consistent with our proposed scenario.

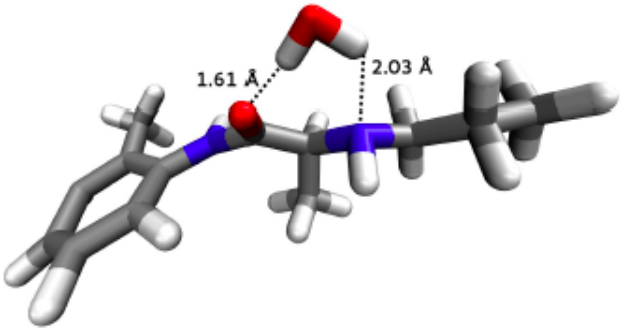

FIGURE 4.13: Plot depicting a single water molecule forming two hydrogen bonds, as donor to both -C=O oxygen and N2 amine nitrogen. (bottom) The distribution of orientations indicate that although the preferential orientation is somewhat broad, it is highly likely that a single water molecule will form two hydrogen bonds on prilocaine. Figure taken from reference Silva-Santisteban et al., 2017

4.4 Conclusions

The increase of relaxation times and that of T_g, as well as the decrease of σ_{dc}, are all indications that a tighter hydrogen bond network is present in hydrated prilocaine compared to the pure compound. However, a tighter H-bond network is likely present also in other hydrated systems displaying the usual plasticizing effect of water.

The formation of prilocaine-water complexes such as water-bridged monomers or dimers could instead rationalize the observed antiplasticizer effect, given that water-prilocaine complexes would display, with respect to pristine prilocaine, specific relaxation modes, higher molecular weight, and larger steric hindrance against reorientation, all factors which would enhance the glass transition temperature.

It is interesting to note that the two molecules that display an antiplasticizing water effect (prilocaine and N-ethyl acetamide) are both amides, in which the C=O group is actually part of a non-terminal peptide unit. Further studies on non-terminal amides could be helpful to investigate the role of the peptide-water interaction in the antiplasticizing effect of water. In order to investigate the veracity of the antiplasticizing effect caused by aggregation of dimers and monomers, experiments in confined systems have been carried out, as explained in Chapter 5.

Chapter 5

Prilocaine - H_2O confined system

5.1 Motivations for confining the system

The experiments and data analysis presented in Chapter 4 showed that the addition of water to the prilocaine liquid phase led to an antiplasticizing effect, portrayed by a significant increase of its T_g and α-relaxation time. It was hypothesized that the formation of prilocaine-water complexes such as water-bridged monomers or dimers could rationalize the observed antiplasticizing effect, given that water-prilocaine complexes would display, with respect to pristine prilocaine, combined relaxation modes, higher effective molecular weight, and larger steric hindrance against reorientation, all factors which would enhance the glass transition temperature. Nevertheless conclusive data on this regard are needed to test the hypothesis.

There is another motivation behind the study presented in this chapter. Not only bulk water is relevant for life as we know it, but also aqueous solutions in different types of geometrical confinements are key to understanding many processes. Since most of the water molecules in our bodies are never more than about 5 Å from other types of molecules, almost all water in our bodies can be considered as confined or interfacial (Middendorf, 1996). Studying the behavior of water in confined conditions is therefore of central importance in biology.

When absorbed by the human body, prilocaine binds to the intracellular surface of sodium channels and blocks the subsequent influx of sodium into the cell. This blocking prevents the propagation of an action potential and thus nerve function, resulting in the anesthetic effect of this drug. This blockage is reversible and when the drug diffuses away from the cell, the function of the sodium channel is restored and nervous signal communication reestablished (*https://www.drugbank.ca/drugs/DB00750*).

Understanding how the prilocaine molecule behaves in confined spaces, such as

sodium channels, may be helpful to develop more effective drugs and/or formulations of prilocaine itself.

Added to the intrinsic importance of both water and prilocaine in confined spaces, such system has been chosen for the current experiments in order to test the hypothesis of the formation of water bridged prilocaine monomers and dimers that may be causing the observed antiplasticizing effect. Molecular sieves of pore size allowing just a few (order of 2 or 3) prilocaine (PLC) molecules inside have been chosen, in order to test whether such structures are enough to see the antiplasticizing effect or if, on the contrary, a larger PLC-H_2O clusters are needed.

As shown by Silva-Santisteban et al., 2017 the length of the prilocaine molecule is about 12 Å whereas the diameter of its ring is estimated to be 5 Å. At the same time, the pores of the molecular sieves have, in average, a minimum effective diameter of about 5 Å. This means that whereas some holes could only allow one prilocaine molecule inside, many others would have room for a few water-bridged prilocaine monomers and/or dimers. In order to gain more insight into these structures and their dynamics, BDS and DSC experiments have been carried out on pure and hydrated prilocaine confined inside molecular sieves.

Such systems represent a relevant environment not only for understanding the behavior of PLC and water under confinement, but also to test the origin of the results presented on the previous chapter. The current results show that the antiplastization of prilocaine by the addition of water is still observed in the confined material.

5.2 Sample preparation and experimental techniques

The prilocaine and hydrated prilocaine solutions mentioned in Chapter 4 were analyzed through BDS and DSC, both in the bulk and confined inside nanoporous molecular sieves.

The experiments presented on this chapter were done in the facilities of Centro de Física de Materiales (CFM) in Donostia, Vasque Country. The BDS and DSC experiments in pure and hydrated PLC, previously shown in Chapter 4 were repeated at the CFM, in order to identify any difference that may arise due to the use of different measuring equipment.

5.2.1 Sample Preparation

Prilocaine hydrochloride was purchased from Sigma Aldrich and purified to obtain pure prilocaine: (N- (2 methylphenyl) - 2(propylamino) propanamide, chemical formula: $C_{13}H_{20}N_2O$). The pure prilocaine and hydrated prilocaine solutions described in Chapter 4 were analyzed through ambient pressure BDS and DSC, both in the bulk and confined systems.

Bulk PLC and hydrated PLC

The saturated solution was achieved by mixing equal amounts of purified water and pure prilocaine, melting it at 323 K and letting it rest in a thermal bath at the same temperature for 2 days. This allowed the system to separate into the two phases, prilocaine-rich and water-rich solutions, as explained in Chapter 4.

Confined PLC and hydrated PLC

Molecular sieves were used as confining environment. These are generally made of a crystalline substance with pores of molecular dimensions which permit the passage of molecules below a certain size. Molecular sieves are commercialized in the shape of beads of different geometries. In the present work tubular beads provided by *Sigma Aldrich*, made of disordered silicates were used. They present an approximate diameter of 2 mm and length of about 7 mm. The pores of the confining system do not have a defined geometry, but present an average effective diameter of 5 Å.
In order to ensure that no water (moisture) is initially present inside the confining material, the beads were dried in a vacuum oven at 373 K for two days. The dried molecular sieves were then immersed into two different containers with liquid pure and hydrated prilocaine, respectively. The whole process was carried out inside a sealed vacuum glove box, in order to prevent hydration. The flasks were hermetically sealed and left inside the vacuum chamber at a temperature of 323 K for two months, in order to allow the liquid to fill the pores of the molecular sieves.
With the aim of ensuring that the BDS and DSC measurements were done over the material filling the molecular sieves, and not over any remains of liquid that may have been left on their surface, the molecular sieves studied were first cleaned. The studied beads were briefly washed individually in ethanol and quickly dried with tissue paper. Then they were put either into the DSC capsules or BDS electrodes, as

appropriate.
Five different samples were studied by each technique; bulk prilocaine, bulk hydrated prilocaine, confined prilocaine, confined hydrated prilocaine and empty molecular sieves.

5.2.2 Experimental Techniques

Differential Scanning Calorimetry (DSC)

A differential scanning calorimeter DSC TA Instrument Q1000 as described in Chapter 3 was used in standard mode to control the glass transition and possible crystallization of the samples. Standard DSC measurements were performed using cooling and heating rates of 8 K/min. Hermetic aluminum pans provided by Perkin Elmer were used for all the materials with sample weights of about 10 mg. In the case of confined samples, empty molecular sieves were used as reference. For bulk samples, empty capsules were used for this purpose.
The thermal protocol used was the same as the one presented in Chapter 4, section 4.3.1.

Broadband Dielectric Spectroscopy (BDS)

In order to study the dynamics in these systems, ambient pressure broadband dielectric spectroscopy measurements in the frequency range($10^{-2} - 10^{7}$) Hz were carried out. The equipment used was a Novocontrol Alpha analyzer, as the one described in Chapter 3. The samples were placed between parallel gold-plated electrodes with a diameter of 30 mm. The sample thickness was typically 0.1 mm. The sample temperature was controlled with stability better than 0.1 K.
Before depositing the sample into the electrodes, they were warmed up to 323 K in order to prevent the material under study to crystallize. The impedance analyzer was precooled to 200 K, and the bulk and confined samples were placed inside. Isothermal frequency scans recording the complex dielectric susceptibility were performed every 2 or 3 K until ambient temperature was reached. Measurements on empty molecular sieves were done every 5 K from 140 K to ambient temperature.

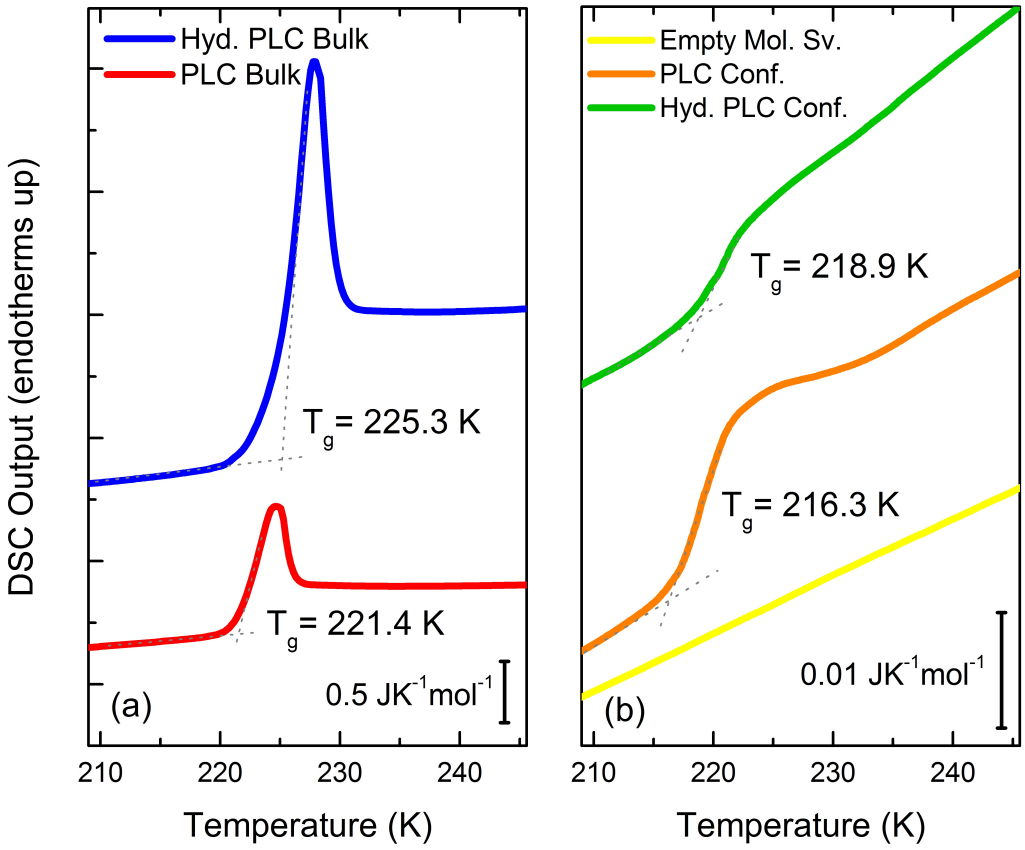

FIGURE 5.1: Effect of water and confinement on the glass transition temperature of prilocaine. DSC scans measured upon heating at 8 K/min right after aging during 1 hour at 215.2 K. (a) DSC scans of pure (red) and hydrated prilocaine (blue) in bulk state. (b) DSC scans of samples confined in molecular sieves with pore diameter 5Å. Orange: pure prilocaine. Green: hydrated prilocaine. Yellow: empty molecular sieves. Dotted gray lines indicate the tangents used to mark the onset glass transition temperature, T_g. All T_g values have an error of $\pm 0.5K$.

5.3 Results

5.3.1 DSC

Both bulk and confined systems were analyzed by DSC using the same thermal protocol explained in Chapter 4, section 4.3.1. Dried empty molecular sieves were analyzed as well so as to have a reference of the signal produced by the porous matrix. The heating scans corresponding to step 11 of the thermal protocol are shown in figure 5.1.

The DSC scans measured upon heating at 8 K/min right after aging during 1 hour at 215.2 K show the effect of water and confinement on the glass transition

temperature (figure 5.1). Panel (a) portrays with a red trace the characteristic glass transition of pure bulk prilocaine, while the blue line shows the thermogram for hydrated prilocaine. Gray dotted lines mark the tangents used to obtain the onset of the glass transition temperatures, which have been found to be (221.4 $\pm$ 0.5) K and (225.3 $\pm$ 0.5) K for the pure and hydrated samples, respectively.
DSC scans of samples confined in molecular sieves with 5Å pore diameter and of the empty molecular sieves are shown in panel (b). The yellow line corresponds to the empty confining matrix, while the orange and green traces correspond to the pure and hydrated confined substance, respectively.
The scan of the empty molecular sieves show that the confining material does not experience any phase transition in the temperature domain studied. On the other hand, by observing the T_g values obtained for the confined pure and hydrated PLC, (216.3 $\pm$ 0.5) K and (218.9 $\pm$ 0.5) K respectively, it can be noted that the antiplasticizing effect observed in bulk samples is visible also in the confined material. The DSC thermograms shown in figure 5.1 present a decrease in T_g in the confined samples with respect to the bulk ones. This decrease is significant and accounts to about 6 K for both pure and hydrated PLC.

5.3.2 BDS

The bulk and confined dynamics of prilocaine and hydrated prilocaine were studied by performing the experiments outlined in section 5.2.2.

Bulk PLC and hydrated PLC

Bulk PLC and hydrated PLC were analyzed by BDS, as done on the previous experiments presented in 4.3.2. The dielectric loss spectra were fitted as the sum of a relaxation process, represented by an Havriliak-Negami profile, and a background proportional to reciprocal frequency representing the dc conductivity.
The Arrhenius plots of both anhydrous and hydrated prilocaine follow a Vogel-Fulcher-Tammann dependence on temperature, given by eq 1.7. The extrapolated T_g are (217.9 $\pm$ 0.5) K for pure prilocaine, and (219.7 $\pm$ 0.5) K for hydrated prilocaine. The very small difference (approximately 0.4 K) between these values and those obtained in Chapter 4 is likely to reside in slight differences in the synthesis process of the PLC drug and the different apparatus used for the experiments.

The T_g values obtained by this method are lower than those found with DSC, because in BDS cooling of the sample is done in a much more rapid rate, since the liquid sample is placed inside the precooled experimental setup. This produces a less stable glass that shows a lower T_g value.

Confining matrix

In order to characterize the confining system, and to be able to separate the signal arising from it, from that coming from the sample, the dried molecular sieves were analyzed. Measurements were done every 5 K from 140 K to ambient temperature. Three Cole-Cole functions were needed to account for all processes in the confinement material (panel (a) figure 5.3). Such relaxations probably correspond to Maxwell-Wagner-Sillars polarization processes, which arise from the space-charge polarization caused by accumulation of charges at regions with different characteristics (conductivity, permittivity) such as pores and interstitial space between molecular sieves.

Confined PLC and hydrated PLC

Figure 5.2 shows the dielectric spectra obtained for pure PLC confined in molecular sieves for temperatures ranging from 243 to 258 K. Just as in the bulk case, a prominent relaxation can be identified in the high frequency portion of the spectra. This peak shifts to higher frequencies with increasing temperature.

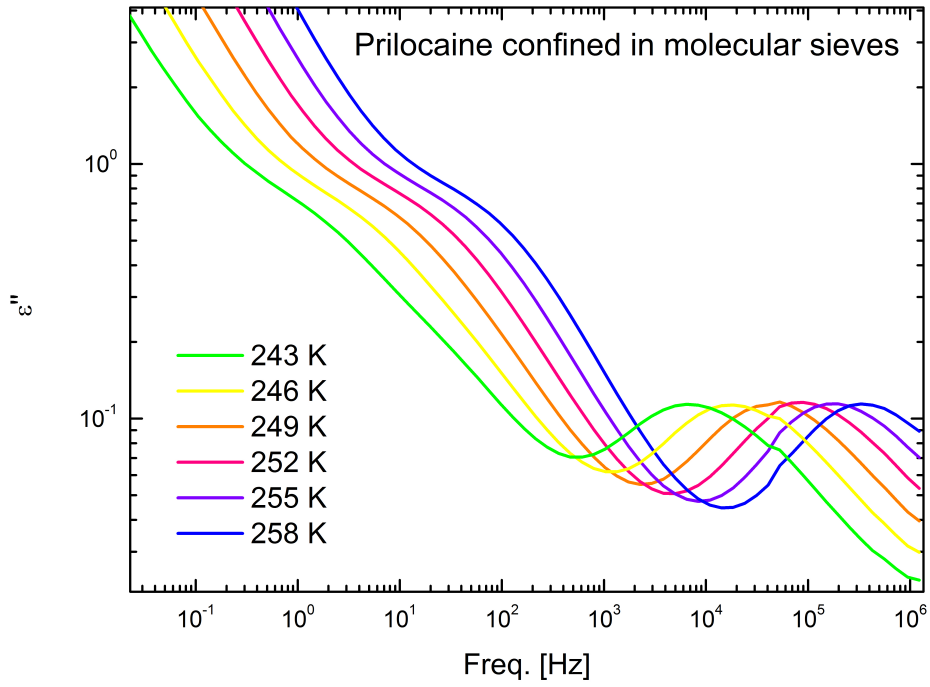

FIGURE 5.2: Dielectric loss spectra of pure prilocaine confined in molecular sieves of 5Å pore size. Temperatures go from 243 to 258 K, every 3 K.

As indicated above, empty molecular sieves measurements were fitted with 3 Cole-Cole relaxations, while both pure and hydrated bulk PLC (without confinement) were fitted with an HN profile for the primary relaxation and a background for conductivity. Figure 5.3 shows the comparison between the dielectric loss profiles obtained at 240 K for empty molecular sieves, bulk PLC and confined prilocaine in panels (a), (b) and (c), respectively. In all cases empty dots present data points and the overlapping traces indicate the resulting total fit for each spectrum.

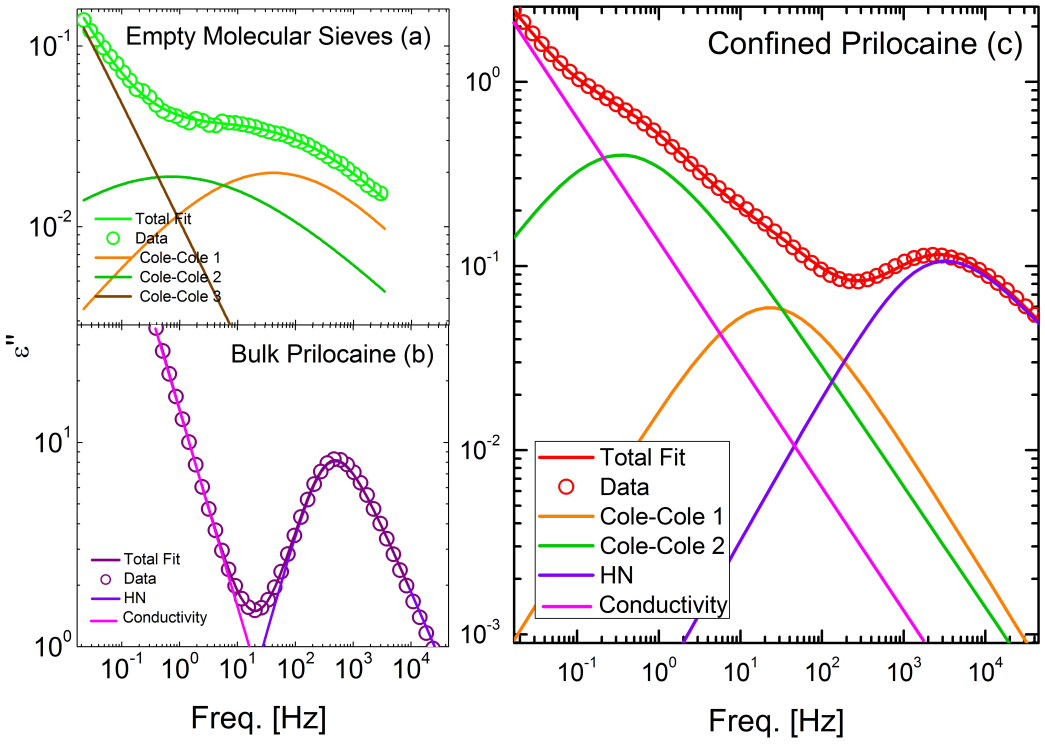

FIGURE 5.3: Dielectric loss as a function of frequency at 240 K. In all cases empty dots represent data points and the overlapping traces indicate the resulting total fit, sum of the fitting functions used for each measurement. (a) Empty molecular sieves. Three Cole-Cole functions (orange, green and brown) add up to the resulting fitting function. (b) Bulk PLC. An HN profile (violet) fits the primary α relaxation and a conductivity component (pink) is added. (c) Confined PLC. Two Cole-Cole processes (orange and green), added to an HN relaxation (violet) and conductivity (pink) were used to fit the data.

Three relaxation peaks and a dc conductivity profile were identified in the data shown in panel (c) of figure 5.3, corresponding to the measurement of confined prilocaine. The relaxation observed at highest frequency was fitted with an HN function, motivated by the observed α relaxation behavior of bulk prilocaine (panel (b) and Chapter 4). The other two peaks were fitted with Cole-Cole functions so as to account for the interfacial processes that arise from the molecular sieves as a confinement matrix (panel (a)). The process indicated as Cole-Cole 3 in figure 5.3 (a) is hidden at all temperatures by the conductivity background in the case of confined PLC, and for this reason only two Cole-Cole functions have been used in this case, and not three.

The strength of the HN process compared to that of the Cole-Cole functions depends on several factors, such as the size and geometry of the pores, and the amount of

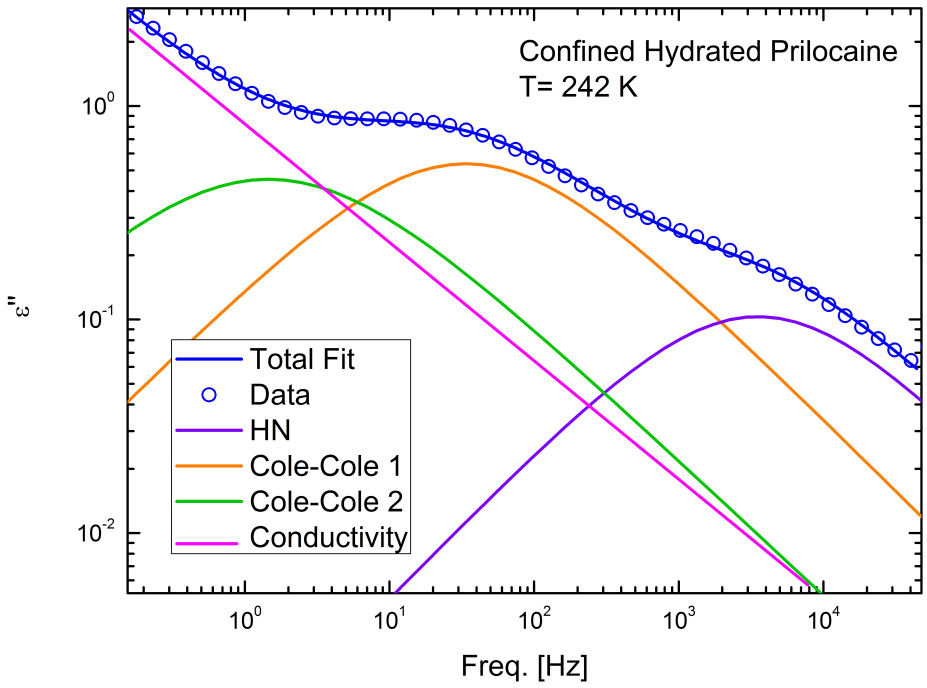

FIGURE 5.4: Data (empty circles) and fit (full lines) of the dielectric loss spectra of hydrated PLC confined in molecular sieves obtained at 242 K. Green and orange lines portray the two Cole-Cole relaxations used to fit the data, while the violet and pink lines show the HN and conductivity contribution respectively.

them successfully filled with solution.

Analogously, the data of confined hydrated PLC were fitted using an HN relaxation, two Cole-Cole functions and a dc conductivity contribution. Figure 5.4 shows in blue empty dots the experimental values obtained at 242 K, and the fitting trace sum of all contributions in blue. In the case of pure confined prilocaine, the Cole-Cole 3 function observed at low frequencies in the empty molecular sieves is hidden by the conductivity contribution at all measured temperatures.

Dielectric spectra Comparison

In order to correctly identify each relaxation process, an Arrhenius plot showing all relaxations is shown in figure 5.5. Red circles correspond to the α relaxation times in pure prilocaine, and blue circles show α relaxation times in hydrated prilocaine. Empty circles represent the α relaxations of bulk samples, while full circles portray the same process in confined samples. Continuous and dotted lines are the VFT function used to fit the processes. Triangles and squares represent the Cole-Cole

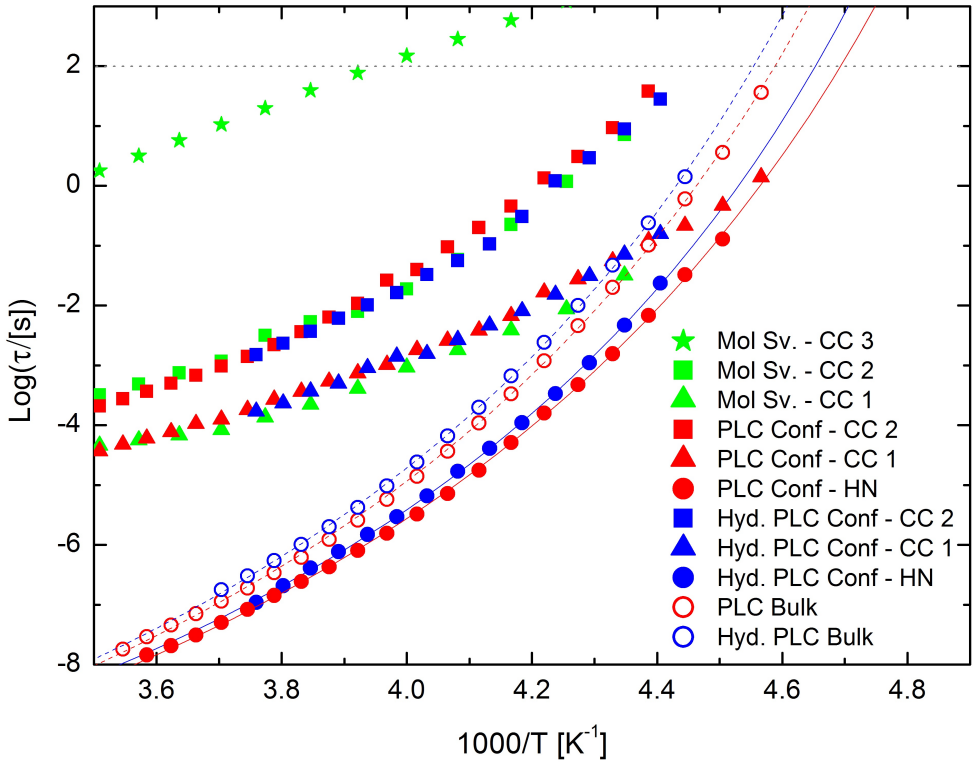

FIGURE 5.5: Arrhenius plot of the relaxation times τ of the fitting functions used for pure and hydrated prilocaine both in the bulk and confined cases, as well as for the empty molecular sieves. Red circles correspond to the α relaxations in pure prilocaine, and blue circles to the α relaxations in hydrated prilocaine. Empty circles represent the α relaxations in bulk samples, while full circles portray the same process in confined samples. Full and dotted lines are fits with the Vogel-Fulcher-Tammann function (Eq. 1.7). Triangles and squares represent the Cole-Cole process 1 and 2 of the molecular sieves respectively, where green corresponds to the empty sieves and colors red and blue to sieves filled with prilocaine and hydrated prilocaine, respectively. Finally, green stars represent the Cole-Cole process number 3, only observed in the empty confining material.

processes 1 and 2 of the molecular sieves respectively. Of these green markers correspond to the empty material and red and blue markers to prilocaine and hydrated prilocaine in the confined systems respectively. Finally, green stars represent the Cole-Cole process number 3, which, as previously explained, was only identified in the empty molecular sieves.

It may be observed that the relaxation times corresponding to the Cole-Cole functions overlap quite reasonably, bearing in mind that the geometry, position and amount of the molecular sieves in the three experiments (on the empty molecular sieves, confined PLC and confined hydrated PLC) is not necessarily the same. The

superposition of the characteristic time of the processes is enough though to identify such relaxations with a process that arises from the confinement environment and not the confined material.

The relaxation times marked by the filled circles were found to follow a Vogel-Fulcher-Tammann temperature dependence, as the main relaxation observed in the bulk case (Eq. 1.7). Given the resemblance of these processes in the confined material to those of PLC and hydrated PLC in the bulk material, such processes have been identified as the collective primary α relaxations in the confined systems.

The extrapolation of the VFT fits to a τ of 100 s. allows one to find the extrapolated T_g values of each substance, as previously done. At the same time, the curvature of the VFT plot in the same region gives the fragility index m in each material. Table 5.1 shows the obtained values for the fragility parameters m and extrapolated T_g values in each case.

Environment	Substance	Extrapolated T_g (K)	Fragility m
Bulk	PLC	217.9 ± 0.5	17 ± 2
	Hyd. PLC	219.7 ± 0.5	18 ± 2
Confined	PLC	213.0 ± 0.5	16 ± 2
	Hyd. PLC	214.8 ± 0.5	17 ± 2

TABLE 5.1: Fragility m and extrapolated T_g calculated for each of the studied systems.

It can be observed in Fig.5.5 that the curvatures of the hydrated samples, both in the bulk and confined systems, are higher than that of the pure compound. This entails a slightly higher kinetic fragility index (Angell, 1985a; Böhmer et al., 1993) (see chapter 1 section 1.4.1) m of hydrated prilocaine compared with the pure compound, that is visible not only in the bulk material, but remains when confining the system.

5.3.3 Comparing DSC and BDS

After evaluating the results obtained both by BDS and DSC experiments on the bulk and confined systems, it may observed that:

PLC vs. hydrated PLC

- T_g is approximately 3.9 K higher in hydrated PLC bulk than PLC bulk by DSC and 1.8 K by BDS.
- T_g is approximately 2.6 K higher in hydrated PLC bulk than hydrated PLC confined by DSC and 1.8 K by BDS.

Confined vs. bulk system

- T_g is approximately 5.1 K higher in PLC bulk than PLC confined by DSC and 4.9 K by BDS.
- T_g is approximately 6.4 K higher in hydrated PLC bulk than hydrated PLC confined by DSC and 4.9 K by BDS.

5.4 Discussion

5.4.1 PLC vs. hydrated PLC: Anti-plasticizing effect of water

Addition of water to pure PLC produces a systematic and consistent effect of lowering T_g that could be observed both by DSC and BDS techniques, not only for the bulk substances (as observed in Chapter 4) but also in the confined one.
The current results in confined systems strongly suggest that the addition of water to the prilocaine molecules produces the formation of water bridged prilocaine monomers and dimers, rather than larger water-prilocaine clusters, in which the water-mediated interactions make a more compact structure and bring the PLC molecules closer together. This effect produces an antiplasticizing effect.

5.4.2 Bulk vs. confined dynamics: The effect of the extension of the H-bond network

By confining the PLC and hydrated PLC samples the observed T_g values were lowered by around 5 K with respect to the bulk. This effect could be consistently observed with both experimental techniques used.
The reason for this lowering in the glass transition temperature resides very likely in the fact that within the bulk system, prilocaine and water molecules are linked through strong hydrogen bonds. When confining the system, the amount of H bonds diminishes and hence the water-PLC clusters are less stable. An equivalent process takes place at the surface of ice. H bonds on the superficial layer are not enough to

hold the ice structure of the surface upon heating. The disruption of the hydrogen bonding network at the interface causes superficial ice to melt at a higher temperature than bulk ice (Kroes, 1992). Analogously, the few molecules inside each hole in the molecular sieves prevent the formation of an extended H-bond network, leading to a smaller variation in T_gs in the confined system compared to the ones observed in the bulk material.

5.5 Conclusions

The experiments performed on bulk PLC and hydrated PLC presented in Chapter 4 suggested that the antiplasticizing effect observed by the addition of water to the PLC molecule could probably be caused by the formation of prilocaine monomers and dimers connected by a water molecule binding to the O-C of the PLC molecule. The formation of these units would cause the relaxation dynamics of hydrated prilocaine to be different from that of the pure compound, given that these complexes would have a higher molecular weight and enhanced hindrance.

The previously observed antiplasticizing effect of water in the bulk prilocaine substance was systematically observed in the confined system in the experiments shown in the present chapter. By confining PLC and hydrated PLC solution, only a few PLC molecules fill the pores of the molecular sieves. These molecules are responsible for the collective relaxation observed as the α relaxation in the BDS measurements and thus for the glass transition peak in the DSC. This implies that only small clusters are needed in order to observe the antiplasticizing effect. Bigger molecular structures are very unlikely to form in the confined system because of the average size of the cavities. Consequently, as suggested by the experiments in Chapter 4, the reason for the change in dynamics by the addition of water, has to be the formation of water bridged prilocaine monomers and dimers.

Not only the addition of water to the PLC molecule produces a lowering in T_g, but also confining the system triggers the same effect. This implies that the effects of confinement dominate over those of the surface interaction. The smaller extent of the H-bond network with respect to the bulk material, produces a less stable amorphous structure within the pores of the molecular sieves, leading to a lower glass transition temperature.

The experiments presented in this chapter confirm the origin of the antiplasticizing effect previously observed in the bulk substance.

Chapter 6

Stiripentol

6.1 Introduction

6.1.1 The importance the amorphous phase in drugs

By means of formulation in amorphous phase, many drugs with originally poor aqueous solubility have reached the drug development stage during the last decade (Yin et al., 2005; Qian et al., 2007; Wu and Yu, 2006). Although the detailed microscopic mechanisms governing the kinetic stability of amorphous Active pharmaceutical ingredients (API's) remain unknown, the crystallization kinetics appears to be determined by a large number of factors such as preparation method, thermal and mechanical treatments employed during formulation, storage temperature, application of pressure, or exposure to humidity (Patterson et al., 2005; Yu, 2001). It is then of utter importance to find out which are the mechanisms taking place in the amorphous to crystalline transformation, so as to be able to find optimum production and storage conditions of the formulated drug (Aso, Yoshioka, and Kojima, 2000; Hancock, Shamblin, and Zografi, 1995; Andronis and Zografi, 1998; Yoshioka and Aso, 2005; Alie et al., 2004; Kolodziejczyk et al., 2013; Wojnarowska et al., 2013b).

6.1.2 Thermodynamics and kinetics of the crystallization process

Many factors are involved in the stability of a substance. In this chapter the crystallization kinetics and the molecular dynamics of a material will be studied. Thermodynamic quantities such as differences in free energy between the phases involved and interfacial energies, play a role as they determine the stable phase of the system and the energetic cost of having a mixed-phase sample. However, thermodynamic quantities mostly reflect equilibrium behavior, and only to a smaller extent the kinetics to reach the equilibrium state.

It is well-known that there are two main relevant factors for the recrystallization process, thermodynamics and kinetics (Graesera et al., 2009). In this respect, it is interesting to note that a recent review indeed suggested that the molecular mobility (rather than thermodynamic quantities) appears to be the most important factor governing the crystallization rate (Grzybowska, Capaccioli, and Paluch, 2016). It is also recognized that the complexity of the problem makes difficult, at present, the establishment of clear correlations between molecular mobility and physical stability. This happens mainly due to two factors. Firstly, the complexity of the involved molecular entities and their inter- and intramolecular interactions. Secondly, due to the different time scales involved in amorphous materials, not only the so-called 'global mobility' which refers to the structural relaxation (α-relaxation).

As for the thermodinamical aspect of recrystallization, lowering the temperature of the supercooled liquid decreases the steady state nucleation and growth rates, but, according to the kinetics, it increases the liquid's viscosity which is responsible for delaying the recrystallization (Grzybowska, Capaccioli, and Paluch, 2016). The problem is even more difficult because nucleation and growth are commonly simultaneous effects that cannot be set apart. The case of Stiripentol is an unusual and outstanding case because nucleation is unlikely and only growth plays a role within the recrystallization process.

Possible correlations between the crystallization kinetics and the molecular dynamics have been analyzed, finding that the crystallization time has a sublinear dependence on the cooperative relaxation time, as is the case in other substances reported in the scientific literature. This could suggest a general correlation of these parameters, at least at temperatures above T_g. The low nucleation rate is an interesting feature in the quest of possible mechanisms that allow enhancing the physical stability of amorphous drugs.

6.1.3 Stiripentol

Stiripentol (STP; 1-(1,3-benzodioxol-5-yl)-4,4-dimethyl-1-penten-3-ol, $C_{14}H_{18}O_3$) is an anticonvulsant drug, structurally unrelated to the currently available antiepileptics (Trojnar et al., 2005). Figure 6.1 depicts the drugs's molecular structure. Stiripentol is used for the treatment of Dravet syndrome or severe myoclonic epilepsy in infancy (SMEI) in conjunction with sodium valporate and clobazam when seizures

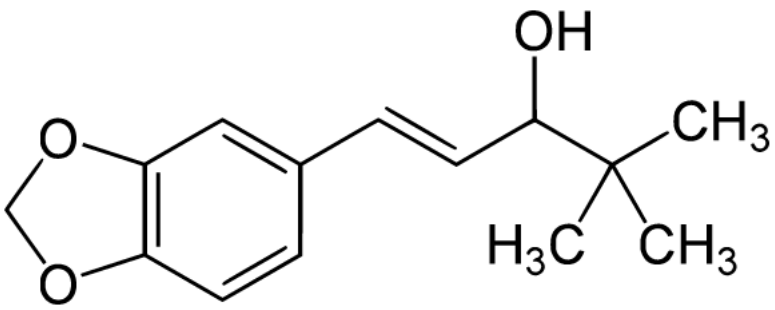

FIGURE 6.1: Stiripentol's molecular structure.

are not adequately controlled with the association of these two medications (Wirrell et al., 2013; Stiripentol, 2002).

STP is practically insoluble in water and aqueous fluids (Afifi, 2015; Bebin and Bleck, 1994), and hence it is commercialized in the form of gelatin capsules or in the form of granules for a drinkable suspension (Diacomit®). The state of the art in STP research is of great impact and relevance. Around 1% of the world's population suffer from epilepsy of different types, among which one third still don't have effective anti-epileptic drugs clinically available. It has been recently reported that STP is an LDH inhibitor that suppresses neural activity and seizures, and is in fact the first antiepileptic drug that acts on metabolic pathways, mimicking the effect of ketogenic diets used in drug-resistant epilepsy (Sada et al., 2015).

Given the low solubility of STP in water, it might be interesting if its amorphous phase could be stabilized to improve its dissolution rate in the body and hence its bioavailability, while avoiding crystallization. In this work, the molecular dynamics and isothermal crystallization of STP have been studied and the possible correlation between the crystallization time and the characteristic time of molecular relaxations has been analyzed. Despite the fact that the crystallization kinetics does not follow the Avrami law (see section 1.3.2), the same sublinear correlations between the cooperative relaxation time and the crystallization time observed in other amorphous drugs have been found (Mehta et al., 2016a; Johari, Kim, and Shanker, 2007; Larini et al., 2008; Bhugra et al., 2008). Finding a correlation model between the cooperative alpha relaxation time and the crystallization time would be of great interest since it would help predicting the crystallization kinetics of a substance at different temperatures, enabling the development of stabilization protocol approaches.

6.2 Experimental Techniques

STP was acquired from Biocodex Laboratoire with purity higher than 99%.

6.2.1 DSC

Differential scanning calorimetry experiments by means of the Q100 from TA Instruments described in Chapter 3 were done by melting, cooling and reheating STP samples inside an aluminum capsule. Measurements were performed in the temperature range from 203 K to 393 K, with a heating/cooling rate of 2 K/min with masses around 10 mg and under nitrogen atmosphere.

6.2.2 BDS

The *Novocontrol Alpha analyzer* for ambient pressure measurements described in Chapter 3 was used for Broadband Dielectric Spectroscopy measurements. The sample was placed in a stainless steel parallel-plate capacitor specially designed for the analysis of liquids, with the two electrodes kept at fixed distance by means of silica spacers of 50 μm diameter. Two different BDS experiments were carried out, in order to study the relaxation dynamics and the crystallization kinetics of the material. In the former case, the sample in crystalline state was placed in the capacitor, melted at 373.2 K, and quenched to 120 K inside cryostat. Successive isothermal measurements were done every 2 K, from 180 K to 296 K in the frequency (f) range between 10^{-2} Hz to 10^{6} Hz.

The second BDS experiment, designed to study the isothermal crystallization kinetics of STP, consisted in measuring the decrease of strength of the dielectric loss as a function of time during the crystallization of the supercooled material at different fixed temperatures. To this end, the molten sample was placed inside a precooled cryostat at 233 K (about 13 K below T_g) and then the temperature was raised at a rate of 10 K/min until reaching the desired temperature of the experiment, (T_e). The recrystallization was measured at five different T_e temperatures between 273 and 293 K in the frequency range from 10^2 to $10^6 Hz$. These dielectric measurements were carried out on the same sample, which was re-melted and re-vitrified prior to each experimental run.

6.2.3 X-Ray powder diffraction

In order to discard the existence of a possible polymorphism of STP at ambient pressure, high-resolution X-ray powder diffraction data were recorded. A horizontally mounted INEL cylindrical position-sensitive detector (CPS-120) with a Debye-Scherrer geometry was used, with angular step of ca. $0.029^\circ - 2\theta$ over a 2θ-range from 2 to 60°. The system works with monochromatic $CuK\alpha_1$ radiation ($\lambda = 1.5406$ Å, 40 kV and 25 mA) and is equipped with a liquid nitrogen 700 series Cryostream Cooler from Oxford Cryosystems (accuracy of 0.1 K). STP samples were loaded at ambient conditions into a 0.5-mm-diameter Lindemann capillar, which could rotate around its axis during data collection in order to minimize the effect of preferential orientation.

6.2.4 Optical Microscope

An optical microscope and an annexed web cam were used to follow and register the crystallization process of STP. The collected images provided insightful information about the kinetics of the crystallization transformation.

6.3 Results and discussion

6.3.1 Relaxation Dynamics

Primary and secondary processes

Figure 6.2 shows the loss spectra, i.e imaginary part of the complex relative dielectric permittivity, of STP in its supercooled liquid state and glass state, as measured upon heating from low temperature (only some measurements from 140 K to 282 K are shown, for clarity).

STP exhibited three dynamic processes, namely a collective primary relaxation at lower frequency (α process), a secondary dynamics at higher frequency (β process) and a γ relaxation arising from intramolecular motions. The acquired dielectric loss spectra were analyzed by fitting the loss features with Havrilak-Negami (HN) functions (equation 3.8 in Chapter 3). A background proportional to reciprocal frequency was added to model the conductivity contribution to the loss spectra.

The primary relaxation is observed, visible as an asymmetric peak in the loss spectra of Fig. 6.2 (a). This relaxation corresponds to the collective reorientation of the STP

molecules, as will be shown later. Upon decreasing the temperature, this feature shifts to lower frequency. At low-temperature a second relaxation (β process) is observed, indicated by the arrow at the bottom of panel (a) and in the middle of panel (b). Finally, for temperatures lower than 240 K, another relaxation (γ) can be observed, as marked in panel (b). The two latter relaxations were fitted with *Cole-Cole* functions (Eq. 3.5 in Chapter 3).

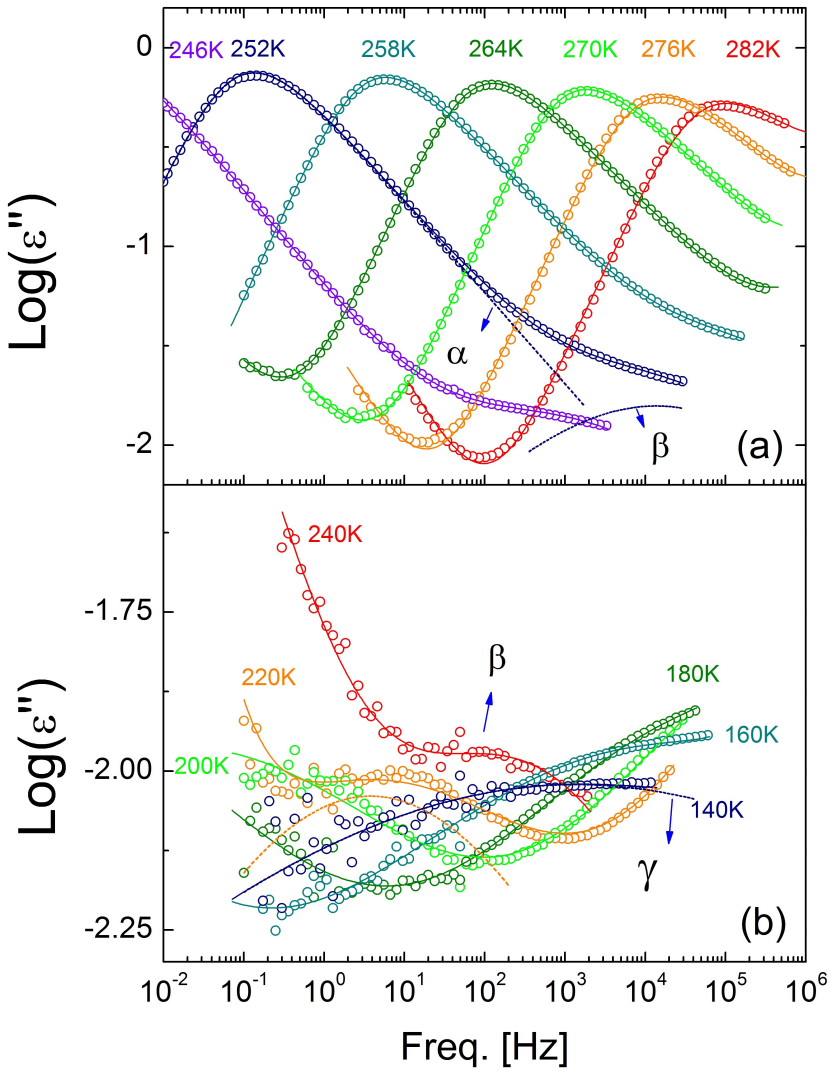

FIGURE 6.2: (a): Loss spectra of STP measured between 246 and 282 K. Fits of α and β relaxations are displayed for the spectrum at 252 K. (b): Loss spectra of STP measured between 140 and 240 K. Fits of β and γ relaxations can be seen in the measurements at 220 and 140 K, respectively.

The Arrhenius plot of the characteristic times (τ) corresponding to α, β and γ relaxations, as obtained from the fitting procedure, is shown in Fig. 6.3. The γ relaxation follows Arrhenius behavior with an activation energy $E_a = 23.5 \pm 0.1$ J/mol

K (see Chapter 1). The β relaxation displays two different Arrhenius regimes with $E_a = 98.2 \pm 0.2$ J/mol K below T_g, and $E_a = 249 \pm 5$ J/mol K above T_g.

Insight into the α relaxation

The continuous line is the fit of τ_α using the Vogel-Fulcher-Tammann equation, as formulated in Eq. 1.7 in Chapter 1. The obtained values for the corresponding parameters of the fits were: $Log(\tau_0/(s)) = -16.2 \pm 0.3$, $D = 10.3 \pm 0.5$ and $T_{VF} = 198 \pm 1$ K. The horizontal dashed line indicates the value of τ_α which is conventionally taken to mark the glass transition temperature ($Log(\tau_\alpha) = 2$, *i.e* $\tau_\alpha = 100$ s). The intersection of the VFT fit and this dashed line gives a glass transition temperature of $T_g = 246.2 \pm 0.5$ K.

The inset of Fig. 6.3 (a) shows the calorimetry thermogram of STP, which was acquired upon heating from below T_g, after previously cooling the sample from the molten state at a rate of $2K/min$. The arrow indicates the onset T_g value obtained from the two tangents (dashed lines), which is 248 ± 1 K, in agreement with the data obtained from the BDS experiments and with the previously reported T_g value (Céolin et al., 1991).

In agreement with the VFT model (see 1.4.1), T_{VF} is lower than T_g. The VFT temperature dependence becomes more pronounced when approaching the glass transition, which is a typical feature of correlated glass forming systems.

The kinetic fragility index m, can be obtained by using equation 1.8 (Böhmer et al., 1993). For the case of STP this parameter has a magnitude of $m = 93 \pm 7$. This drug is then a fragile glass former.

Insight into the secondary relaxations

The interpretation of secondary relaxations is not as straightforward as for the primary one; a secondary relaxation may relate either to intramolecular motions involving the displacement of polar side-groups, or else it may be a Johari-Goldstein relaxation, as seen in 2.2.2. The latter type of process involves the whole molecule and can be interpreted as the single-molecule relaxation, precursor of the cooperative α-relaxation according to the Coupling model (Ngai and Paluch, 2004; Ngai, 1998; Ngai, 2011; Ngai, 2003; Capaccioli et al., 2012b, see 2.2.4).

For the obtained shape parameters (α, β) of the HN function employed to fit the primary relaxation, and by using equations 2.8 and **??** the corresponding time τ_{CM} is

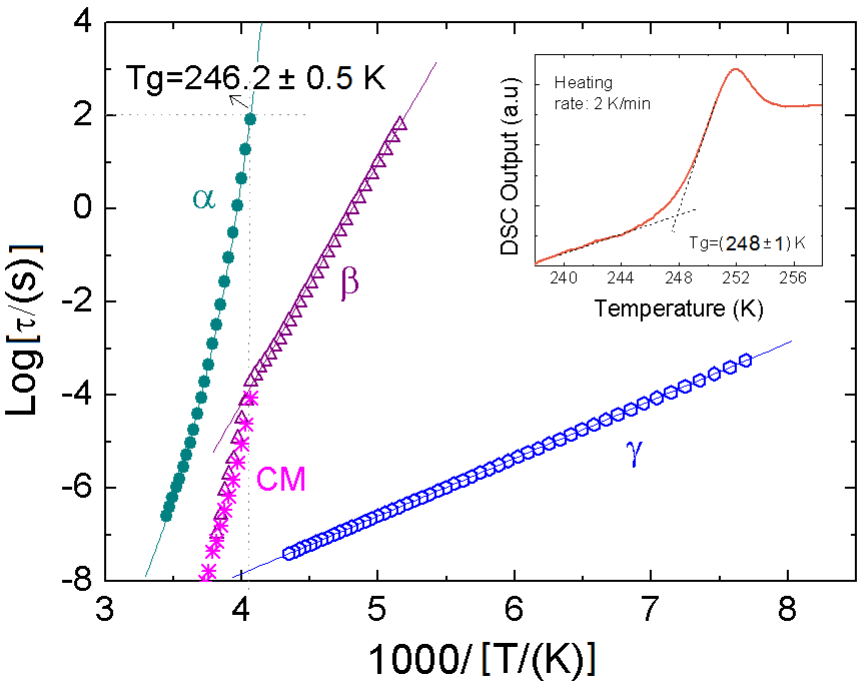

FIGURE 6.3: Arrhenius plot of the primary (α, filled green circles) and secondary (β, purple triangles and γ, blue empty circles) relaxation times, as extracted from the loss spectra displayed in Fig. 6.2. The continuous green line is the fit of τ_α using the Vogel-Fulcher-Tammann equation 1.7. The horizontal dashed line indicates the glass transition temperature. Pink asterisks portray the values obtained for τ_β using the Coupling model (see text) (Ngai, 1998; Ngai, 2007). Inset: DSC thermogram acquired upon heating from the glass. The arrow indicates the onset T_g value obtained from the two tangents shown with dashed lines.

obtained. The results are shown in the Arrhenius plot in Fig. 6.3 (pink asterisks). The calculated Coupling Model values are virtually identical to the experimental ones. Hence, the β relaxation can be considered the precursor of the α process and it is a whole-molecule process. Consequently, the observed γ process must be an intramolecular process, linked to the dynamics of a subpart or side-group of the non-rigid STP molecule.

6.3.2 Crystallization kinetics

Isothermal crystallization through BDS experiments

In order to characterize the crystallization process from the supercooled liquid state into the stable crystalline state, we performed experiments at five fixed temperatures (T_e) above T_g, namely: 273.0, 275.5, 278.0, 283.0 and 293.0 K ($\pm$ 0.1) K. The decrease of $\Delta\epsilon$ over time (at a fixed temperature) is a quantitative measure of the amorphous fraction of the sample and thus of the kinetics of the (isothermal) recrystallization process, since the number of molecules participating in the cooperative α relaxation is proportional to the dielectric strength $\Delta\epsilon$ (Kremer and Schönals, 2002). During crystal growth, in fact, some molecules are removed from the supercooled liquid phase (where they are mobile), and form crystallites (where all motion stops). As an example, Fig. 6.4 shows the real *(a)* and imaginary *(b)* part of complex dielectric permittivity, ϵ' and ϵ'' respectively, recorded at T_e=278.0 K in consecutive spectra (one every 190 seconds, approximately) during crystallization. The arrows indicate the spectral changes as crystallization progresses.

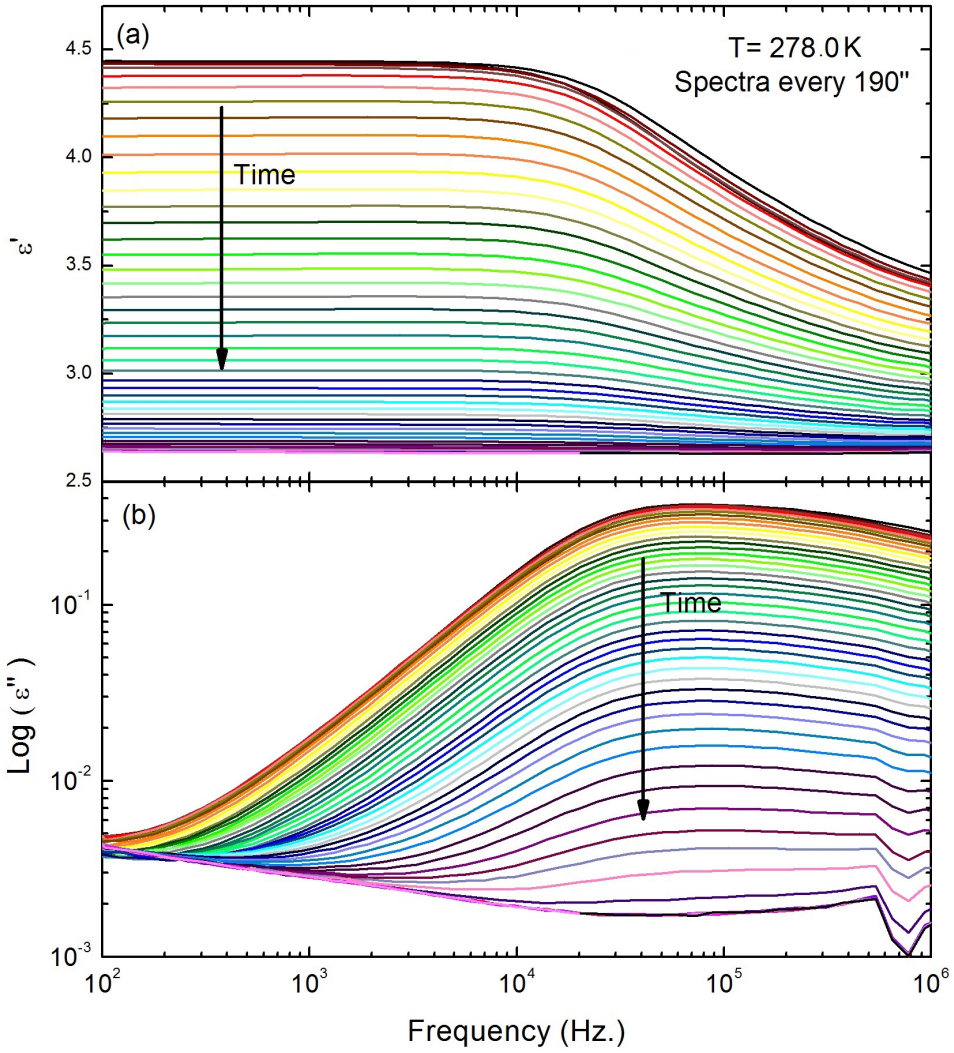

FIGURE 6.4: Spectra of the real *(a)* and imaginary *(b)* part of complex dielectric permittivity, ϵ' and ϵ'' respectively, recorded at T_e=278.0 K every 190 seconds during crystallization. The arrows indicate the evolution in time as crystallization progresses.

It can be observed that the recrystallization process produces a decrease in the intensity of the α relaxation peak, in the imaginary part of the dielectric permittivity, and correspondingly a decrease of static permittivity ϵ_s, and thus of the dielectric strength in the real part.

Fig. 6.5 shows the values of ϵ_s at 100 Hz, during isothermal crystallization at T_e = 278.0 K. The plateau at long times indicates full crystallization of the sample. The inset to Fig. 6.5 shows a zoom-in at short times, where the intersection of two tangents marks the crystallization onset at time t_o. In each series of isothermal spectra, the static permittivity was taken to be the value of the real permittivity at a fixed frequency varying between 10^2 and 10^4 Hz depending on the measuring temperature,

but always representing the low-frequency plateau value of the real permittivity.

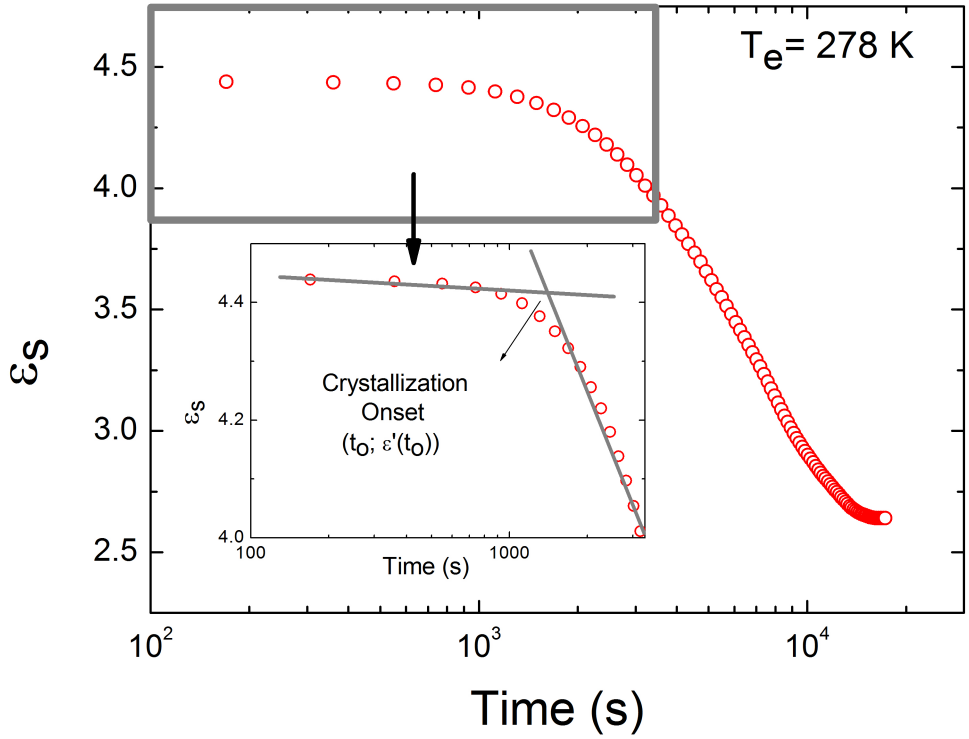

FIGURE 6.5: Evolution of the real static permittivity, ϵ_s, at 100 Hz as a function of time, for the data of Fig. 6.4 at $T_e = 278.0K$. The inset shows a zoom-in at short experiment times, where the intersection of the two gray lines marks the crystallization onset.

To analyze the crystallization kinetics of STP, we have studied the time evolution of the normalized static-permittivity difference, as defined by *D'Amore et al.* (D'Amore et al., 1990):

$$\hat{\epsilon} = \frac{\epsilon_s(SL) - \epsilon_s(t)}{\epsilon_s(SL) - \epsilon_s(C)}. \tag{6.1}$$

Here, $\epsilon_s(SL)$ and $\epsilon_s(C)$ are the static permittivity of the supercooled liquid and the crystalline phase, respectively. The first value can be obtained by extracting ϵ_s at time zero (right after supercooling), and the second by doing the same thing at the end of the crystallization process, where the sample is completely crystalline and no further change is observed in ϵ_s (See Fig. 6.5). $\epsilon_s(t)$ is the static permittivity of the mixed-phase sample as a function of the time elapsed from the start of the isothermal measurements. Fig. 6.6 shows the $\hat{\epsilon}$ values obtained for all five experiments

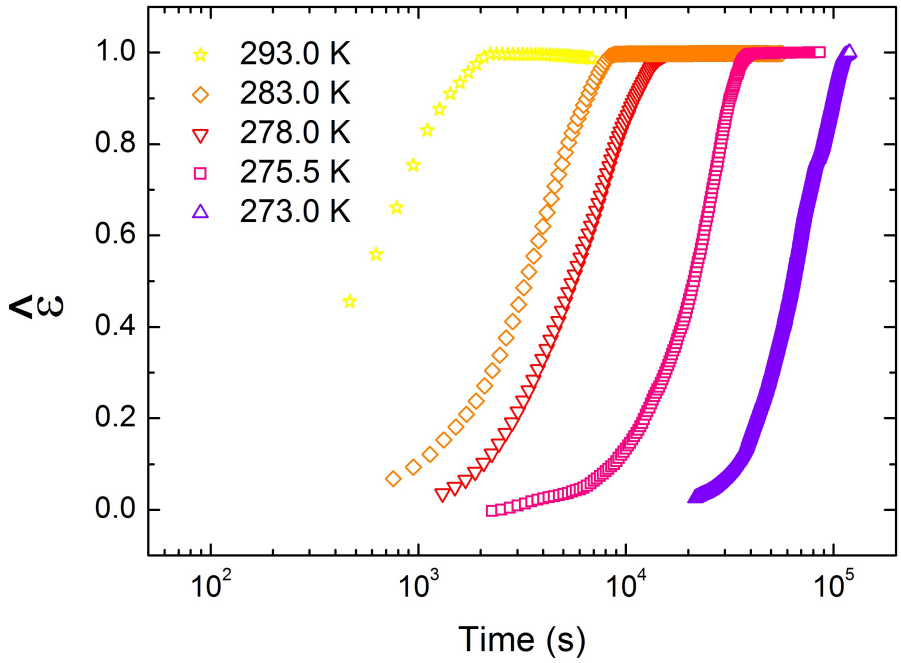

FIGURE 6.6: Time evolution of the normalized static-permittivity difference $\hat{\epsilon}$ during crystallization, as a function of the time elapsed since crystallization onset of each isothermal measurement (logarithmic scale) Stars, diamonds, inverted triangles, squares and triangles represent temperatures 293.0, 283.0, 278.0, 275.5 and 273.0 K respectively.

as a function of time. At short times $\hat{\epsilon} = 0$, since the sample is mainly in the supercooled state and the numerator vanishes. As the sample crystallizes, the value of $\epsilon_s(t)$ decreases approaching $\epsilon_s(C)$, until complete crystallization when $\hat{\epsilon}$ becomes unity.

Correlation between τ_α and tc through BDS

In order to find a possible correlation between the relaxation time of the α relaxation and the characteristic crystal growth time of STP the characteristic crystallization time (t_c) has been determined as the time interval between the crystallization onset (t_o) and the time at which $\hat{\epsilon}$ becomes 0.25. This value has been chosen since at this stage all samples shown in 6.6 have overcome the change in slope that is experienced upon triggering of the crystallization process.

In Fig. 6.7 the obtained t_c values are plotted as a function of the relaxation time of the cooperative dynamics, in logarithmic scale. For comparison, similar data obtained from the literature (Mehta et al., 2016b) for the drugs celecoxib and indomethacin is displayed as well.

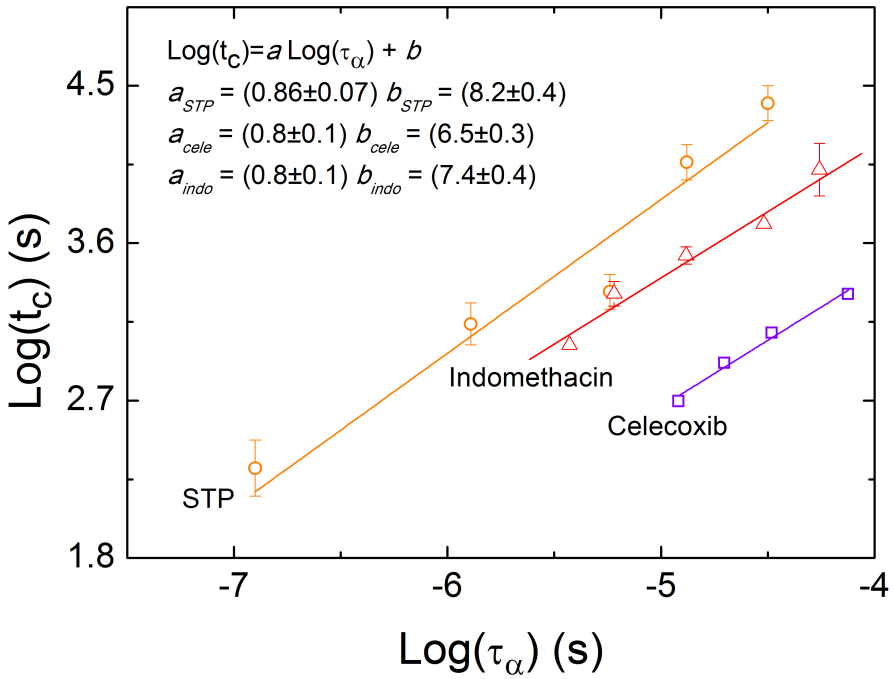

FIGURE 6.7: Plots of characteristic crystallization time (t_c) versus average α relaxation time above T_g in STP (circles), indomethacin (triangles) and celecoxib (squares). Values for indomethacin and celecoxib were obtained from reference (Mehta et al., 2016b). Error bars are provided when n = 3; otherwise, the crystallization time is the average of two determinations.

There is a clear correlation between the two times in all cases. A linear regression gives for STP a slope value of (0.86 ± 0.07), whereas that reported for indomethacin and celecoxib is 0.8 ± 0.1. Interestingly, the experimental range of the slopes overlap, suggesting a possible universal slope value, at least above T_g. Nevertheless, further substances should be studied to be able to postulate a possible general model that could predict t_c for a given τ_α. It is also interesting to note that the dependence of t_c on τ_α is sublinear.

If the temporal dependence of the crystallization were Avrami-like (Avrami, 1939; Avrami, 1940), then the normalized static-permittivity difference would follow the equation 1.3 (Adrjanowicz et al., 2010). Fig. 6.8*(a)* displays the Avrami plot at all studied temperatures. The normalized static-permittivity difference $\hat{\epsilon}$ is shown as a function of the time elapsed from the crystallization onset $(t - t_o)$ for each crystallization temperature. The inset shows the Arrhenius plot of the onset time, t_o. If the Avrami law were obeyed, each isothermal curve should look like a straight line, with constant slope equal to n. However, this is clearly not the case in Fig. 6.8 *(a)*.

To better visualize this fact, in Fig. 6.8 *(b)* we have plotted the value of the effective (time-dependent) Avrami exponent for the temperature at which crystallization is slowest (namely, 273.0 K), defined as:

$$n = \frac{d(Ln(-Ln(1-\epsilon')))}{d(Ln(t-t_o))} \tag{6.2}$$

It is evident from Fig. 6.8 *(b)* that the Avrami exponent is far from constant. In order to unambiguously state that the Avrami's law is not followed by this compound the errors affecting the data have been calculated using a block average technique. As it can be seen in Fig. 6.8 *(b)* the variation of the curve is greater than the calculated errors, supporting again that Avrami's law is not followed. The inset in the same figure shows a curve obtained by the subtraction of a linear curve to the experimental one in order to investigate if the exponent is constant or not in the most straightforward way. Again, the points seem not to follow an Avrami law, taking into account the obtained errors. Finally, a different choice of t_o was analyzed, in order to find out whether this could be possibly causing the variations on the Avrami exponent. However t_o is only affecting an horizontal and vertical displacement of the curve of Fig. 6.8 *(b)* and, thus, it cannot cause a deviation from linearity in Fig. 6.8 *(b)*. At higher isothermal crystallization temperature, the effective Avrami coefficient is observed to vary between 1 and 2 (not shown). A value in this range would suggest a one-dimensional crystallization of STP into needle-like crystallite (Tripathi et al., 2015), which is however not observed (see below). It is worth pointing out that similar departures from the Avrami law have been observed also in other compounds (Sanz and Niss, 2017).

XRD experiments

To understand the reason underlying the failure of the Avrami law diffraction experiments and observations of the crystallization process with an optical microscope were performed. Three samples were measured: the crystalline powder (as received from the manufacturer), the supercooled liquid during the crystallization process, and a fully recrystallized sample. The first and last were measured at ambient temperature (300 K), while the second was studied at 273 K.

One possible cause of failure of the Avrami law, could be the existence of different polymorphs of STP, leading to the formation of crystallites with distinct structures

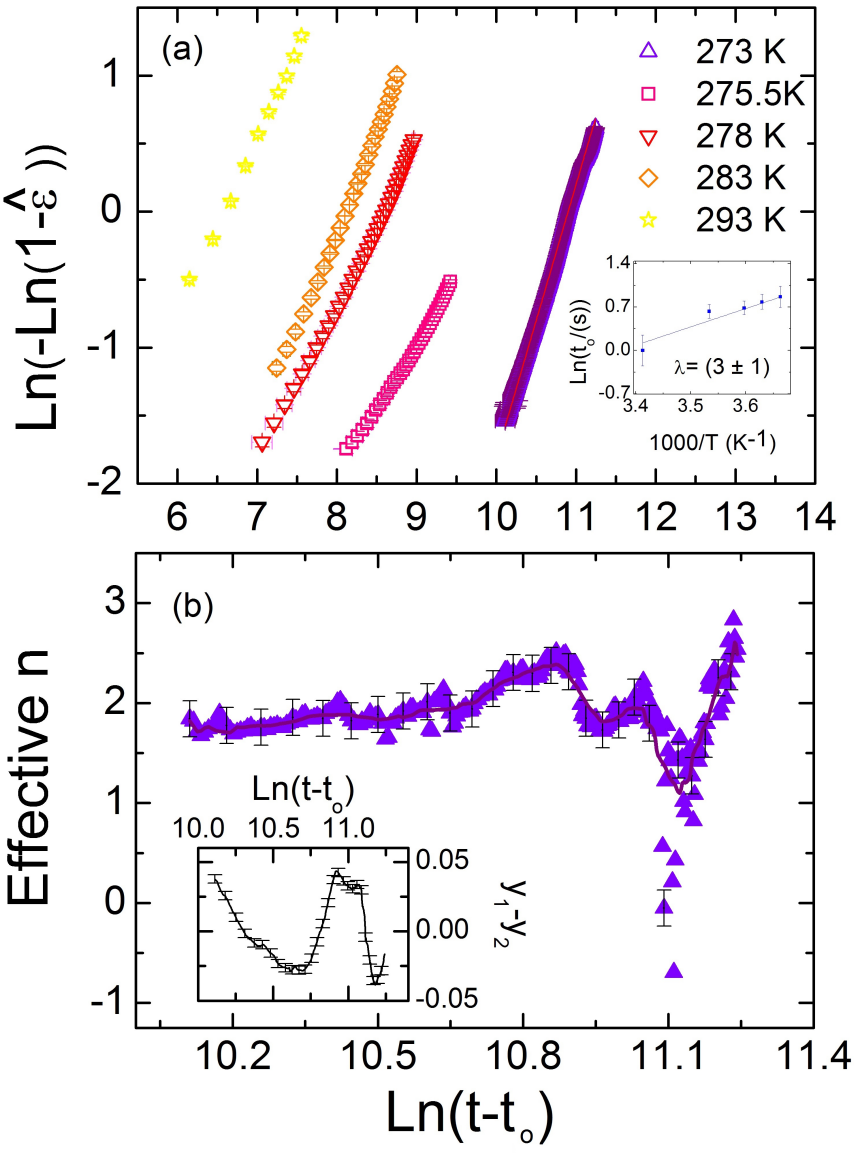

FIGURE 6.8: *(a)* Avrami plot of the normalized static-permittivity difference $\hat{\epsilon}$ as a function of the time elapsed from the crystallization onset $(t - t_o)$, for all five isothermal crystallization temperatures studied. Inset: Arrhenius plot of the onset time t_o. *(b)* Effective Avrami exponent (Eq. 6.2), as a function of the time elapsed from the crystallization onset, for the measuring temperature of 273.0 K. Inset: Curve obtained by the subtraction of a linear curve to the experimental one.

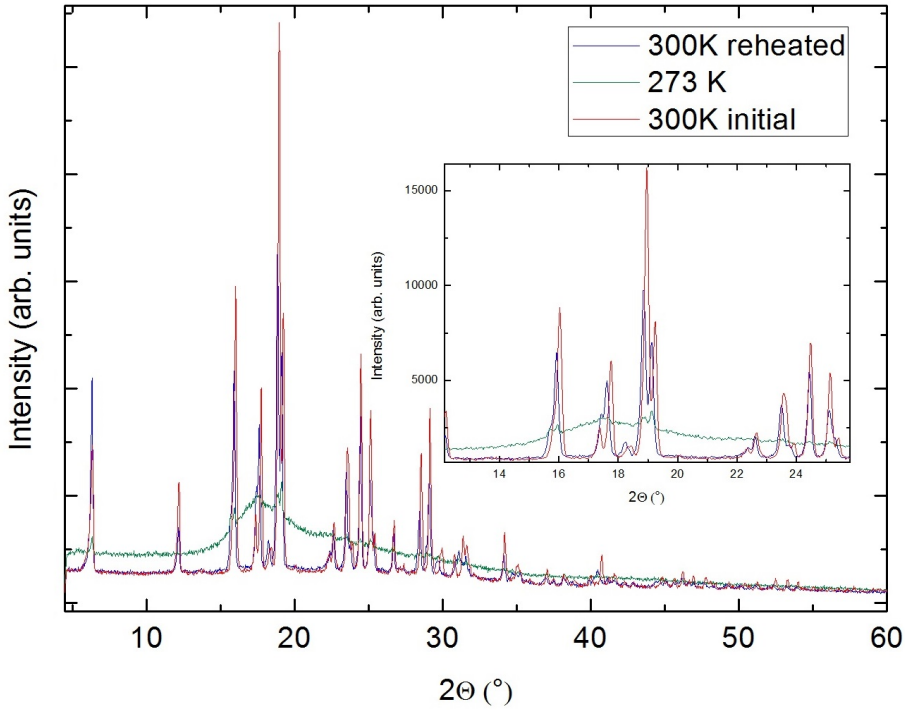

FIGURE 6.9: X-ray diffraction pattern of the as-received STP powder at 300 K (blue), supercooled liquid at 273 K (green) and recrystallized sample at 300 K (red). Inset: Zoom-in of the data at low scattering angles.

and morphology, for example, as it happens for many pharmaceutical compounds (Espeau et al., 2005; Barrio et al., 2009; Barrio et al., 2012; Toscani et al., 2016; Céolin et al., 2008; Gana et al., 2015). This possibility is discarded by our X-ray diffraction measurements. Fig. 6.9 shows the diffractograms obtained at (300 $\pm$ 1) K on the as-stored crystalline material, at (273 $\pm$ 1) K right after quenching from liquid state and at (300 $\pm$ 1) K after reheating.

It can be observed that the initial and recrystallized material display the same structure, and that the supercooled sample is indeed of glassy nature, as evidenced by the broad amorphous background. Within this broad feature, some crystalline Bragg reflections can be observed at $2\theta = 6, 15.6, 15.9, 18.8$ and 19.1. These correspond to the presence of a fraction of crystalline material. This behavior coincides with that observed by optical microscopy on molten drops at ambient temperature: while some drops recrystallized within approximately 10 minutes, some others remained liquid for much longer times.

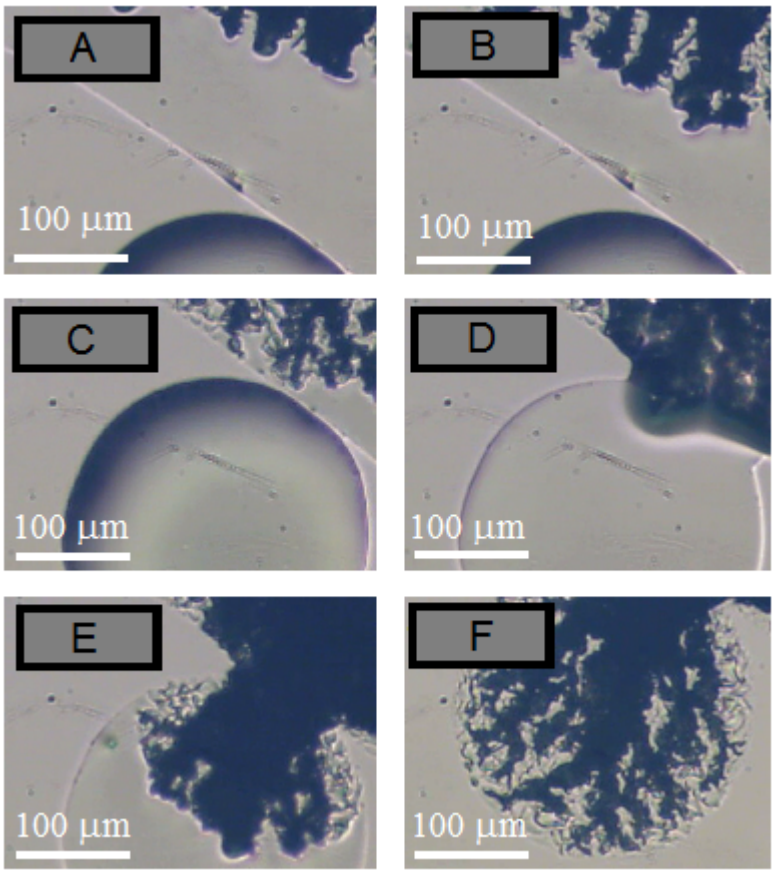

FIGURE 6.10: Crystallization of STP observed through an optical microscope with back-light illumination.

Crystallization observation through optical microscope

Fig. 6.10 shows of the crystallization of pure STP as observed with an optical microscope. In the first photograph two regions can be clearly distinguished: a circular drop on the bottom and a bigger liquid domain on top, whose boundary is signaled by a white line. The dark region on the top right corner is the part of STP that is already crystalline. As time advances the growth of the crystal is observed. It can be noted in the first three photographs that the process is not unidirectional but rather results in a fractal 3D-morphology. Moreover, no other nucleation site appears in the liquid portion, apart from the first crystal. In other words, it is hard for STP crystals to nucleate, so that recrystallization generally proceeds from a single point (seed) towards the rest of the available liquid in all possible directions. This is evident also in the center and lower panels of Fig. 6.10, where a circular drop of liquid STP is visible. Such drop only starts to crystallize when crystallization of the larger liquid domain is complete. In picture *D* the growing crystal reaches the boundary with the single drop breaking its surface. As soon as the liquid of the second drop comes in contact with the crystal, it produces a burst of further crystal growth. In *E* the remaining part of the smaller drop is half crystallized and at *F* the process is complete. Black regions indicate higher crystalline structures, which are out of focus with respect to the height of the original liquid. It can be then affirmed that the crystalline phase grows as a function of the shape and size of the domains of the supercooled liquid, and that nucleation is the limiting step for crystallization. This, together with the fractal-like crystal growth, helps rationalizing why the Avrami theory is not fully satisfied. The Avrami exponent can in fact change during crystallization if the growth morphology changes (Jensen et al., 2015).

6.4 Conclusions

It can be concluded that Stiripentol in its supercooled liquid and glass state, presents three different relaxations: the α relaxation peak, corresponding to the collective reorientation of the STP molecules, a Johari Goldstein β relaxation that is the precursor of the α process according to the Coupling model, and a γ relaxation which corresponds to an intramolecular relaxation. The T_g of the material was determined both by dielectric spectroscopy and calorimetry, obtaining $T_g = 246.2 \pm 0.5$ K and $T_g = 248 \pm 1$ K, respectively.

Isothermal crystallization of STP was studied at temperatures between 273.0 and 293.0 K. It was found that the Avrami law is not obeyed. This happens because STP has difficulties when nucleating, and possibly also because the crystalline phase grows in a fractal 3D morphology. It appears that supercooled liquid STP requires in general relatively high temperatures to produce a crystalline nucleus, from which crystal growth proceeds so fast, that no other nucleation site is generated during crystallization of a given liquid domain. As observed by means of X-ray diffraction, the initial solid and the recrystallized material display the same structure, which indicates that no other polymorph of STP appears at ambient pressure. A sublinear correlation is found between the characteristic crystal-growth time and the collective relaxation dynamics. This correlation was observed also in other substances, and suggests a general correlation at temperatures above T_g to predict a substance's crystallization time as a function of temperature. Further materials should be studied so as to test this possibility.

Chapter 7

Conclusions

For pharmaceutical products the aggregation phase is of the uttermost importance, since there is a very delicate balance between producing a drug that has a high dissolution rate, and being able to keep the substance free from phase transformation for a long period of time. The glass state presents a higher free energy than the crystalline phase, and for this reason it dissolves more rapidly, improving its bioavailability. Nevertheless, the same property makes it prone to crystallizing and for this reason, being able to understand the amorphous-phase dynamics and crystallization kinetics of drugs is a very powerful tool in order to develop more efficient products.
In this thesis the relaxation dynamics of the prilocaine and stiripentol drugs and the kinetics of crystallization of the latter have been studied. Both substances can be vitrified forming structural glasses. These phases are non-equilibrium states that maintain the orientational and translational disorder of the liquid from which they derive, but behave mechanically like solids. Whenever vitrification of the supercooled liquid cannot be achieved, both prilocaine and stiripentol transform into the crystalline stable phase. Both materials show a primary α relaxation associated with the collective motion of the molecules, which is halted at the glass transition temperature, T_g.
For the prilocaine drug studied in pure and hydrated forms in bulk and under confinement inside a nanoporous material, it could be observed that:

- A single primary α relaxation, characterizing the collective reorientation of the molecules, was consistently observed in all cases. This implies that the water molecules in the hydrated prilocaine drug are strongly bonded to the prilocaine matrix and do not show a separate relaxation behavior.

- The addition of water to the prilocaine drug produces an antiplasticizing effect that is expressed in a reproducible increase in the glass transition temperature. After studying the bulk system it was hypothesized that the formation of prilocaine-water complexes such as water-bridged prilocaine dimers could rationalize the observed antiplasticizing effect, due to the fact that water-prilocaine complexes would display, with respect to pristine prilocaine, hybrid relaxation modes, higher molecular weight, and larger steric hindrance against reorientation, all factors which would enhance the glass transition temperature. By confining the pure and hydrated substance in molecular sieves where only a few of these molecules may fit, the proposed hypothesis could be confirmed.

- By comparing the bulk and the confined geometries for this drug, it was observed that the addition of water to the prilocaine drug in glass phase produces a stable structure that is more resistant to crystallizing upon heating the broader the matrix is. Increasing the amount of H-bonds in the glassy material has a direct impact on its stability against phase transformation.

In the case of the stiripentol drug, the following conclusions could be drawn:

- In the amorphous state it presents three different relaxations: the α relaxation, corresponding to the collective reorientation of the STP molecules, a Johari Goldstein β relaxation that follows the predictions of the Coupling model, and a γ relaxation which corresponds to an intramolecular relaxation.

- The supercooled liquid transforms at high temperatures (around $T_g + 30K$) into the crystalline phase by growing from a single nucleation site in a fractal 3D morphology at a relatively fast rate. The crystallization process does not follow the Avrami law, possibly because the condition of random nucleation over the entire material is not fulfilled.

- A sublinear correlation linking the characteristic crystal-growth time and the collective relaxation dynamics of stiripentol is found. This correlation was observed also in other substances, and suggests a general correlation at temperatures above T_g that may allow predicting a substance's crystallization time as a function of temperature.

The results obtained in this Thesis shed light into the phase stability of both substances, and provide important observations that could be generalized to other materials. The antiplasticizing effect observed in prilocaine is quite rare, and it would be interesting to identify other drugs which show the same behavior, as increasing the T_g is one of the methods to enhance the metastability of the amorphous phase of a drug. At the same time, the analysis carried out of the stiripentol drug, not only provides valuable information of the drug dynamics but also suggests a correlation between the characteristic crystal-growth time and the collective relaxation times. If this relation is found to be general to a broader range of substances it would allow one to foresee the phase transformation of the material and find the optimum formulating and storing conditions.

Appendix A

List of publications from this thesis

- G.N. Ruiz, M. Romanini, A. Hauptmann, T. Loerting, E. Shalaev, J.LL. Tamarit, L.C. Pardo and R. Macovez. Genuine antiplasticizing effect of water on a glass-former drug. *Sci. Rep.* **7** 7470 (2017).
- G.N. Ruiz, M. Romanini, M. Barrio, J.LL. Tamarit, L.C. Pardo and R. Relaxation dynamics vs crystallization kinetics in the amorphous state: the case of stiripentol. *Mol. Pharm.* **14** 3636 (2017).
- A. Silva-Santisteban, N. Steinke, A.J. Johnston, G.N. Ruiz, L.C. Pardo and S.E. McLain. On the structure of prilocaine in aqueous and amphiphilic solutions. *Phys. Chem. Chem. Phys.*, **19** 12665 (2017).
- G.N. Ruiz, I. Combarro-Palacios, S.E. McLain, J.LL. Tamarit, L.C. Pardo, S. Cerveny and R. Macovez. Insigths of antiplasticizing effect of water on a glass-former drug in confined systems (in preparation).

Appendix B

Agradecimientos

Sinceramente, el proceso de esta tesis doctoral fue para mi una experiencia que disfruté mucho, tanto a nivel laboral como personal. Quiero agradecer enormemente a Josep LLuis Tamarit y el Grupo de Caracterización de Materiales de UPC en su conjunto por haberme dado esta posibilidad, por haber escuchado mis intereses personales y por darme las herramientas para crecer como científica y muchas veces también como persona.

Para mis directores, Roberto y Luis Carlos, no me alcanzan las palabras de agradecimiento. Creo que sus formas de enseñar son tan diferentes como complementarias, y les voy a estar siempre agradecida por su tiempo, paciencia, esfuerzo, enseñanzas, y por su amistad. Tuve una suerte enorme de tenerlos como mentores. Gracias.

A Michi, gurú del laboratorio y amiga personal, gracias de todo corazón. Es un honor aprender y trabajar con una mujer tan empoderada como vos. A María, Lola y Pol, gracias por siempre acompañar, por incluirme y ayudarme a crecer como científica. A mis compañerxs y amigxs doctorandxs: Efi, Ale, Manesh, Pragya, Jin, Andrés, Johnny, Ara, Sofi y Yago cada unx a su manera única hicieron este camino más rico, más fácil, más feliz. Gracias.

I would like to thank as well Sylvia Mclain who was a fruitful collaborator and teacher to me, y a Silvina Cerveny, que confió en mi y supo estimularme y acompañarme en mis proyectos académicos.

A mi familia, la biológica y la construida, la de éste lado del Atlántico, y la del otro, la de dos patas y la de cuatro. Ustedes son el motor de mi energía y la chispa que enciende mi alegría cada día. Gracias por acompañar, gracias por nutrirme, por estimularme, por hacerme sentir tan querida.

A Lucho, por ser un compañero de vida excepcional, por animarse y saltar de la mano, por el amor. A Frishi, Juli y Belén por su sororidad inquebrantable y su amor

gigantesco. A San San por el punto de luz que no se apaga. A Marian, por siempre volver. A Robi, por la dulzura transparente. A Lore, Haizea y Vane por ser familia. A mi vieja, que me enseñó el empoderamiento, a mi viejo que siempre está, a mis hermanxs que siempre le ponen el cariño y el cuerpo a todas. A Eli, Nachi y Albert, por hacerme sentir parte y querida. Y finalmente, pero no menos importante, gracias a las Bonitas, Lxs Colgadxs, a Can Batlló y a mi amado mundo en Barcelona, que hicieron de estos años un viajazo increíble. Lo lamento si estos agradecimientos son demasiado sensibleros, pero sinceramente siento que tengo todo por agradecer. Gracias, totales.

Bibliography

Abiad, M.G., M.T. Carvajal, and O.H. Campanella (2009). "A Review on Methods and Theories to Describe the Glass Transition Phenomenon: Applications in Food and Pharmaceutical Products". In: *Food Eng. Rev.* 1, p. 105.

Adrjanowicz, K. et al. (2010). "Dielectric Relaxation and Crystallization Kinetics of Ibuprofen at Ambient and Elevated Pressure". In: *J. Phys. Chem. B* 114, p. 6579.

Afifi, S. (2015). "Solid Dispersion Approach Improving Dissolution Rate of Stiripentol: a Novel Antiepileptic Drug". In: *Iranian J. Pharm. Research* 14, p. 1001.

Aichayawanich, S. et al. (2011). "Agglomeration Mechanisms of Cassava Starch During Pneumatic Conveying Drying". In: *Carbohydr. Polym.* 84, p. 292.

Alie, J. et al. (2004). "Dielectric study of the molecular mobility and the isothermal crystallization kinetics of an amorphous pharmaceutical drug substance". In: *J. Pharm. Sci.* 93, p. 218.

Alvarez, F., A. Alegria, and J. Colmenero (1991). "Relationship between the time-domain Kohlrausch-Williams-Watts and frequency-domain Havriliak-Negami relaxation functions". In: *J. Phys. Rev. B* 4, p. 7306.

Andronis, V. and G. Zografi (1998). "The molecular mobility of supercooled amorphous indomethacin as a function of temperature and relative humidity". In: *Pharm. Res.* 15, p. 835.

Angell, C. A. (1990). "Dynamic processes in ionic glasses". In: *Chem. Rev.* 90, p. 523.

Angell, C.A. (1985a). "Spectroscopy simulation and scattering, and the medium range order problem in glass". In: *J. Non-Cryst. Solids* 73, p. 1.

— (1985b). "The old problems of glass and the glass transition, and the many new twists". In: *Proc. Natl. Acad. Sci. USA* 92, p. 6675.

— (1988). "Structural instability and relaxation in liquid and glassy phases near the fragile liquid limit". In: *J. Non-Cryst. Solids* 102, p. 205.

— (2002). "Liquid Fragility and the glass transition in water aqueous solutions". In: *Chem. Rev.* 102, p. 2627.

Angell, C.A. (2008). "Insights into phases of liquid water from study of its unusual glass-forming properties". In: *Science* 319, p. 582.

Angell, C.A. et al. (2000). "Relaxation in glassforming liquids and amorphous solids". In: *J. Appl. Phys.* 88, p. 3113.

Ashcroft, N.W. and N.D. Mermin (1976). *Solid state physics*. Holt, Rinehart and Winston.

Aso, Y., S. Yoshioka, and S. Kojima (2000). "Relationship Between the Crystallization Rates of Amorphous Nifedipine, Phenobarbital, and Flopropione, and Their Molecular Mobility as Measured by Their Enthalpy Relaxation and ^{1}H NMR Relaxation Times". In: *J. Pharm. Sci.* 89, p. 408.

Avrami, M. (1939). "Kinetics of Phase Change. I General Theory". In: *J. Chem. Phys.* 7, p. 1103.

— (1940). "Kinetics of Phase Change. II Transformation - Time Relations for Random Distribution of Nuclei". In: *J. Chem. Phys.* 8, p. 212.

Badr, A.M., H.A. Elshaikh, and I.M. Ashraf (2011). "Impacts of Temperature and Frequency on the Dielectric Properties for Insight into the Nature of the Charge Transports in the Tl_2S Layered Single Crystals". In: *Journal of Modern Physics* 2, p. 12.

Ball, P. (2008). "Water as an Active Constituent in Cell Biology". In: *Chem. Rev.* 108, p. 74.

Barrio, M. et al. (2009). "Polymorphism of progesterone: relative stabilities of the orthorhombic phases I and II inferred from topological and experimental pressure-temperature phase diagrams". In: *J. Pharm. Sci.* 98, p. 1657.

Barrio, M. et al. (2012). "Pressure-Temperature State Diagram for the Phase Relationships Between Benfluorex Hydrochloride Forms I and II: A Case of Enantiotropic Behavior". In: *J. Pharm. Sci.* 101, p. 1073.

Barsoum, M. (1997). *Fundamentals of Ceramics*. McGraw-Hill, New York.

Barthel, J., H. Krienke, and W. Kunz (1998). *Physical chemisty of electrolyte solutions. Vol. 5*. Springer (Steinkopff-Verlag: Darmstadt).

Bauer, T. et al. (2010). "Relaxation dynamics and ionic conductivity in a fragile plastic crystal". In: *J. Chem. Phys.* 133, p. 144509.

Bebin, M. and T.P. Bleck (1994). "New anticonvulsant drugs. Focus on flunarizine, fosphenytoin, midazolam and stiripentol". In: *Drugs* 48, p. 153.

Bellavia, G. et al. (2009). "Thermal denaturation of myoglobin in water-disaccharide matrixes: relation with the glass transition of the system". In: *J. Phys. Chem. B* 113, p. 11543.

Bengtzelius, U., W. Götze, and A. Sjölander (1984). "Dynamics of supercooled liquids and the glass transition". In: *J. Phys. C* 17, p. 5915.

Bhugra, C. et al. (2008). "Different measures of molecular mobility: comparison between calorimetric and thermally stimulated current relaxation times below Tg and correlation with dielectric relaxation times above Tg". In: *J. Pharm. Sci.* 97, p. 4498.

Bobrov, V.B., S.A. Trigger, and G.J.F. van Heijstand P.P.J.M. Schram (2010). "Kramers-Kronig relations for the dielectric function and the static conductivity of Coulomb systems". In: *Europhysics Letters* 90.1, p. 10003.

Böhmer, R. et al. (1993). "Nonexponential relaxations in strong and fragile glass formers". In: *J. Chem. Phys.* 99, p. 4201.

Böttcher, C.J.F. and P. Bordewijk (1978). *Theory of electric polarization, vol. II. Dielectrics in time-dependent fields*. Elsevier Amsterdam, Oxford, New York.

Brand, R., P. Lunkenheimer, and A. Loidl (2002). "Relaxation dynamics in plastic crystals". In: *J. Chem. Phys.* 116, p. 10386.

Brodin, A. et al. (1984). "Phase Diagram and Aqueous Solubility of the Lidocaine-Prilocaine Binary System". In: *J. Pharm. Sci.* 73, p. 73.

Buchenau, U. et al. (1992). "Interaction of soft modes and sound waves in glasses". In: *Phys. Rev, B* 46, p. 2798.

Capaccioli, S. et al. (2012a). "Many-Body Nature of Relaxation Processes in Glass-Forming Systems". In: *J. Phys. Chem. Lett.* 3, pp. 735–743.

Capaccioli, S. et al. (2012b). "Many-Body Nature of Relaxation Processes in Glass-Forming Systems". In: *J. Phys. Chem. Lett.* 3, p. 735.

Céolin, R. et al. (1991). "Solid state studies on stiripentol: a novel anticonvulsant drug". In: *Int. J. Pharm.* 74, p. 77.

Céolin, R. et al. (2008). "Overall monotropic behavior of a metastable phase of biclotymol, 2,2′−methylenebis(4-chloro-3-methyl-isopropylphenol), inferred from experimental and topological construction of the related P-T state diagram". In: *J. Pharm. Sci.* 97, p. 3927.

Ceolin, R. et al. (2010). "Liquid-Liquid Miscibility Gaps and Hydrate Formation in Drug-Water Binary Systems: Pressure-Temperature Phase Diagram of Lidocaine

and Pressure-Temperature-Composition Phase Diagram of the Lidocaine-Water System". In: *J. Pharm. Sci.* 99, p. 2756.

Céolin, R. et al. (2010). "Liquid-liquid miscibility gaps and hydrate formation in drug-water binary systems: Pressure-temperature phase diagram of lidocaine and pressure-temperature-composition phase diagram of the lidocaine-water system". In: *J. Pharm. Sci.* 99, p. 2756.

Chang, Y.P., P.B. Cheah, and C.C. Seow (2000). "Plasticizing-Antiplasticizing Effects of Water on Physical Properties of Tapioca Starch Films in the Glassy State". In: *J. Food Sci.* 65, p. 445.

Cole, K.S. and R.H. Cole (1941). "Dispersion and absorption in dielectrics I. Alternating current characteristics". In: *J. Chem. Phys.* 9, p. 341.

Contard, N. and S. Ring (1996). "Edible wheat gluten film: influence of water content on glass transition temperature". In: *J. Agric. Food Chem.* 44, p. 3474.

Corezzi, S. et al. (1999). In: *Phys. Rev. E* 60, p. 4444.

D'Amore, A. et al. (1990). "Dynamic-mechanical and dielectric characterization of PEEK crystallization". In: *Polym. Eng. Sci.* 30, p. 314.

Davidson, D.W. and R.H. Cole (1950). "Dielectric relaxation in glycerine". In: *J. Chem. Phys.* 18, p. 1417.

— (1951). "Dielectric relaxation in glycerol, propylene glycol and n-propanol". In: *J. Chem. Phys.* 19, p. 1484.

Debenedetti, P.G. and F.H. Stillinger (2001). "Supercooled liquids and the glass transition". In: *Nature* 410, p. 259.

Debye, P. (1929). *Polar Molecules*. New York: Chem. Catalog.

Do, C. et al. (2013). "Li+ transport in poly(ethylene oxide) based electrolytes: neutron scattering, dielectric spectroscopy, and molecular dynamics simulations". In: *J. Chem. Phys.* 111, p. 018301.

Drugbank. *https://www.drugbank.ca/drugs/DB00750*.

Dyre, J.C. (2006). "Colloquium: The glass transition and elastic models of glass-forming liquids". In: *Rev. Mod. Phys.* 78, p. 953.

Ediger, M.D., C.A. Angell, and S.R. Nagel (1996). "Supercooled Liquids and Glasses". In: *J. Phys. Chem.* 100, p. 13200.

Elliott, S.R. (1992). "A Unified Model for the Low-Energy Vibrational Behaviour of Amorphous Solids". In: *EuroPhys. Lett.* 19, p. 201.

Emsley, J. (1980). "Very Strong Hydrogen Bonds". In: *Chemical Society Reviews* 9, p. 91.

Espeau, P. et al. (2005). "Polymorphism of paracetamol: relative stabilities of the monoclinic and orthorhombic phases inferred from topological pressure-temperature and temperature-volume phase diagrams". In: *J. Pharm. Sci.* 94, p. 524.

Evain, M. et al. (1993). "Potential of the INEL X-ray position-sensitive detector: a general study of the Debye-Scherrer setting". In: *J. Appl. Cryst.* 26, p. 563.

Ewing, S. et al. (2016). *Low-Temperature Mobility of Water in Sugar Glasses: Insights from Thermally Stimulated Current Study. In: G. Gutiérrez-López, L. Alamilla-Beltrán, M. del Pilar Buera, J. Welti-Chanes, E. Parada-Arias and G. Barbosa-Cánovas (eds). Water Stress in Biological, Chemical, Pharmaceutical and Food Systems. Food Engineering Series*. Springer, New York, NY, pp. 75–87.

Fahy, G.M. et al. (1984). "Vitrification as an Approach to Cryopreservation". In: *Cryobiology* 21, p. 407.

Fontanet, S. et al. (1997). "Effect of water on mechanical behaviour of extruded flat bread". In: *J. Cereal Sci.* 25, p. 43.

Gana, I. et al. (2015). "An integrated view of the influence of temperature, pressure, and humidity on the stability of trimorphic cysteamine hydrochloride". In: *Mol. Pharm.* 12, p. 2276.

Garcia-Belmonte, G., F. Henn, and J. Bisquert (2006). "Dielectric relaxation strength in ion conducting glasses caused by cluster polarization". In: *Chem. Phys.* 330, p. 113.

Gerhardt, R. (1994). "Impedance and dielectric spectroscopy revisited: Distinguishing localized relaxation from long-range conductivity". In: *J. Phys. Chem. Solids* 55, p. 1491.

Gondek, E. and P.P. Lewicki (2006). "Antiplasticization of cereal-based products by water Part II: breakfast cereals". In: *J. Food Ing.* 77, p. 644.

Gordon, M. and J.S. Taylor (1952). "Ideal copolymers and the second-order transitions of synthetic rubbers". In: *J. Appl. Chem.* 2, p. 493.

Götze, W. (1985). "Properties of the glass instability treated within a mode coupling theory". In: *Z. Phys. B* 60, p. 195.

Götze, W. and M.R. Mayr (2000). "Evolution of vibrational excitations in glassy systems". In: *Phys. Rev. E* 61, p. 587.

Götze, W. and L. Sjögren (1992). "Relaxation processes in supercooled liquids". In: *Rep. Progr. Phys.* 55, p. 241.

Graesera, K.A. et al. (2009). "Correlating thermodynamic and kinetic parameters with amorphous stability". In: *European J. of Pham. Sci.* 37, p. 492.

Griffiths, P. and J. A. De Haseth (2007). *Fourier Transform Infrared Spectrometry*. John Wiley and Sons.

Grzybowska, K., S. Capaccioli, and M. Paluch (2016). "Recent developments in the experimental investigations of relaxations in pharmaceuticals by dielectric techniques at ambient and elevated pressure". In: *Adv. Drug Del. Rev.* 100, p. 158.

Halek, G.W., S.W. Paik, and K.L. Chang (1989). "The effect of moisture content on mechanical properties and texture profile parameters of corn meal extrudates". In: *J. Texture Stud.* 20, p. 43.

Hancock, B.C., S.L. Shamblin, and G. Zografi (1995). "Molecular mobility of amorphous pharmaceutical solids below their glass transition temperatures". In: *Pharm. Res.* 12, p. 799.

Hancock, B.C. and G. Zografi (1994). "The relationship between the glass transition temperature and the water content of amorphous pharmaceutical solids". In: *Pharm. Res.* 11, p. 471.

Havriliak, S. and S. Negami (1966). "A complex plane analysis of α-dispersions in some polymer systems". In: *J. Polym. Sci. C* 16.14, p. 99.

— (1967). "A complex plane representation of dielectric and mechanical relaxation processes in some polymers". In: *Polymer* 8, p. 161.

Hedvig, P. (1977). *Dielectric Spectroscopy of Polymers*. Bristol: Hilger.

Hench, L.L. and J.K. West (1990). *Principles of electronic ceramics*. Wiley, New York.

Hodge, I.M., M.D. Ingram, and A.R. West (1976). "Impedance and modulus spectroscopy of polycrystalline solid electrolytes". In: *J. Electroanal. Chem.* 74, p. 125.

Hoehne, G. and W. Hemminger andH.J. Flammersheim (1996). *Differential Scanning Calorimetry*. Springer.

IUPAC (2006). *Compendium of chemical terminology. 2nd ed. (the 'Gold book')*. A.D. McNaught and A. Wilkinson.

Jackson, J.D. (1998). *Classical Electrodynamics (3 rd ed.)* John Wiley and Sons.

Jena, A.K. and M.C. Chaturvedi (1992). *Phase Transformations in Materials*. Prentice Hall. ISBN: 0-13-663055-3.

Jensen, M. et al. (2015). "A systematic study of the isothermal crystallization of the mono-alcohol n-butanol monitored by dielectric spectroscopy". In: *J. Chem. Phys.* 143, p. 134501.

Johari, G.P. and M. Goldstein (1970). "Viscous Liquids and the Glass Transition. II. Secondary Relaxations in Glasses of Rigid Molecules". In: *J. Chem. Phys.* 53, p. 2372.

Johari, G.P., S. Kim, and R.M. Shanker (2007). "Dielectric Relaxation and Crystallization of Ultraviscous Melt and Glassy States of Aspirin, Ibuprofen, Progesterone, and Quinidine". In: *J. Pharm. Sci.* 96, p. 1159.

Jonscher, A.K. (1977). "'Universal' Dielectric Response". In: *Nature* 267, p. 673.

J.Perdomo et al. (2009). "Glass Transition Temperatures and Water Sorption Isotherms of Cassava Starch". In: *Carbohydr. Polym.* 76, p. 305.

Kalichevsky, M., J. Blanshard, and P. Tokarczuk (1993). "Effect of water content and sugars on the glass transition of casein and sodium caseinate". In: *Int. J. FoodTechnol.* 28, p. 1390.

Kalichevsky, M., E.M. Jaroszkiewicz, and J.M.V. Blanshard (1992). "Glass transition of gluten. 1: Gluten and gluten-sugar mixtures". In: *Int. J. Biol. Macromol.* 14, p. 257.

Karpov, V.G., M.I. Klinger, and F.N. Ignatiev (1983). "Theory of the low-temperature anomalies in the thermal properties of amorphous structures". In: *Sov. Phys. JETP* 84, p. 760.

Katkov, I.I. and F. Levine (2004). "Prediction of the glass transition temperature of water solutions: comparison of different models". In: *Cryobiology* 49, p. 62.

Knight, C. and G.A. Voth (2012). "The curious case of the hydrated proton". In: *Acc. Chem. Res.* 45, p. 101.

Kohlrausch, R. (1847). In: *Pogg. Ann. Phys.* 12, p. 393.

— (1854). "Theorie des elektrischen Rückstandes in der Leidener Flasche". In: *Ann. Phys. Chem. (Poggendorff)* 56, p. 91.

Kolodziejczyk, K. et al. (2013). "Relaxation dynamics and crystallization study of sildenafil in the liquid and glassy states". In: *Mol. Pharm.* 10, p. 2270.

Konopacka, D., W. Plocharsky, and T. Beveridge (2002). "Water sorption and crispness of fat-free apple chips". In: *J. Food Sci.* 67, p. 87.

Kremer, F. and A. Schönals (2002). *Broadband Dielectric Spectroscopy*. Springer.

Kroes, G.J. (1992). "Surface melting of the (0001) face of TIP4P ice". In: *Surface Science* 275, p. 365.

Kudlik, A. et al. (1999). "The dielectric response of simple organic glass formers". In: *J. Mol. Structure* 479, p. 201.

Larini, L. et al. (2008). "Universal scaling between structural relaxation and vibrational dynamics in glass-forming liquids and polymers". In: *Nature Phys.* 4, p. 42.

Larson, J.W. and T.B. McMahon (1984). "Gas-phase bihalide and pseudobihalide ions. An ion cyclotron resonance determination of hydrogen bond energies in XHY-species (X, Y = F, Cl, Br, CN". In: *Inorganic Chemistry* 23, p. 2029.

Lazaridou, A., C.G. Biliaderis, and V. Kontogiorgos (2003). "Molecular weight effects on solution rheology of pullulan and mechanical properties of its films". In: *Carbohydrate Polymers* 52, p. 151.

Leutheuser, E. (1984). "Dynamical model of the liquid-glass transition". In: *Phys. Rev. A* 29, p. 2765.

Levine, H. and L. Slade (1988). "Water as a Plasticizer: Physico-Chemical Aspects of Low-Moisture Polymeric Systems". In: *Water Science Reviews* 3, p. 79.

Levy, Y. and J.N. Onuchic (2006). "Water mediation in protein folding and molecular recognition". In: *Annu. Rev. Biophys. Biomol. Struct.* 35, p. 389.

Li, X. et al. (2014). "Comparative study of dynamics in glass forming mixtures of Debye-type N-ethyl acetamide with water, alcohol, and amine". In: *J. Chem. Phys.* 141, p. 104506.

Li, Y., K.M. Kloeppel, and F. Hsieh (1998). "Texture of glassy corn cakes as function of moisture content". In: *J. Food Sci.* 63, p. 869.

Lindsay, C.P. and G.D. Patterson (1980). "Detailed comparison of the Williams-Watts and Cole-Davidson functions". In: *J. Chem. Phys.* 73, p. 3348.

Lower, S. (2016). *Chem1 - States of matter*. Simon Fraser University.

Lunkenheimer, P. and A. Loidl (2002). "Dielectric spectroscopy of glass-forming materials: α-relaxation and excess wing". In: *Chem. Phys.* 284.284, p. 205.

Lunkenheimer, P. et al. (2000). "Glassy dynamics". In: *Contemporany Physics* 41, p. 15.

Macedo, P.B., C.T. Moynihan, and R. Bose (1972). "The Role of Ionic Diffusion in Polarisation in Vitreous Ionic Conductors". In: *Phys. Chem. Glasses* 13, p. 171.

Malinovsky, V.K., V.N. Novikov, and A.P. Sokolov (1987). "Investigation of structural correlations in disordered materials by Raman scattering measurements". In: *J Non-Cryst Solids* 90, p. 485.

Mallamace, F. et al. (2016). "Energy Landscape in Protein Folding and Unfolding". In: *Proc. Natl. Acad. Sci. USA* 113, p. 3159.

Martin, Steve W., Wenlong Yao, and Kyle Berg (2009). "Space Charge Polarization Measurements as a Method to Determine the Temperature Dependence of the

Number Density of Mobile Cations in Ion Conducting Glasses". In: *Materials Sciences and Applications* 223, p. 1379.

Marzec, A. and P.P. Lewicki (2006). "Antiplasticization of cereal-based products by water Part I: Extruded flat bread". In: *J. Food Ing.* 73, p. 73.

McCrum, N.G., B.E. Read, and G. Williams (1991). *Anelastic and Dielectric Effects in Polymeric Solids*. John Wiley and Sons.

M.Chaplin (2014). *Chaplin*. www.lsbu.ac.uk/water.

Mehta, M. et al. (2016a). "Correlation between Molecular Mobility and Physical Stability in Pharmaceutical Glasses". In: *Mol. Pharm.* 13, p. 1267.

Mehta, M. et al. (2016b). "Correlation between Molecular Mobility and Physical Stability in Pharmaceutical Glasses". In: *Mol. Pharm.* 13, p. 1267.

Middendorf, H.D. (1996). "Neutron studies of the dynamics of biological water". In: *Physica* 226, p. 113.

Mitchell, H.H. et al. (1945). "The chemical composition of the adult human body and its bearing on the biochemistry of growth". In: *Journal of Biological Chemistry* 158, p. 625.

Myshakina, N.S., Z. Ahmed, and S.A. Asher (2008). "Orientational and translational dynamics in room temperature ionic liquids". In: *J. Phys. Chem. B* 112, p. 11873.

Ngai, K. (1998). "Relation between some secondary relaxations and the α relaxations in glassforming materials according to the coupling model". In: *J. Chem. Phys.* 109, p. 6982.

— (2003). "An Extended Coupling Model Description of the Evolution of Dynamics with Time in Supercooled Liquids and Ionic Conductors". In: *J. Phys. Condens. Matter* 15, S1107.

— (2007). "Why the glass transition problem remains unsolved?" In: *J. Non-Cryst. Solids* 353, p. 709.

— (2011). *Relaxation and Diffusion in Complex Systems*. Springer: New York.

Ngai, K. and M. Paluch (2004). "Classification of secondary relaxation in glass-formers based on dynamic properties". In: *J. Chem. Phys.* 120, p. 857.

Novocontrol. *http://www.novocontrol.de/*.

Nyqvist-Mayer, A.A., A.F. Brodin, and S.G. Franck (1985). "Phase Distribution Studies on an Oil-Water Emulsion Based on a Eutectic Mixture of Lidocaine and Prilocaine as the Dispersed Phase". In: *J. Pharm. Sci.* 74, p. 1192.

Nyqvist-Mayer, A.A., A.F. Brodin, and S.G. Franck (1986). "Drug Release Studies on an Oil-Water Emulsion Based on an Eutectic Mixture of Lidocaine and Prilocaine as the Dispersed Phase". In: *J. Pharm. Sci.* 75, p. 365.

Orford, P.D. et al. (1989). "Effect of water as a diluent on the glass transition behavior of malto-oligosaccharides, amylose and amylopectin". In: *Int. J. Biol. Macromol.* 11, p. 91.

Paluch, M. (2001). "Effect of temperature, pressure and volume on long time relaxation dynamics in fragile glass-forming liquid". In: *J. Chem. Phys.* 115, p. 10029.

Paluch, M., S. Pawlus, and C. M. Roland (2002). "Pressure and Temperature Dependence of the α-Relaxation in Poly(methyltolylsiloxane)". In: *J. Chem. Phys.* 35, p. 7338.

Paluch, M., C.M. Roland, and S. Pawlus (2002). "Temperature and pressure dependence of the α-relaxation in polymethylphenylsiloxane". In: *J. Chem. Phys.* 116, p. 10932.

Paluch, M. et al. (1996). "Isothermal and high-pressure studies of dielectric relaxation in supercooled glycerol". In: *J. Phys.: Condens. Matter* 8, p. 10885.

Paluch, M. et al. (1998). "On the isothermal pressure behaviour of the relaxation times for supercooled glass-forming liquids". In: *J. Phys.: Condens. Matter* 10, p. 4131.

Paluch, M. et al. (2002). "Effect of pressure on the α relaxation in glycerol and xylitol". In: *J. Chem. Phys.* 116, p. 9839.

Patterson, J. et al. (2005). "The influence of thermal and mechanical preparative techniques on the amorphous state of four poorly soluble compounds". In: *J. Pharm. Sci.* 94, p. 1998.

Peleg, M. (1994). "A model of Mechanical Changes in Biomaterials at and Around Their Glass Transition". In: *Biotechnol. Prog.* 20, p. 385.

— (1995). "Formation of Glasses from Liquids and Biopolymers". In: *Science* 267, p. 1924.

Petry, W. and J. Wuttke (1995). "Quasielastic neutron scattering in glass forming viscous liquids". In: *Transp. Theory Stat. Phys.* 24, p. 1075.

Pittia, P. and G. Sacchetti (2008). "Antiplasticization effect of water in amorphous foods". In: *Food Chem.* 106, p. 1417.

Pollak, M. and T.H. Geballe (1961). "Low-frequency conductivity due to hopping processes in silicon". In: *Phys. Rev.* 122, p. 1742.

Pungor, E. (1995). *A practical guide to instrumental analysis*. Florida: Boca Raton.

Qian, F. et al. (2007). "Mechanistic Investigation of Pluronic® Based Nano-crystalline Drug-polymer Solid Dispersions". In: *Pharm. Res.* 24, p. 1551.

Raihan, R. et al. (2015). "Composite Materials Damage Modeling Based on Dielectric Properties". In: *Materials Sciences and Applications* 6, p. 1033.

Rietveld, I.B. et al. (2013a). "Liquid-liquid miscibility gaps in drug-water binary systems: crystal structure and thermodynamic properties of prilocaine and the temperature-composition phase diagram of the prilocaine-water system". In: *Mol. Pharm.* 10, p. 1332.

Rietveld, I.B. et al. (2013b). "Liquid-Liquid Miscibility Gaps in Drug-Water Binary Systems: Crystal Structure and Thermodynamic Properties of Prilocaine and the Temperature-Composition Phase Diagram of the Prilocaine-Water System". In: *Mol. Pharm.* 10, p. 1332.

Romanini, M. et al. (2017). "Thermodynamic Scaling of the Dynamics of a Strongly Hydrogen-Bonded Glass-Former". In: *Sci. Rep.* 7, p. 1346.

Roos, Y. and M. Karel (1991). "Plasticizing Effect of Water on Thermal Behavior and Crystallization of Amorphous Food Models". In: *J. Food Sci.* 56, p. 38.

Roos, Y.H. (1995). *Phase Transitions in Foods. Academic Press, Inc.* Elsevier.

Rössler, E., V.N. Novikov, and A.P. Sokolov (1997). "Toward a general description of the dynamics of glass formers". In: *Phase Transitions* 63, p. 201.

Roudaut, G., C. Dacremont, and M. Le Meste (1998). "Influence of water on the crispness of cereal based foods: acoustic, mechanical, and sensory studies". In: *J. Texture Stud.* 29, p. 199.

Sabin, J.R. (1971). "Hydrogen bonds involving sulfur. I. Hydrogen sulfide dimer". In: *J. Am. Chem. Soc.* 93, p. 3613.

Sada, N. et al. (2015). "Epilepsy treatment. Targeting LDH enzymes with a stiripentol analog to treat epilepsy". In: *Science* 347, p. 1362.

Sanz, A. and K. Niss (2017). "Coupling between Molecular Mobility and Kinetics of Crystal Growth in a Hydrogen-Bonded Liquid". In: *Cryst. Growth Des.* 17, p. 4628.

Schaumann, G.E. and E. LeBoeuf (2005). "Glass Transitions in Peat: Their Relevance and the Impact of Water". In: *J. Environ. Sci. Technol.* 39, p. 800.

Schirmacher, W., G. Diezemann, and C. Ganter (1998). "Harmonic Vibrational Excitations in Disordered Solids and the 'Boson Peak'". In: *Phys. Rev. Lett.* 81, p. 136.

Schönals, A. (1997). *Dielectric spectroscopy of polymeric materials*. ACS-Books.

Seow, C.C., P.B. Cheah, and Y.P. Chang (1999). "Antiplasticization by water in reduced moisture food systems". In: *J. Food Sci.* 64, p. 576.

Seow, C.C., C.K. Vasanti Nair, and B.S. Lee (1995). "Effects of processing on textural properties of food phytosystems". In: *Barbosa-Canovas GV, Welti-Chanes J, editors. Food preservation by moisture control* 21, p. 697.

Shalaev, E.Y. and G. Zografi P.L. Steponkus (2010). "Occurrence of Glass Transitions in Long-Chain Phosphatidylcholine Mesophases". In: *J. Phys. Chem. B* 114, p. 3526.

Silva-Santisteban, A. et al. (2017). "On the structure of prilocaine in aqueous and amphiphilic solutions". In: *Phys. Chem. Chem. Phys.* 19, p. 12665.

Sippel, P. et al. (2015). "Importance of liquid fragility for energy applications of ionic liquids". In: *Sci. Rep.* 5, p. 13922.

Skoog, D. A., F. J. Holler, and T. A. Nieman (1998). *Principles of instrumental analysis*. Boston: Thomson Learning.

Slade, L., H. Levine, and D.S. Reid (1991). "Beyond Water Activity: Recent Advances Based on an Alternative Approach to the Assessment of Food Quality and Safety". In: *Crit. Rev. Food Sci. Nutr.* 30, p. 79.

Spackman, C.W. and S.J. Schmidt (2009). "Characterizing the physical state and textural stability o sugar gum pastes". In: *Food Chem.* 119, p. 490.

Stanley, H.E. (1971). *Introduction to phase transitions and critical phenomena*. Oxford Science Publications.

Staveren, M.P.J.van, H.B. Brom, and L.J. Jongh (1991). "Compounds and Universal Features of the Hopping Conductivity of Solids". In: *Phys. Rep.* 208, p. 1.

Stillinger, F.H. (1995). "A topographic view of supercooled liquids and glass formation". In: *Science* 267, p. 1935.

Stiripentol (2002). "BCX 2600". In: *Drugs in R &D* 3, p. 220.

Sugisaki, M., H. Suga, and S. Seki (1968). "Calorimetric study of the glassy state. IV. Heat capacities of glassy water and cubic ice". In: *Bull. Chem. Soc. Jpn.* 41, p. 41.

Surana, R. et al. (2003). "Determination of Glass Transition Temperature and in Situ Study of the Plasticizing Effect of Water by Inverse Gas Chromatography". In: *Pharm. Res.* 20, p. 1674.

Symon, K. (1971). *Mechanics. 3rd ed.* Addison-Wesley.

Talja, R.A. and Y.H. Roos (2001). "Phase and state transition effects on dielectric, mechanical, and thermal properties of polyols". In: *Thermochim. Acta* 380, p. 109.

Tarjus, G., D. Kivelson, and S. Kivelson (1976). *The glass transition and the nature of the glassy state. In: Goldstein M, Simha R (eds)*. Annu. New York Acad. Sci. 279.

Thayyil, M. Shahin et al. (2008). "Is the Johari-Goldstein β relaxation universal?" In: *Philosophical Magazine* 88.33-35, pp. 4007–4013.

Toscani, S. et al. (2016). "Stability hierarchy between Piracetam forms I, II, and III from experimental pressure-temperature diagrams and topological inferences". In: *Int. J. Pharm.* 497, p. 96.

Tripathi, P. et al. (2015). "Collective relaxation dynamics and crystallization kinetics of the amorphous Biclotymol antiseptic". In: *Int. J. Pharm.* 495, p. 420.

Trojnar, M.K. et al. (2005). "Stiripentol. A novel antiepileptic drug". In: *Pharmacol. Rep.* 57, p. 154.

Vrentas, J.S., J.L. Duda, and H. Ling (1988). "Antiplasticization and volumetric behavior in glassy polymers". In: *Macromol* 21, p. 1470.

Walden, P.Z. (1906). "Organic solvents and ionization media. III. Interior friction and its relation to conductivity". In: *J. Phys. Chem.* 55, p. 207.

Wang, Q. et al. (2016). "The decisive role of free water in the determining homogeneous ice nucleation behavior of aqueous solutions". In: *Sci. Rep.* 6, p. 26831.

Williams, G. and D.C. Watts (1970). "Non-symmetrical dielectric relaxation behaviour arising from a simple empirical decay function". In: *Trans. Faraday Soc.* 66, p. 80.

Wirrell, E.C. et al. (2013). "Stiripentol in Dravet syndrome: results of a retrospective U.S. study". In: *Epilepsia* 54, p. 1595.

Wojnarowska, Z. et al. (2013a). "Decoupling of conductivity relaxation from structural relaxation in protic ionic liquids and general properties". In: *Sci. Rep.* 15, p. 9205.

Wojnarowska, Z. et al. (2013b). "Molecular dynamics, physical stability and solubility advantage from amorphous indapamide drug". In: *Mol. Pharm.* 10, p. 3612.

Wojnarowska, Z. et al. (2015). "Dynamic properties of glass-formers governed by the frequency dispersion of the structural α-relaxation: examples from prilocaine". In: *J. Phys. Chem. B* 119, p. 12699.

Wu, T. and L. Yu (2006). "Surface Crystallization of Indomethacin Below T_g". In: *Pharm. Res.* 23, p. 2350.

Wunderlich, B. (1976). *Macromolecular Physics. Crystal Nucleation, Growth, Annealing, Vol. 2*. Academic Press: London.

Yin, S.X. et al. (2005). "Bioavailability enhancement of a COX-2 inhibitor, BMS-347070, from a nanocrystalline dispersion prepared by spray-drying". In: *J. Pharm. Sci.* 94, p. 1598.

Yoshioka, S. and Y. Aso (2005). "A quantitative assessment of the significance of molecular mobility as a determinant for the stability of lyophilized insulin formulations". In: *Pharm. Res.* 22, p. 1358.

Yoshioka, S. and V.J.Stella (2002). *Stability of drugs and dosage forms*. Kluwer Academic Publishers.

Yu, L. (2001). "Amorphous pharmaceutical solids: preparation, characterization and stabilization". In: *Adv. Drug Deliv. Rev.* 48, p. 27.

Zachariah, M. et al. (2015a). "Molecular diffusion and DC conductivity perfectly correlated with molecular rotational dynamics in a plastic crystalline electrolyte". In: *Phys. Chem. Chem. Phys.* 17, p. 16053.

Zachariah, M. et al. (2015b). "Self-Diffusion, phase behavior, and Li+ ion conduction in succinonitrile-based plastic co-crystals". In: *J. Phys. Chem.* 119, p. 27298.

Zachariah, M. et al. (2015c). "Water-triggered conduction mediated by proton exchange in a hygroscopic fulleride and its hydrate". In: *J. Phys. Chem. C* 19, p. 685.

Zhao, L.S., Z.X. Cao, and Q. Wang (2015a). "Glass Transition of Aqueous Solutions Involving Annealing-Induced Ice Recrystallization Resolves Liquid-Liquid Transition Puzzle of Water". In: *Sci. Rep.* 5, p. 15714.

— (2015b). "Glass transition of aqueous solutions involving annealing-induced ice recrystallization resolves liquid-liquid transition puzzle of water". In: *Sci. Rep.* 5, p. 15714.

Zhu, F. (2015). "Composition, Structure, Physicochemical Properties, and Modifications of Cassava Starch". In: *Carbohydr. Polym.* 122, p. 456.